Detection and characterization of the structural determinants of temperature sensitivity in TRPM8.

Tesis entregada a

LA UNIVERSIDAD DE VALPARAÍSO

en Cumplimiento Parcial de los requisitos para optar al grado de

Doctor en Ciencias con Mención en Neurociencia

Facultad De Ciencias

Por

Natalia Alejandra Raddatz Cárdenas

Mes, xx 2013

Dirigida por: Ramón Latorre de la Cruz
Co-Dirigida por: Osvaldo Álvarez

FACULTAD DE CIENCIAS

UNIVERSIDAD DE VALPARAÍSO

INFORME DE APROBACION

TESIS DE DOCTORADO
Se informa a la Facultad de Ciencias que la Tesis de Doctorado presentada por:

Natalia Alejandra Raddatz Cárdenas

Ha sido aprobada por la comisión de Evaluación de la tesis como requisito para optar al grado de Doctor en Ciencias con mención en Neurociencia, en el examen de Defensa de Tesis rendido el día XX del Mes de XXXX de 20XX

Director/a de Tesis:
Dr/a. .....

Co-Director/a de Tesis:
Dr/a. .....

Comisión de Evaluación de la Tesis

Dr/a. .....

Dr/a. .....

Dr/a. .....

Dr/a. .....

TABLE OF CONTENTS

LIST OF TABLES

LIST OF FIGURES

LIST OF ABBREVIATIONS

°C	degree centigrade
ΔG_0	standard Gibbs free energy change
ΔH	enthalpy change
ΔS	entropy change
σ^2	variance
τ_{act}	time constant of activation
τ_{deact}	time constant of deactivation
A	Activated conformation of the sensors.
2-APB	2-aminoethyldiphenyl borate
µg	microgram
µl	microliter
µM	micromolar
ADP	Adenosine diphosphate
C	Allosteric factor describing interaction between channel opening and temperature sensor activation
C-terminal	carboxy-terminal
$CaCl_2$	calcium chloride
cDNA	complementary DNA
CIRB	calmodulin IP_3-receptor binding site
C. elegans	*Caenorhabditis elegans*
D	Allosteric factor describing interaction between channel opening and voltage sensor activation.
d	delay (ms)
DNA	desoxyribonucleic acid
DRG	dorsal root ganglion
$E^{\ddagger}$	activation energy
E	Allosteric factor describing interaction between voltage-sensor activation and temperature sensor
EGTA	ethylene glycol-bis (2-amino-ethylether)N,N,N',N'-tetra acetic acid
ER	endoplasmatic reticulum
F	Faraday constant (96,485.3365 C/mol)
G	conductance

HEK 293	human embryonic kidney cells 293
HEPES	4-2-hydroxyethyl-1-piperazineethanesulfonic acid
</I>	average current and variance, □2,
I	current
i	unitary current
IP_3	ionositol triphosphate
J	equilibrium constant for the voltage sensor
J_0, z_J	The zero voltage value of J and its partial charge, respectively.
K	equilibrium constant for the temperature sensor
k	rate constant at the absolute temperature
KCl	potassium chloride
kDA	kilo Dalton
kHz	kilohertz, 10^3 Hz
L	equilibrium constant between the closed and open states being the voltage and temperature sensors in resting
L_0, z_L	The zero voltage value of L and its partial charge, respectively.
LED	Light-emitting diode
LiCl	Lithium chloride
MΩ	megaohm
$MgCl_2$	magnesium chloride
MHR	TRPM homology regions
min	minute
mL	milliliter(s)
mM	millimolar
MO	mustard oil
mRNA	messenger RNA
ms / msec	milliseconds
mV	milli volt
N-terminal	amino-terminal
N	number
nA	nanoampere(s)
NaCl	sodium chloride
NaOH	sodium hydroxide
ng	nanogram
nL	nanolitre
nM	nanomolar(s)

nm	nanometre
NUDT9	nucleoside diphosphate linked moiety X-type motif 9
pA	picoampere(s)
PCR	polymerase chain reaction
PDZ	**P**ost synaptic density protein (PSD95), **D**rosophila disc large tumor suppressor (Dlg1), and **Z**onula occludens-1 protein (zo-1)
PIP_2	phosphatidylinositol bisphosphate
PKA	protein kinase A
PKD	polycystic kidney disease
PLC	phospholipase C
Po	open probability
Q_{10}	value change in the rate of reaction when temperature is increased by 10°C
R	Resting conformation of the sensors
R	universal gas constant (8.3144621 $J\,K^{-1}\,mol^{-1}$)
RNA	Ribonucleic acid
s / sec	second(s)
s.e.m	standard error of the mean
T	absolute temperature
t	time (ms)
TG	trigeminal ganglion
TM	transmembrane
TRP	transient receptor potential
TRPA	transient receptor potential ankyrin
TRPC	transient receptor potential classical
TRPL	transient receptor potential -like
TRPM	transient receptor potential melastatin
TRPN	transient receptor potential no mechanoreceptor potential C (nompC)
USB	Universal Serial Bus
V	membrane potential
$V_{0.5}$	voltage for half-maximal activation
z	voltage dependency for this constant

1. ABSTRACT

Transient Receptor Potential Melastatin 8 (TRPM8) is a Ca^{2+} permeable non-selective cation channel activated by cold temperatures and chemical agonists, such as menthol. The channel is largely closed at 28 °C and is mainly open at 10 °C. Their conductance increases about 24 times when the temperature drops 10 °C, indicating that the gating process in TRPM8 channels is 8 times more sensitive to changes in temperature that, for example, voltage-dependent K^+ channels (Q_{10} ~3). Analysis of the conductance-voltage curves in the TRPM8 wild type, showed that values of the voltage at which the open probability is 0,5 ($V_{0.5}$) saturate at high and low temperatures. This is a demonstration of the existence of a temperature sensor and a voltage sensor that determine the open probability of the channel. Furthermore, the quantification of the open probability at different temperatures shows that the voltage is a partial activator of channel. Analysis of the limiting slope of the open channel probability as a function of voltage and deactivation time constant at very negative potential values shows that the opening of the channel is independent of voltage. Finally, analyses of the activation kinetics suggest that TRPM8 channels undergo one or more transitions along a series of closed states before opening. The C-terminal of TRPM8 is an important molecular domain that defines the channel sensitivity to temperature. In order to determine which regions of the C-terminal are the molecular determinants of cold sensitivity of TRPM8, a series of deletions were performed in the distal region of this structure. The temperature sensitivity of each mutant was determined using electrophysiological techniques. A thermodynamic analysis of the results indicates that the coiled-coil structure, located between amino acids 1064 and 1104, play a key role in temperature sensing of TRPM8 channels. Thus, all these data allow us to demonstrate: first the existence of independent temperature and voltage sensors coupled through allosteric interactions to channel

gating and second, that the coiled-coil structure confers specific thermal sensitivity in TRPM8.

2. INTRODUCTION

In this section, I will briefly present the main characteristics of the family of the TRPs channels, to continue with a concise description of those that are temperature sensitive. Next, I will focus on the main actor of this thesis work, TRPM8, focused mainly to study of the contribution of the C-terminal domain to the channel temperature sensitivity. Finally, I will describe allosteric model, with the purpose of setting a theoretical framework to account for our experimental observations.

2.1. Time line of the discovery of the TRP channels

*T*ransient *R*eceptor *P*otential genes (*trp*) were first described in the late 1960s in the fruit fly, *Drosophila melanogaster* (Cosens and Manning, 1969). The name is derived from a spontaneously occurring mutation in the fly *Drosophila* that shows a defect in visual transduction. The eyes of these mutant flies elicit a transient electric response to continuous light instead of a continuous response, as it is the case of the wild type flies. Twenty years late Montel and Rubin reported that the *trp* gene encoded a large protein, the TRP channel, consisting of 1275 amino acid residues displaying eight putative transmembrane (TM) segments (Montell and Rubin, 1989). In addition, the amino acid sequence did not present any clear homology with any other known ion channel. Just four years late, in 1992, Phillips found a new gene that he called trp-like (*trpl*). The protein encoded by *trpl* showed structural homologies with *Drosophila trp* and also with the superfamily of voltage gated channel genes (Phillips et al., 1992). On the same year, Hardie and Minke demonstrated that the *trp* gene coded for a highly Ca^{2+} permeable channel (Hardie and Minke, 1992). In 1995, Petersen demonstrated that TRP related proteins were also present on vertebrates such as *Xenopus laevis* and mice cDNA libraries (Petersen et al., 1995). The same year Wes and Zhu, reported the full sequence of the first human

homologue, TRPC1 (Wes et al., 1995; Zhu et al., 1995) sharing 37% identity with the *Drosophila trp* gene. Today, we can list more than 100 channels (table 1) (Nilius and Owsianik, 2011) within this family (invertebrate and vertebrate combined).

2.2. Structure and function of the TRP superfamily

The TRP superfamily comprises a large number of ion channels with diverse functions. The division into subfamilies on the basis of amino acid sequence and structural similarity does not provide functional classification for TRP proteins. For example, some members of the TRPV subfamily are involved in thermal and nociceptive sensing whereas others are insensible to temperature but are highly selective to Ca^{2+} participating in the epithelial Ca^{2+} transport. Moreover, thermal sensing is not restricted to members of the TRPV subfamily. TRPM8 and TRPA1, also functions in thermal sensing. All members of the TRP family include six putative transmembrane domains, cytosolic N- and C-terminal tails and an ion pore between transmembrane domains 5 and 6 (Montell, 2005). According to their amino acid sequence homology TRP channels are grouped into seven subfamilies (Figure 1) which, in turn, are classified into groups 1 and 2 based on sequence and topological differences (Figure 2) (Montell et al., 2002a). The Group 1 TRPs, composed of TRPC (classical), TRPV (vanilloid), TRPM (melastatin-related), TRPA (ankyrin), and TRPN (NOMP-C homologues) show a strongest sequence homology with the founding member of the superfamily, *Drosophila* TRP (Montell and Rubin, 1989), while the Group 2 comprising TRPP (polycystin) and TRPML (mucolipin) are distant relatives. TRPP and TRPML proteins share sequence homology over the transmembrane segments and contains a large loop separating the first two transmembrane domains (see Figure 1). An eighth subfamily, TRPY, Y for yeast TRPs, is distantly related to the Group 1 and Group 2 TRPs (Palmer et al., 2001; Denis and Cyert, 2002).

TABLE1

Composition of the TRP superfamily of the fruit fly *Drosophila melanogaster,* the worm *Caenorhabditis elegans*, the sea squirt *Ciona intestinalis,* the puffer fish (Seifuku, *Fugu rubripes*), the zebrafish (*Danio rerio*), mouse and human. Adapted from (Nilius and Owsianik, 2011)

	Drosophila melanogaster	Caenorhabditis elegans	Ciana intestinalis	Fugu rubripes	Danio rerio	Mus musculus	Homo sapiens
TRPC	3	3	8	8	8	7	6
TRPV	3	5	2	4	4	6	6
TRPM	1	4	2	6	6	8	8
TRPA	4	2	4	1	2	1	1
TRPN	1	1	1	-	1	-	-
TRPML	4	1	9	2	2	3	3
TRPP	1	1	1	4	4	3	3
Total	**17**	**17**	**27**	**25**	**27**	**28**	**27**

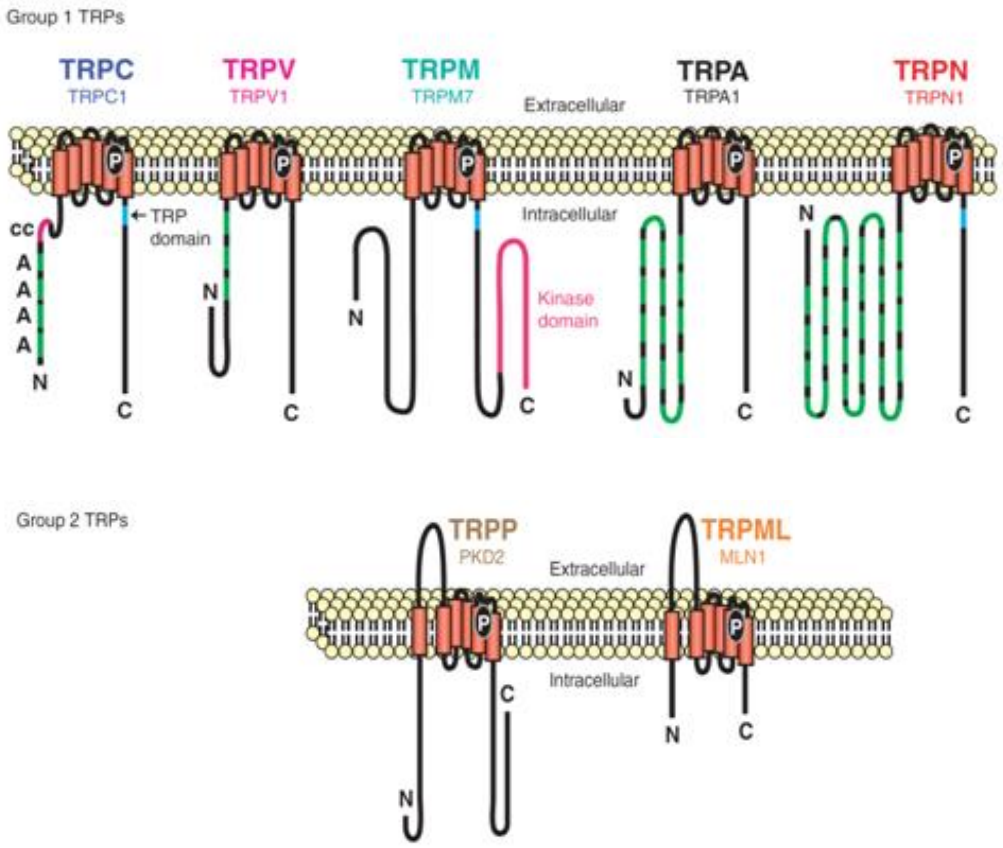

Figure 1. ***The seven TRP subfamilies***. Representatives of the five group 1 and two group 2 subfamilies are indicated at the top and bottom, respectively. Several domains are indicated: ankyrin repeats (A), coiled-coil domain (cc), protein kinase domain (TRPM6/7 only), transmembrane segments, and the TRP domain. Adapted from Venkatachalam and Montell (Venkatachalam and Montell, 2007).

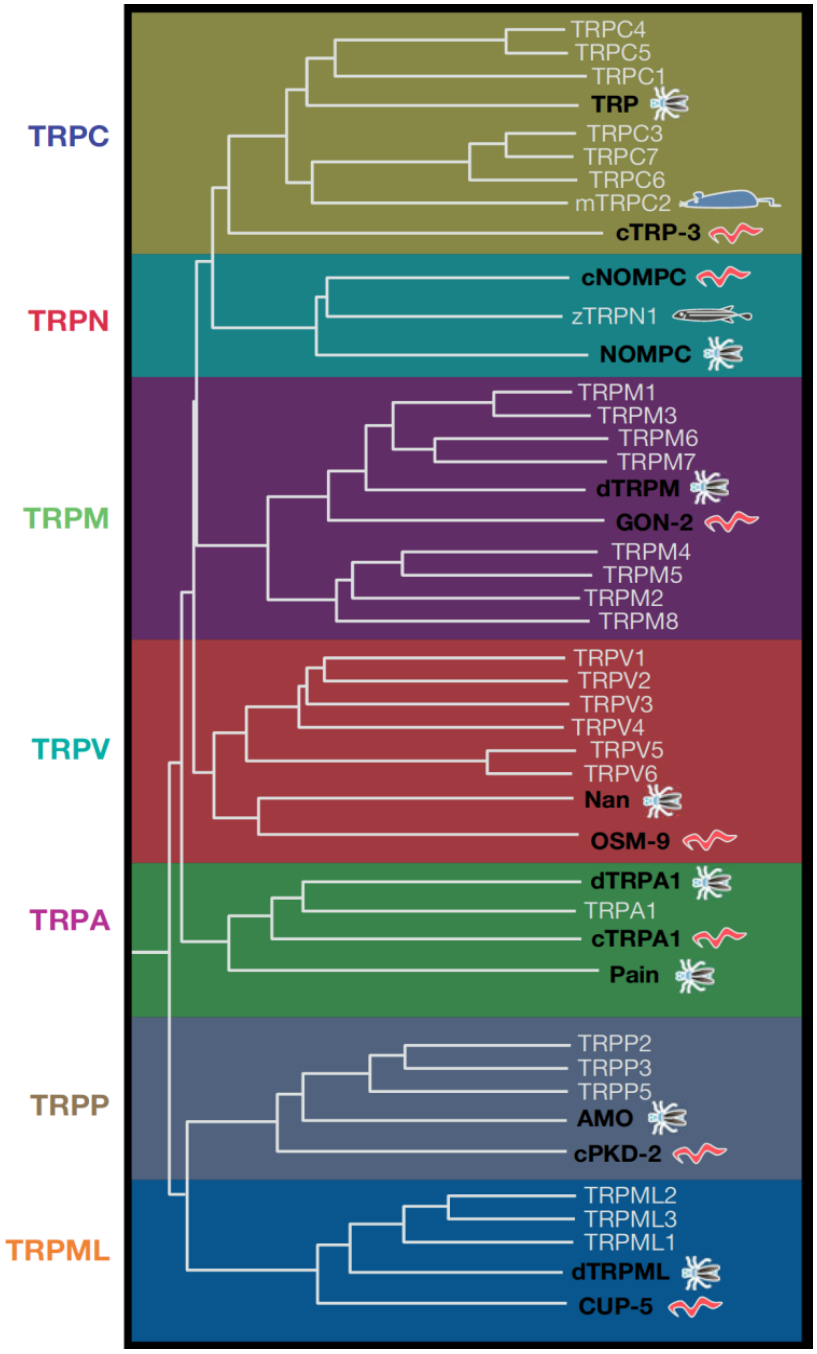

Figure 2: ***Phylogenetic tree showing the relatedness of the TRP proteins*****.** The dendrogram of vertebrate TRPs includes mostly human TRPs, except for mouse TRPC2 (cartoon of a mouse) and zebrafish TRPN1 (cartoon of a zebrafish). Black text and cartoons highlight the TRP proteins from worms and flies. One *C. elegans* and one *Drosophila* member of each subfamily are included.

2.2.1. GROUP 1 SUBFAMILIES

2.2.1.1. TRPC (classical)

TRPC channels are ubiquitously expressed among cell types and mediate signals in response to phospholipase C (PLC)-coupled receptors (Clapham, 2003; Montell, 2005). They have four ankyrin repeats, a TRP box, a homer-binding region, a calmodulin IP_3-receptor binding site (CIRB) and PDZ domain in TRPC4 and 5.

The first mammalian homologues of *Drosophila* TRPs were referred to as TRPC1, TRPC2, and TRPC3 (Wes et al., 1995; Zhu et al., 1995). Since then, seven mammalian TRPC proteins (TRPC1–7) have been described (Montell et al., 2002b). TRPC channels have been proposed to be activated by a variety of signals including Ca^{2+} store depletion, membrane lipids, and vesicular insertion into the plasma membrane. As nonspecific cation channels, TRPC channel opening results in the entry of both Na^{+} and Ca^{2+} ions into the cell.

2.2.1.2. TRPV (vanilloid)

The TRPV subfamily of ion channels contains three ankyrin repeats and calmodulin binding site. Consists of six members, of which, TRPV1-4 are non-selective cation channels and temperature sensitive, whereas TRPV5 and TRPV6 are insensible to temperature and are the most Ca^{2+} selective (PCa^{2+}/PNa^{+} > 100) channels of the mammalian TRPs (Montell, 2005). Three mammalian TRPV channels, TRPV1, TRPV2 and TRPV4 are involved in sensing osmolarity changes and mechanical stimuli (Kim et al., 2003; Gong et al., 2004).

2.2.1.3. TRPM (melastatin-related)

TRPM channels share four regions of high homology (TRPM homology regions-MHRs) in their N-terminal cytoplasmic segment. The TRPM subfamily contains eight members, TRPM1-TRPM8. They have diverse C-terminal domains but share a cytoplasmic coiled-coil domain. The C-terminal domain distal to the coiled-coil region varies significantly between different TRPM

family members and may contain structures that are important in controlling the ion channel activation mechanism. TRPM6 and TRPM7 are designated as chanzymes since their C-terminal contains catalytic domains able to show protein kinase activities (Nadler et al., 2001; Runnels et al., 2001; Schlingmann et al., 2002; Walder et al., 2002). TRPM2 is also a chanzyme with a C-terminal ADP-ribose pyrophosphatase domain (NUDT9 homology domain) (Perraud et al., 2001; Sano et al., 2001). TRPM2, TRPM4 and TRPM5 are heat activated whereas that TRPM8 is activated by cold temperature. In contrast to all other TRPs, both TRPM4 and 5 form ion channels permeable to monovalent cations but impermeable to Ca^{2+} (Launay et al., 2002; Hofmann et al., 2003; Nilius et al., 2003). Finally, studies in HEK-293 cells indicate that the activity of TRPM3 is increased by reduction of extracellular osmolarity (Grimm et al., 2003).

2.2.1.4. TRPA (ankyrin)

TRPA family includes only one member present in human, TRPA1. The N-terminal region of the TRPA1 protein comprises 17 ankyrin repeats, which are common structural motifs that mediate protein–protein interactions (Gaudet, 2008). It is activated by different chemical compounds including psychoactive component in marijuana (delta-9-tetrahydrocannabinol), environmental irritants, and pungent compounds of wasabi, garlic (allicin), cinnamon oil (cinnamaldehyde), mustard oils (allyl isothiocyanate) and tear gas (acrolein) (Jordt et al., 2004). Acrolein also is present in air pollution, vehicle exhaust, and cigarette smoke (Bautista et al., 2006). TRPA1 has been reported as a cold receptor (Story et al., 2003).

2.2.1.5. TRPN (no mechanoreceptor potential C (NOMP-C) homologues)

This family has a single member that can be found in worms, flies, and zebrafish (Littleton and Ganetzky, 2000; Walker et al., 2000; Sidi et al., 2003), whereas mammals do not encode any TRPN homologues. TRPNs lack the TRP domain; however they do have the conserved TRP-box. Apparently they have a role in mechanotransduction (Walker et al., 2000).

2.2.2. GROUP 2 SUBFAMILIES

2.2.2.1. TRPP (polycystin)

The TRPP subfamily is formed by the polycystic kidney disease (PKD) proteins or polycystins. TRPP channels carry an EF-hand motif and an ER retention signal. TRPP channels are present on both motile and primary cilia, and they may function to sense fluid flow, osmolarity, and mechanical stretch (Stayner and Zhou, 2001; Nauli et al., 2003; Venkatachalam and Montell, 2007).

2.2.2.2. TRPML (mucolipin)

The TRPML subfamily is defined by a human protein, TRPML1 (mucolipidin1; ML1) (Bargal et al., 2000; Bassi et al., 2000; Sun et al., 2000). Mutations in this protein are responsible for the lysosomal storage disorder mucolipidosis IV, which is characterized by severe neurodegeneration. In addition to TRPML1, mammals encode two other closely related proteins referred to as TRPML2 and TRPML3. TRPML1 and TRPML2 are expressed in the lysosomal membrane while TRPML3 resides predominantly in the endoplasmic reticulum, ER, membrane in cultured cells (Manzoni et al., 2004; Kiselyov et al., 2005; Venkatachalam et al., 2006). Finally, the only member of this subfamily reported to form a nonselective Ca^{2+} channel is TRPML1 (LaPlante et al., 2002).

2.3. ThermoTRP channels

2.3.1. Overview of thermo-TRPs

The neurons that allow us to sense temperature are located in the trigeminal ganglia (TG) innervating the face and head, and the dorsal root ganglia (DRG) for the rest of the body. The DRG are clusters of sensory neuron cell bodies that are located along the vertebral column just

lateral to the spine. DRG neurons are functionally classified as proprioceptors, low-threshold mechanoreceptors, and cells that sense pain and temperature. Nociceptive (pain) neurons detect noxious thermal, mechanical (high-threshold) or chemical stimuli (Campero et al., 1996; Cain et al., 2001), whereas thermosensitive neurons detect temperature either in the noxious range (making up a subset of nociceptive neurons) or in the innocuous range. The process of thermosensation begins through specific receptor proteins, such as thermo-TRP channels, that are located within the free nerve endings in the skin. Thus, for example at 15 °C, TRPM8 channels are open and allow sodium and calcium ions to flow into the nerve terminals leading to depolarization, which in turn activate sodium channels, triggering action potentials firing (Babes, 2009).

Cloning and characterization of a temperature sensitive subclass of the TRP channels (the thermo-TRPs) have opened up our understanding of the molecular basis of thermal sensation. To date, six TRP channels have been reported to be directly activated at specific temperature ranges from noxious heat to painful cold: TRPV1, TRPV2, TRPV3 and TRPV4 are heat-activated, whereas TRPM8 and TRPA1 are activated by cold (McKemy, 2002; Peier, 2002; Story et al., 2003; Talavera et al., 2005; Dhaka et al., 2006; Huang et al., 2006; Togashi et al., 2006). Three other TRPs (TRPM2, TRPM4 and TRPM5) also show temperature sensitivity but are not usually included in the thermo-TRP family because they are not expressed in primary somatosensory neurons. Table 2 summarizes the activation of the thermo-TRPs by temperature and agonists, and describes some functions of these ion channels.

2.3.1.1. TRPV1.

This TRP channel was first characterized by McNaugthon and his group (Cesare and McNaughton, 1996), and was subsequently cloned by the group of David Julius (Caterina et al., 1997). TRPV1 is a non- selective cation permeable channel activated by a wide range of stimuli (see Table 2) including capsaicin, low pH (< 6) and by physical factors such as heat and membrane depolarization (Tominaga et al., 1998; Voets et al., 2004). The activation by

TABLE2

Thermo-TRP channels, with examples of agonists acting on each receptor and suggested functions of the receptor in the intact animal. Adapted from L. Vay (Vay et al., 2012).

Channel	Temperature sensitivity	Non-thermal agonists	Function
TRPV1	≥ 42 °C	Capsaicin, low pH, ethanol, anadamide, NADA, 12-HPETE, camphor, resiniferatoxin, allicin, 2-APB, lidocaine, gingerol, shogaol, piperine monoacylglycerols, ω-3 fatty acids, membrane stretch	Noxious heat sensor; also involved in inlammatory pain, thermal hyperalgesia, hippocampal long-term depression, diabetes, obesity, bladder function, hypertension, gastrointestinitis, hypothermia, renal excretory function.
TRPV2	≥ 52 °C	2-APB, cannabidiol, membrane stretch	Possible extreme heat sensor ; innate immune system
TRPV3	32°C~39°C	2-APB, camphor, carvacrol (from oregano), incensole acetate, thymol, eugenol	Warmth; possible involvement in noxious heat detection
TRPV4	27°C~34°C	Membrane stretch, phorbol ester, 5,6-EET, anandamide, arachidonic acid, BAA	Warm temperature sensation and volume regulation; possible involvement in noxious mechanical pain and thermal hyperalgesia
TRPM8	25°C~34°C	Menthol, icilin, eucalyptol	Innocuous cold perception, behavioural thermoregulation, cold-mediated analgesia; cold nociception in some neurons
TRPA1	≤17°C	Cinnamaldehyde, acrolein, chlorine, ROS, formalin, fatty acids, mustard oil, allicin, icilin, gingerol, prostanoids, NSAIDs, isoflurane, propofol, etomidate, dihydropyridines, clotrimazole, nicotine, menthol	Cold, mechanical and chemically induced nociception, cold hyperalgesia

temperature is in the range of 41-43 °C, likely reaching a maximum over 50 °C. This channel, can be directly activated by ethanol (Trevisani et al., 2002), by a variety of endogenous lipids for example endocannabinoid, anandamide and N-arachidonoyl dopamine (Ross, 2003; De Petrocellis et al., 2004), by metabolic products of lipoxygenase (Hwang et al., 2000), by the topical analgesic as camphor (Xu et al., 2005), the pungent compounds present in black pepper (piperine) (McNamara et al., 2005) and garlic (allicin) (Macpherson et al., 2005). Thus, TRPV1 is viewed as a signaling integrator for many noxious stimuli. TRPV1$^{-/-}$ mice show impaired responses to heat and vanilloid compounds, and have reduced inflammatory thermal hyperalgesia. However, these mice are relatively normal in their response to noxious heat stimuli and the mechanical hyperalgesia is little affected (Caterina et al., 2000; Davis et al., 2000).

2.3.1.2. TRPV2.

Although this channel shares a 50% sequence homology to TRPV1, is insensitive to capsaicin, low pH and responds to higher temperature stimuli, with an activation threshold of 52°C (Caterina et al., 1999). TRPV2 is activated *in vitro* by three different types of physical stimuli: heat, osmotic stress and mechanical stretch (Caterina et al., 1999; Muraki et al., 2003). Also, it is activated by chemicals such as 2-aminoethoxydiphenyborate (2-APB), known to inhibit inositol 1,4,5-trisphosphate receptors and store-operated channels as well as many TRP channels (Hu et al., 2004), and by cannabidiol, a natural component of the marijuana plant (Qin et al., 2008). The physiological role of TRPV2 in thermal nociception remains unknown because TRPV2$^{-/-}$ mice showed no evident deficits in thermal sensation (Park et al., 2011).

2.3.1.3. TRPV3.

This ion channel is implicated in the perception of warmth in the skin with an activation threshold of 34-38 °C (Peier et al., 2002; Smith et al., 2002; Xu et al., 2002). TRPV3 is activated by 2-APB (Chung et al., 2004) and by various natural compounds such as carvacrol, thymol and eugenol, which are present in the essential oils from herbs and spices: thyme (*Thymus vulgaris*),

oreganum (*Origanum syriacum*), and clove (*Caryophilli flos*) (Moqrich et al., 2005; Xu et al., 2006). In late 2008, Patapoutian and his colleagues identified five single point mutations that specifically abolish heat-activation, but do not perturb chemical activation or voltage modulation of this channel. These amino acid residues are located in the 6th transmembrane segment and the adjacent extracellular loop of the pore domain (Grandl et al., 2008). These findings are very important because demonstrate that temperature-sensitivity of TRPV3 is separable from all other activation mechanisms such as voltage sensing and agonist binding. Finally, the TRPV3$^{-/-}$ mice shows some deficits in sensing hot temperatures in the innocuous to noxious range (Moqrich et al., 2005).

2.3.1.4. TRPV4.

It is a nonselective cation channel that shares ~40% amino acid identity with TRPV1 (Liedtke et al., 2000; Strotmann et al., 2000; Delany et al., 2001). This thermo-TRP is activated by moderate temperature; the activation is measurable from 27°C–34°C (Watanabe et al., 2002a). In addition to temperature, TRPV4 is activated by hypotonic solutions, suggesting that it serves as a sensor for osmolarity or mechanical stretch (Liedtke et al., 2000; Strotmann et al., 2000; Wissenbach et al., 2000; Delany et al., 2001; Alessandri-Haber et al., 2005), also can be activated by phorbol esters (Watanabe et al., 2002b). Knockout studies suggest that TRPV4 plays a role in thermal hyperalgesia (Todaka et al., 2004).

2.3.1.5. TRPM8.

TRPM8 was the first TRP channels found to sense cold temperature (McKemy, 2002; Peier, 2002). Activation is measurable at ~28°C, with currents increasing in magnitude down to 10°C (McKemy, 2002; Peier, 2002; Brauchi, 2004; Bautista et al., 2007). Furthermore, this channel is activated by voltage (Brauchi, 2004; Voets et al., 2004), and by chemical agonists that mimic cooling such as menthol, eucalyptol or icilin (McKemy, 2002; Peier, 2002; Chuang, 2004; Bodding et al., 2007). Low levels of menthol move the activation threshold of TRPM8 to warmer

temperatures. However, repeated menthol stimulation rapidly desensitizes TRPM8 in a Ca^{2+}-dependent manner (McKemy, 2002; Reid G, 2002). TRPM8 is also activated by the regulatory lipid phosphatidylinositol 4,5-bisphosphate (PIP_2) (Liu and Qin, 2005; Rohacs et al., 2005). Voltage dependence, it is very weak (z=0.6-0.8) compared with z=13 in Shaker K^+ channels (Brauchi, 2004; Voets et al., 2004; Voets, 2007). One possible explanation for it is the scarcity of positive charges in the human TRPM8 S4 domain, having only one arginine residue on the S4 (R842) and one lysine on the S4–S5 (K856) linker (Voets, 2007). The S4 domain also contains a histidine residue that can be positively charged depending of its pK in the protein milieu. Cold temperature and agonist shift the TRPM8 conductance-voltage curve towards more negative potentials (Brauchi, 2004; Voets et al., 2004; Matta and Ahern, 2007). *In vivo* studies of $TRPM8^{-/-}$ mice showed deficits in reaction to cool temperatures, demonstrating that this channel is a major sensor of peripheral innocuous coolness (Bautista et al., 2007; Colburn et al., 2007; Dhaka et al., 2007).

2.3.1.6. TRPA1.

TRPA1 is activated on the noxious cold range of temperatures (~≤ 17°C), suggesting that may be the responsible for detecting painful levels of cold (Story et al., 2003). The active constituents of mustard oil (allyl isothionate) and garlic (allicin) robustly activate TRPA1 currents (Bandell et al., 2004; Jordt et al., 2004; Macpherson et al., 2005). TRPA1 is directly activated by Ca^{2+} binding to an EF-hand domain located within its intracellular N-terminal region. This suggests that the apparent cold sensitivity may result not from direct temperature-sensitive gating but instead from a cold induced increase in intracellular Ca^{2+} (Doerner et al., 2007; Zurborg et al., 2007). Furthermore, analyses $TRPA1^{-/-}$ mice has yielded conflicting data, with one group reporting no deficits in acute cold sensing, a second group observing reduced cold sensitivity in female but not male mice, and a third group showing cold deficits after prolonged exposure to cold (Bautista et al., 2006; Kwan et al., 2006; Karashima et al., 2009).

2.4. The role of the C-terminal domain of TRPM8 channel.

The key domain or residues for thermosensitivity of these channels have not been identified yet. Studies reveal that the C-terminal of thermo-TRPs may be a potential candidate because swapping the C-terminal domain of TRPV1 with TRPM8 exchanges their temperature sensitivity, channel gating kinetics and PIP_2 modulation (Brauchi S., 2006). Furthermore, other study uncover that sequential deletion of the distal half C-terminal in TRPV1 reduced the temperature threshold (Vlachova V, 2003). Thereby, these findings support the idea that the C-terminal domain may contain the thermal sensor. In this section I focus attention on two important domain of the C-terminal of TRPM8: the TRP domain and the coiled-coil domain.

2.4.1. TRP domain

The proximal C-terminus contains a block of ~25 residues, the TRP domain, that has a signature sequence dubbed TRP box (IWKLQR) that is highly conserved in all TRP mammalian subfamilies except TRPA and TRPP (Clapham, 2003; Montell, 2005). Residues within the TRP domain and TRP box, K995, R998 and R1008, are critically involved in the activation of TRPM8 by the signaling membrane lipid, PIP_2, which is necessary for the activation of TRPM8 (Rohacs et al., 2005).

2.4.2. Coiled-coil domain

Coiled-coils are the most common and best understood protein-protein interaction domain (Lupas and Gruber, 2005; Woolfson, 2005). Coiled-coils consist of two to four amphipathic α-helices that twist around one another to form a particularly stable structure. These sequences are characterized by a seven-residue periodicity (heptad repeat) of amino acids (***a****bc****d******e****f****g***)*n*, where ***a*** and ***d*** are hydrophobic, and ***e*** and ***g*** are charged or polar. The hydrophobic amino acids form a nonpolar stripe that promotes the multimerization (Crick, 1953). Electrostatic interactions of the charged residues with the solvent permit a proper alignment, orientation, selectivity and stability of coiled-coils (Figure 3A) (Kohn et al., 1995; Krylov et al., 1998). TRPM channels share

a coiled-coil domain located on the C-terminal domain but only in the case of TRPM8, this region is at the very end of the protein, more specifically in the residues 1064–1104, the last 40 amino acids of the protein (Figure 3B) (Montell, 2005). When this coiled-coil domain is expressed as a fusion protein, forms tetramers, suggesting that are likely to direct channel assembly (Tsuruda et al., 2006). Removal and or mutation in the positions ***a*** and ***d*** of the coiled-coil domain, leads to complete loss of TRPM8 expression and channel activity (Tsuruda et al., 2006). However, other reports show that a TRPM8 deletion construct missing the C-terminal coiled-coil still tetramerizes and traffics to the plasma membrane when expressed heterologously in insect cells (Gaudet, 2007). A second potential coiled-coil domain was identified on the N-terminal domain of TRPM8, however, has a much weaker coiled-coil score compared to the C-terminal domain (40% versus 96% probability for the C-terminal coil) and, is not well conserved among other TRPM family members (Tsuruda et al., 2006).

Recent studies have characterized the X-ray crystal structure of the coiled-coil domain of the channel enzyme TRPM7. This structure revealed that the homotetrameric crystal of TRPM7 coiled-coil shows two α-helical strands going in one direction and two strands going in the opposite direction (Fujiwara and Minor, 2008). An analysis of the primary structure of the coiled-coil domains of other members of this subfamily suggest that they can be divided into two groups: TRPM1, 3, 6, 7, and TRPM2, 4, 5, 8 (Figure 3B). The principal differences between both groups are the coiled-coil lengths and the lack of matching between hydrophobic core compositions, which suggests that is unlikely that heterotetramers will form between groups and that the quaternary structure of the coiled-coil domain of these two groups will be different.

2.4.3. Allosteric model

In the last decade, significant progress has been made in biophysics and thermodynamic characterization of TRPM8 channel (Brauchi et al., 2004; Voets et al., 2004; Hui et al., 2005; Matta and Ahern, 2007). Nevertheless, there is still controversy about which is the kinetic model that best explains this behavior. On the basis of results previously published, I postulate that the

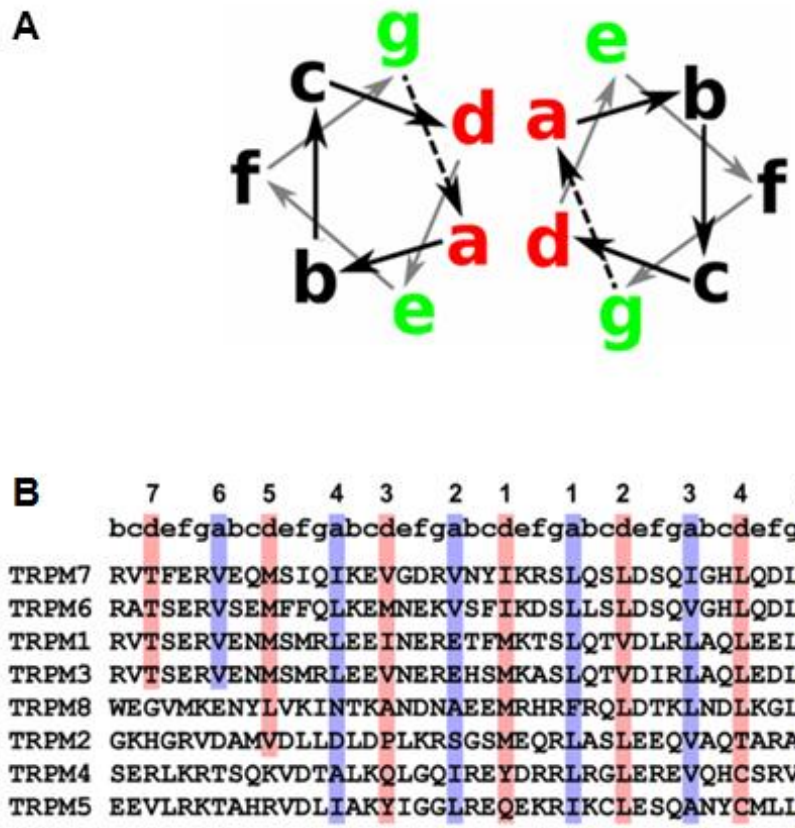

Figure 3: ***The coiled coil structure of the distal C terminus in TRPM channels*****. (A)** Helical wheel diagram of a parallel coiled coil showing the recognition motifs. Red residues represent hydrophobic interactions, while coulomb interactions are occurring between negatively and positively charged residues (green). **(B)** Sequence alignments of TRPM coiled coil domains. Heptad repeat pattern of amino acids ***a***bc***d***efg is shown on top of the coiled coil domains and hydrophobic amino acids ***d*** and ***a*** denoted by red and blue respectively. Asterisk in the sequence of TRPM8 shows the last amino acid in the carboxy terminal region. Image adapted of (Fujiwara and Minor, 2008).

model that could best explains the behavior of TRPM8 channels, is the allosteric model. For this reason, in this section, I briefly explain several characteristics of this kinetic model.

The term allosteric is quite popular in enzyme kinetics. The word was introduced as a combination of the Greek words *allos* and *stereós* to mean *other-form*. A classical usage in this sense is when a ligand binds to a regulatory site of an enzyme and alters the form of the protein resulting in a change in enzyme effectiveness. The regulatory site in the protein can be altogether different from the catalytic site where the chemistry takes place. The Dual-Allosteric Coupling Model is an adaptation of a model originally derived for large conductance Ca^{2+}-activated K^+ channels (Horrigan and Aldrich, 2002). On the basis of this model (scheme 1), with my working group, propose that TRPM8 channel gating involves voltage sensor activation, temperature sensor activation, channel opening, and some interaction among these three processes.

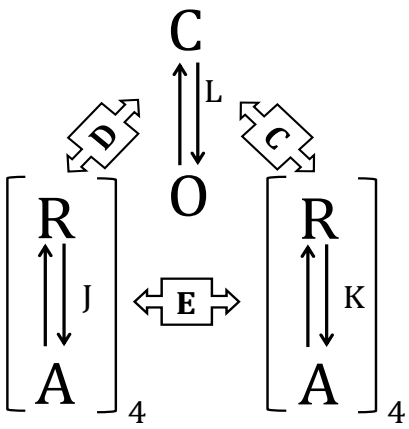

Scheme 1

Thus, the channel undergoes transitions between closed (*C*) and open states (*O*), with an equilibrium constant *L* between the closed and open states being the voltage and temperature sensors in resting. On the other hand, the sensors undergo transitions between resting (R) (R, Resting state, Scheme 1; we must take care not to confuse with the ideal gas constant, *R*) and activated (A) conformations, with equilibrium constants *J* and *K* for the voltage and temperature sensors, respectively. The interaction between sensors by allosteric factors is given by: *C*

coupling temperature sensors with channel gate and *D* coupling voltage sensors with channels opening. Finally, allosteric factor, *E*, establishes the interaction between the voltage and temperature sensors. Thus, when “n” voltage sensor are activated, *L* change to LD^n, when “n” temperature sensor are activated *L* change to LC^n and when both sensor are activated, *L* change to $LC^nD^nE^n$. The homotetrameric nature of TRPM8 allows us to assume that the channel has four voltage sensor and four temperature sensors, so that the channel has seventy possible states and the open probability for any temperature and membrane potential is given by Eq. 1 (see Annex 1)

$$P_o = \frac{1}{1+\frac{(1+J+K+KEJ)^4}{L(1+JD+KC+KCEJD)^4}} \qquad \textbf{Eq. 1}$$

According to the Equation 1 for the open probability of allosteric model, at any membrane potential, and temperature $J=J_0 \exp(z_J FV/RT)$ and $K=\exp(-((\Delta H-T\Delta S))/RT)$. J_0 is the value of equilibrium constant *J* at 0 mV, z_J is the voltage dependency for this constant, *V* is membrane potential, and T is absolute temperature. ΔS and ΔH represent the difference of entropy and enthalpy, respectively, *R* is the universal gas constant, and *F* is Faradays constant.

One of the key features that define the behavior of TRPM8 channel is that neither temperature nor voltage is strictly necessary for channel activation (Brauchi, 2004; Latorre et al., 2007; Matta and Ahern, 2007). Thus, at high temperatures, the channel is activated by large depolarization and when all voltage sensors are resting, the open probability of the channel can be increased by decreasing temperature. This and several other observations, including macroscopic and single channel kinetics (Brauchi, 2004; Matta and Ahern, 2007) led to the idea that both temperature and voltage increase the open probability by an allosteric mechanism. In this work, I present a detailed study of the temperature and voltage dependence of the TRPM8 channel to verify the ability of this model to explain the behavior of the channel. For this, I analyze the effect

of voltage and temperature on steady-state activation parameters and on the kinetics properties of TRPM8 channel, for which I evaluate the conductance versus voltage curves establishing the behavior of $V_{0.5}$ at different temperatures, the open probability versus voltage curves, the limiting slope and the deactivation time constant at very negative potential values and the transitions among closed states of channel before opening by Cole-Moore shift. On the other hand a series of deletions were constructed in the distal region of coiled-coil structure to determine which regions of the C-terminal are the molecular determinants of cold sensitivity of TRPM8. Thus, I demonstrate that gradual deletions of this region promoted a gradual decrease in the temperature sensitivity of TRPM8 channel, without greatly affecting the voltage dependence.

In summary, with these results it is established the importance of coiled-coil structure in the thermoregulation of channel and that the voltage and temperature sensors are localized in different structural domains, confirming that the TRPM8 channel behavior is explained by an allosteric mechanism.

3. MATERIALS AND METHODS

3.1. Composition of solutions

3.1.1. Oocytes Solution

3.1.1.1. Oocyte Ringer 2 Solution (OR-2)

–	NaCl	82.5	mM
–	KCl	2.5	mM
–	$MgCl_2$	1	mM
–	Na pyruvate	2.5	mM
–	HEPES	5	mM

Adjust with NaOH to pH 7.6

3.1.1.2. ND96 Solution

–	NaCl	96	mM
–	KCl	2	mM
–	$CaCl_2$	1.8	mM
–	$MgCl_2$	1	mM
–	HEPES	5	mM

supplemented with penicillin-streptomycin 10 U/ml.

Adjust with NaOH to pH 7.6

3.1.2. Solutions for electrophysiology

Bath and pipette solutions contained:

–	KMES	140	mM

- KCl 2 mM
- EGTA 5 mM
- HEPES 10 mM

Adjust with KOH to pH 7.5.

The reagents and antibiotic were purchased from Sigma-Aldrich Corp. (St. Louis, MO, USA).

3.2. Methods

3.2.1. Molecular Biology.

cDNAs coding for rat TRPM8 (provided by David Julius, University of California, San Francisco, CA; GenBank accession number NM_134371) was used. DNAs (wild type and truncations) were subcloned into pBSTA vector by using for restriction enzymes, *Not*I and *Kpn*I (New England Biolabs). The pBSTA vector contains a T7 promoter followed by 5′ noncoding β-globin sequences and a multiple cloning site for insertion of exogenous DNA. This site also allows the plasmid to be linearized before *in vitro* transcription. The pBSTA vector also contains a 3' noncoding β-globin sequences and a poly(A) tail (Shih et al., 1998). The addition of 5′ and 3′ noncoding sequences from the *β-globin* gene greatly increases the expression of exogenous proteins in oocytes (Krieg and Melton, 1984). TRPM8 DNA was used as starting point for the generation of every C-terminal truncations. The truncation: TRPM8CTΔ8, TRPM8CTΔ15, TRPM8CTΔ22, TRPM8CTΔ29, TRPM8CTΔ36 y TRPM8CTΔ40 were prepared by PCR-based mutagenesis (Pfu DNA polymerase; Stratagene). Primers were designed to give a product containing the complete cDNA sequence except for the deleted sequence. Sequences of forward primers were as follows: DEL 8, 5´CAG AAG ACC TTT GAG ATC ATT AAG C 3'; DEL15, 5´AAG CTT TGT GTC CAG TTG TCT GAA C 3´; DEL22 5´GAA CCG ATG CCT CAT CTC CTC TG 3´; DEL29 5´TGC GTT GTC GTT GGC CTT CGT G 3´; DEL36 5´GTT GAT CTT GAC AAG GTA ATT CTC C 3´; DEL40 5' GTA ATT CTC CTT CAT GAC GCC CTC C 3'. The same primer was used for all truncations: P3(M8)PBSTA 5´TAA TGG CGA CTA TGC AGG GAT CAA T 3´. The PCR products were purified by agarose gel electrophoresis, the linear plasmids were

dephosphorylated with bovine phosphatase alkaline (Promega Corp., Madison, WI USA) and ligated using T4 DNA ligase (Promega Corp., Madison, WI USA). Competent *Escherichia Coli* cells, DH5α, were transformed with the ligation products. cDNAs from preselected colonies were sequenced in the region of interest (Macrogen Inc. Seul, Corea). The cassettes containing the mutations were cut out using the restriction enzymes *Kpn*I and *Not*I and were subcloned in the vector pBSTA with the original TRPM8 DNA insert. The DNA was afterwards introduced into DH5α competent cells (Hanahan, 1985) and a glycerol stock was prepared from each transformant containing plasmid (75% cells + 15% glycerol) to have a constant supply. This stock was stored at -80 °C.

3.2.2. *In vitro* transcription.

One µg of cDNA was placed in a standard *in vitro* transcription reaction using a T7 mMessage mMachine Kit (Ambion, Austin, TX). The reaction was carried out at 37°C for 2–4 h, followed by the addition of DNase I and incubation for 15 min. Ammonium acetate was added, and RNA was isolated by phenol/chloroform extraction and isopropanol precipitation. After centrifugation, the RNA pellet was resuspended in RNase-free water, and LiCl precipitated to remove residual unincorporated nucleotides. The pelleted RNA was resuspended in RNase-free water, and the quantity and purity were determined by measuring the absorbance at 260 nm. The integrity and size range of total RNA purified was checked by denaturing agarose gel electrophoresis (0.7%) and ethidium bromide staining.

3.2.3. Oocyte Isolation and Injection.

African clawed frogs, *Xenopus laevis,* not bred in captivity (from Santiago de Chile), were anesthetized by submersion in fresh 0.1–0.2% tricaine (3-aminobenzoic acid ethyl ester methanesulfonate) (Sigma, St. Louis, MO) for 5 min and then packed in ice to cause hypothermia (20 min in ice-cold water). One or two ovarian lobes were removed through an abdominal incision, cut into small portions and placed into OR2 solution. Then, the incision was

sutured and the frog was returned to water. The procedures performed comply with the standards required by both Universidad de Valparaíso and Comisión Nacional de Investigación Científica y Tecnológica (CONICYT). Oocytes were prepared as described (Dascal, 1987), and mature stage VI oocytes were injected with 50 nl of TRPM8 mRNA (0.05 ng/nl), TRPM8 mutants mRNA (0.05 µg/µl - 0.5 µg/µl) and/or sterile water for control oocytes, by using a micropipette attached to a hydraulic microinjector (Nanoject, Drummond Scientific, Broomall, PA). Glass micropipettes with a tip diameter of 10–30 µm were pulled in a horizontal pipette puller (Sutter Instruments). Injected oocytes were kept at 18°C for 2-5 days in ND96 medium after RNA injection, which ensured 90% survival. Before of each washing, the damaged oocytes were separated from intact oocytes.

3.3. Electrophysiology

Two to five days after mRNA injection and after the manual removal of the vitelline membrane, currents elicited by the wild type and the different mutant TRPM8 channels were recorded using the patch clamp technique on the cell attached configuration (Hamill et al., 1981) using an Axopatch 200B amplifier (Axon Instruments, Foster City, Calif). Patch pipettes were pulled in a horizontal pipette puller (Sutter Instruments) from glass capillaries of borosilicate (World Precision Instruments, Sarasota, Fl, USA) and to promote high-resistance seal formation, electrodes were fire-polished by positioning the electrode tip close to a heating filament under a microscope. Gigaseals were formed using pipettes with 1-2 MΩ resistances. Those mutants which yielded a low expression level were recorded in cell-attached macropatches of oocyte membrane (pipette resistance, 0.4-1 MΩ and tip diameter, 2-3 µm) (Stuhmer et al., 1987). The procedure for preparing the pipettes for macropatches was essentially the one described above. The macroscopic current was filtered with an 8-pole low pass Bessel filter (900C9L8L, Frequency Devices, Haverhill, MA USA) at 20 or 40 kHz and digitized at a rate of 200 kHz by a NI-PCI-6014 Card (National Instruments). The set up consisted of: an electrophysiological recording chamber constructed in our laboratory with a cavity of approximately 2 ml volume. The

chamber was constructed of aluminum and its surface was glossy. It was placed over the anti-vibration table and under a binocular microscope (PZM, WPI, Sarasota, FL USA). The visualization of the oocyte in the recording chamber was facilitated by an epi-illumination optical system for which was used a LED light connected to the computer's USB port. The position and displacement of the pipette was controlled by micromanipulator (model MX-2, Narishige, Tokyo). Primary data analysis was performed with Analysis Application program (Starace and Bezanilla, 2004) kindly provided by Dr. F. Bezanilla (University of Chicago, USA) and Clampfit 9 (Axon Instruments) software (Brauchi et al., 2007).

3.3.1. Macroscopic Current Analysis

For macroscopic current relaxation experiments, the membrane was held at -90 mV. Each experimental episode consisted on an epoch at the holding potential, followed by a depolarization to different test voltages and ending with an epoch at +100 mV. The duration of each episode was variable due to the need to finding the steady state current at each voltage, for this reason, when the voltage was increased the duration of episode was diminished. The voltage protocol used for all experiments was: voltage steps from -160 to 300 or 500 mV in 10 or 20 mV increments separated by intervals of 2 seconds. The amplitude of tail current (I_{tail}) was determined by fitting of each *trace* of the current obtained at +100 mV with a double exponential function and extrapolating to the time zero. The I_{tail} obtained for each temperature was normalized to I_{tail} maximum and subsequently was plotted as a function of voltage and fitted to a Boltzmann relation of the form:

$$\frac{I_{tail}}{I_{tail}^{max}} = \left[1 + e^{\frac{\left(-z_{eq}F(V-V_{0.5})\right)}{RT}}\right]^{-1} \qquad \textbf{Eq. 2}$$

where $V_{0.5}$ is the voltage at which the open probability is 1/2, z_{eq} is the valence of the charge associated with the closed to open transitions, *R* is the universal gas constant, *T* is the absolute temperature and *F* is the Faraday constant (coulomb/mol).

3.3.2. Cole-Moore shift Analysis

The initial lag of the ionic currents reflects the early transitions of the activation pathway. A large hyperpolarizing prepulse will populate of closed states further removed from the open state, which results in a longer lag in the activation. So, under this principle, I applied the classical Cole-Moore protocol (Cole and Moore, 1960). The cell membrane was hyperpolarized to various potentials (since -200 mV to -40 mV) for 100 ms and immediately thereafter, the current record was tested with a short depolarizing pulse to 260 mV. The shift (in the axis of time, ms) between each trace was evaluated fitting each curve to the following equation:

$$I(t) = I_{max}\left[1 - e^{\left(\frac{-(t-d)}{\tau}\right)}\right] \quad (for\ t\ > 3d) \qquad \textbf{Eq. 3}$$

where I_{max} is the maximum current obtained in the experiment, *t* is time (ms), *d* is the delay (ms) and τ is the activation constant. This procedure was repeated at different temperatures.

3.3.3. Non-stationary noise analysis

The maximum probability of opening for the wild type TRPM8 and mutants channel was determined using non-stationary fluctuation analysis (Alvarez et al., 2002). This type of analysis is used to relate macroscopically observable parameters, such as the total ionic current with microscopic parameters like the single-channel current *i*, the number of functional channels in the patch of membrane *N*, and the probability that the channels are open under a given condition, P_o. Thus, for our purposes, the analysis was performed at various temperatures, for

each of which, 200 individual current traces were taken during consecutive depolarizing pulses, with duration of 20-30 ms preceded for another of -100 mV. The average current <*I*> and variance, σ^2, in each isochrone, were analyzed with Analysis Application program (Starace and Bezanilla, 2004). For a population channels, the mean, $I(t)$, and the current variance, $\sigma_I(t)^2$, are given by

$$I(t) = NiPo(t) \qquad \textbf{Eq. 4}$$

$$\sigma_I(t)^2 = Ni^2Po(t)[1 - Po(t)] \qquad \textbf{Eq. 5}$$

Combining Equations 4 and 5 gives the following expression

$$\sigma^2 = i\langle I\rangle - \frac{\langle I\rangle^2}{N} \qquad \textbf{Eq. 6}$$

where *i* is the unitary current and *N* is the number of channels in the patch. The maximum open probability, P_O^{max}, was obtained according to the relation:

$$P_o^{max} = \frac{I_{max}}{iN} \qquad \textbf{Eq. 7}$$

where I_{max} is the maximum average current measured.

3.3.4. Time Constants Calculation

The time constant of activation (τ_{act}) was determined from a fit of current traces with the eq. 3. The deactivation kinetics were measured by holding the membrane potential at 260 mV for 50

ms to open all of the channels and then stepping to a series of potentials (from −260 to +200 mV). The time constant of deactivation was fitted with a bi exponential function of the form:

$$I(t) = A_1 e^{(-t/\tau_1)} + A_2 e^{(-t/\tau_2)} + C \qquad \textbf{Eq. 8}$$

where $I(t)$ is the current amplitude at any given time t, A_1 and A_2 are the estimated fast and slow intercepts of the components at time zero, τ_1 and τ_2 are the fast and slow time constants of current decay, respectively, and C is the baseline current.

3.3.5. Single Channel Analysis

Single channel events were recorded from cell-attached patches that containing hundreds of channels at voltages where open probability is low ($< 10^{-3}$). Currents were typically filtered at 20 kHz, and were sampled at 50–100 kHz. On a computer screen, two cursor lines were manually set to the displayed single-channel current levels. Thus, the single channel data were then idealized by use of a 50% amplitude criterion (Colquhoun, 1995). The *NPo* was calculated from the sum of open times for each sweep divided by sweep duration. The *Po* was automatically calculated based on the number of channels that were measured by noise analysis (section 3.3.3)

3.3.6. Limiting Slope Analysis

In voltage-dependent channels, the method known as limiting slope introduced by Almers (Almers, 1978), provides the relationship of charge movement and voltage sensitivity, giving the number of effective gating charges coupled to the channel opening. This method, is used for any kinetic model (Sigg and Bezanilla, 1997). For the case of allosteric model, the opening of the channel has an intrinsic voltage dependence (zL) unrelated to the movement of the voltage sensors (zJ). Thus, for the application of this method, the Gigaseals ($> 1G\Omega$) were subjected to

three different and sequential voltage protocols:

- For macroscopic currents, the voltage dependence of the tail current was estimated from voltage steps from -160 to 300 mV in 10 or 20 mV increments separated by intervals of 2 seconds.

- Estimation of the number of channels in a patch of membrane was done by nonstationary noise analysis using the pulse protocol indicated in the section 3.3.3.

- Finally, single-channel experiments were performed keeping the fixed potential by 30 to 90 s, using potential between -40 to -200 mV. More details in the section 3.3.5.

3.3.7. Temperature Control

The recording chamber, made in our laboratory, consisted of a glazed aluminum block which was located above a heating-cooling (Peltier) element. A heat sink made of bronze, was located under the peltier and cooled by water circulation. The temperature feedback signal was obtained by using a miniature thermistor located in the recording chamber allowing me to measure the temperature of the bath. Immediately, it is compared with the desired temperature so that the temperature controller (proportional integral differential) fabricated by Dr. Osvaldo Álvarez (Universidad de Chile, Chile), delivers or removes heat to the system. The control system was built around a digital platform Arduino (www.arduino.cc).

3.4. Determination of thermodynamic parameters

3.4.1. Arrhenius

In the two-state model, the ion channels can undergo conformational transitions between nonconducting (closed state) and ion-conducting states (open state) (Scheme 2)

$$C \underset{}{\overset{K}{\rightleftharpoons}} O$$

Scheme 2

$K = {}^{O}/_{C}$, is the equilibrium constant of the process, where *O* is the number of open channels and *C* is the number of closed channels, respectively. However, when the channel traverses this pathway their structure is neither closed nor opens. This leads to the picture of an energy barrier of height $E^{\ddagger}$ separating both states (Figure 4). Thus, the rate of going over this barrier can be estimated from:

$$k = Ae^{-E^{\ddagger}/RT} \qquad \textbf{Eq. 9}$$

Where *k* is a rate constant at the absolute temperature *T*, *R* is the gas constant, *A* is a constant called Arrhenius frequency factor, that includes the probability of the state change taking place, while that $E^{\ddagger}$, activation energy, is the energy barrier that the molecules must overcome to react and trigger, for example, the channel opening. In transition state theory, *A* depends on the activation entropy and $E^{\ddagger}$ is the activation enthalpy. Then, taking the natural logarithm to both sides of equation 9, leads to

$$lnk = lnA - E^{\ddagger}/RT \qquad \textbf{Eq. 10}$$

To estimate $E^{\ddagger}$ from kinetic data, the ln of the rate of the activation or deactivation time constants versus 1/*T,* was plotted. Then, the activation energy, $E^{\ddagger}$, was calculated directly from the slope of the Arrhenius plots (slope=- $E^{\ddagger}/R$).

The Q_{10} is used to estimate the temperature dependence of a rate constant or of a system, measuring the activity at two different temperatures separated by 10 ºC. The Q_{10} can be related to the activation energy by the following approximate expression

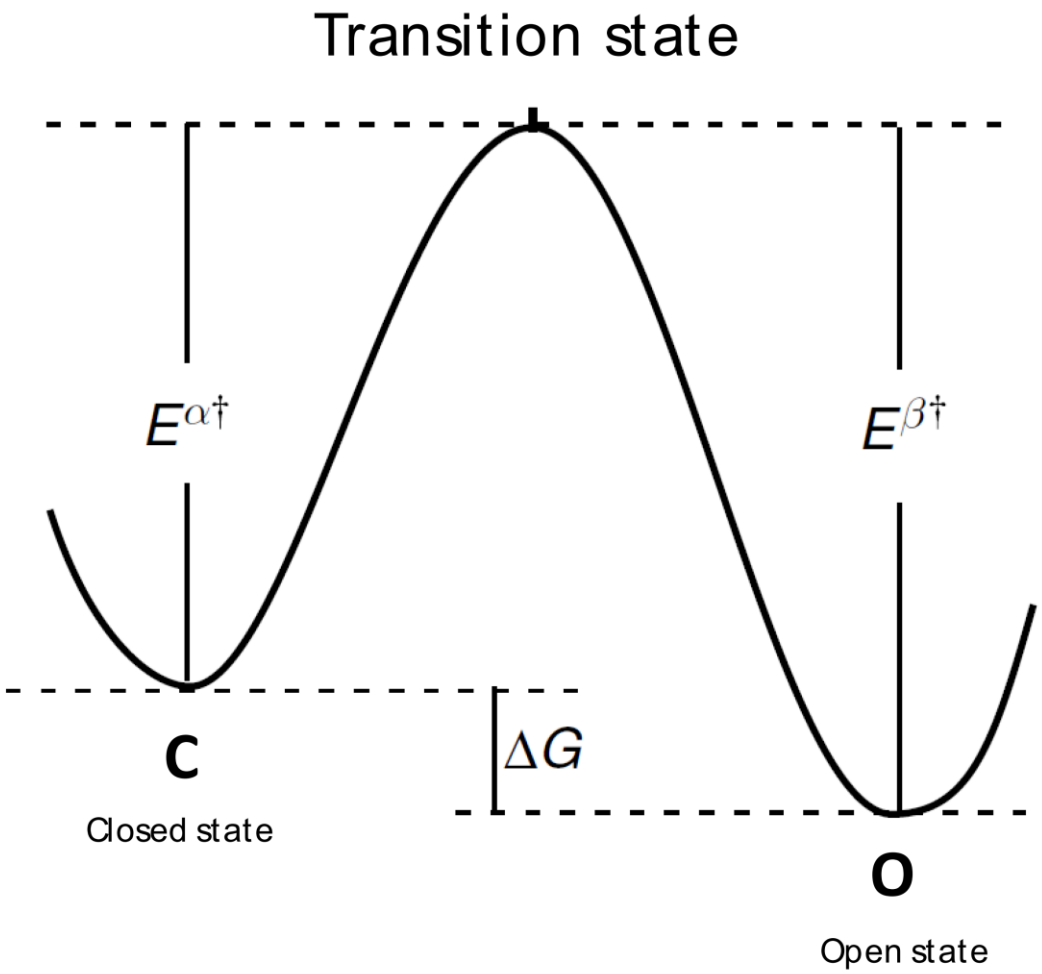

Figure 4: ***The channel opening reaction requires overcoming the activation energy barrier*****.** Plot of the free energy along the reaction coordinate. The wells at C and O correspond to the energies of the closed and open state, respectively and the peak corresponds to the free energy of the transition state.

$$E^{\ddagger} = \frac{RT^2 \ln(Q_{10})}{10}$$ **Eq. 11**

Thus, at typical physiological temperatures, a Q_{10} of 2 gives $E^{\ddagger} \approx 12$ kcal mole^{-1}. Other form to obtain Q_{10}, is using the following equation:

$$Q_{10} = \left(\frac{I_2}{I_1}\right)^{10/(T_2 - T_1)}$$ **Eq. 12**

where I_1 and I_2 are the measured currents at temperatures T_1 and T_2, respectively.

It is noteworthy that a typical voltage gated ion channels have a Q_{10} value between 2 and 4, which can be interpreted as two to four times greater rate of ion flow through the ion channels when temperature increases 10 °C, at a specific voltage (Equation 12). Heat-activated TRP channels have Q_{10} values between 6 and 30, which is well above a typical ion channel. However, in TRPM8 the situation is different, ionic currents decrease when temperature increases, a fact that, in theory, corresponds to Q_{10} values <1. Until now, there is not clarity on how to express the Q_{10} in cold-sensitive channels. For this reason, Voets comments as follows: “As an admittedly arbitrary criterion I propose that a TRP channel must exhibit a minimal Q_{10} value of ≥ 5 (or ≤ 0.2, in case of a cold activated channel)” (Voets, 2012). Thus, in this thesis work, I will use the criterion proposed by Voets to refer to Q_{10}.

3.4.2. Van´t Hoff

Even though the two-state model (Scheme 2) (Voets, 2007) represents an oversimplification of the functioning of the channel, it is the simplest scheme to describe the effects of temperature on TRPM8 channel opening, for this reason for measure their thermodynamic parameters we consider that the open probability is determined by

$$P_o = \frac{O}{O+C} = \frac{1}{1+\frac{1}{K_{eq}}}$$ **Eq. 13**

So, to obtain the open probability, the I_{tail} was measured at different voltages. Additionally, to obtain the actual open probability a noise analysis using a voltage pulse of 260 mV was performed. In this way, it was possible to normalize the tail current-voltage curves, yielding *Po*-V curves at different temperatures. The *Po* measure at 60 mV was used for obtain the *Keq*.

The difference in the standard Gibbs free energy change (ΔG^0) between closed state and open state is given by:

$$\Delta G^0 = -RTlnK_{eq}$$ **Eq. 14**

Furthermore, considering that:

$$\Delta G = \Delta H - T\Delta S$$ **Eq. 15**

Then,

$$lnK_{eq} = \frac{-\Delta H^0}{RT} - \frac{\Delta S^0}{R}$$ **Eq. 16**

This relation corresponds to the Van't Hoff equation, which provides an important way to interpret the temperature dependence of equilibrium between two states. Assuming that ΔH^0 and ΔS^0 are temperature-independent, the slope of the line is equal to ΔH^0 and the intercept is equal to ΔS^0. This procedure was performed between 10 and 30 °C.

3.5. Molecular modeling.

The molecular model to coiled-coil of TRPM8, was constructed using the structure of C-terminus of coiled-coil of TRPM7 (Protein Data Bank (PDB) accession number: 3E7K, X-Ray Diffraction

with resolution of 2.01 Å) as template. The 3D model of the TRPM8 coiled-coil was generated through the MODELLER program (Marti-Renom et al., 2000; Eswar et al., 2006). MODELLER is used for homology or comparative modeling of protein three-dimensional structures for which, the user provides an alignment of a sequence to be modeled with known related structures and MODELLER automatically calculates a model. For construction of coiled-coil of TRPM8, were considered their four respective chains (ABCD) and spatial orientation. The NAMD energy plug-in for VMD (Humphrey et al., 1996) was used to calculate Coulomb and van der Waals interaction energies which provides both a graphical user interface and text commands for evaluating energies using NAMD. The average energies obtained for each of the frames and the sum of such averages give an approximation of the enthalpy of the system. For the calculation, we used a model of TRPM8 channel embedded in a physiological environment, considering each of the coiled coil heptad channel (homotetramer). This energy was obtained from a trajectory of 10 ns Molecular Dynamics.

4. RESULTS

4.1. Effects of Temperature on Ionic Currents

To determine the temperature sensitivity of TRPM8 channels, I exposed TRPM8 channels to temperature from 35 °C to 10 °C in steps of 1 °C. Macroscopic currents were recorded using the patch clamp technique in its cell-attached configuration (Figure 5). Figure 5A shows a family of macroscopic current records obtained from the same patch at different temperatures but at same voltage, 150 mV. Each trace of ionic current is shown in a different color, where red colors represent high temperatures (e.g., 35 °C) and blue colors represent low temperatures. A robust increase in ionic currents when the temperature decreases, was observed. Figure 5B shows a temperature versus current plot. The steady-state current, was obtained at the end of the pulse voltage of 150 mV (t = 80 ms). On lowering the temperature, TRPM8 channel opening becomes appreciable at 27°C, and reaches a plateau at about 15°C, temperature range in which the current increases 25-fold. Importantly, these data are consistent with previously published results obtained using HEK-293 cells (Brauchi et al., 2004), which supports the use of oocytes as an expression system TRPM8.

4.2. *Itail* versus voltage curve of TRPM8 is shifted by temperature.

Figure 6A shows a representative family of macroscopic currents at 15 °C, 20 °C, 25 °C and 30 °C obtained from the same cell-attached patch in response to the voltage protocol shown at the top of the figure. It is clear that the current magnitude increases when the temperature is decreased. Tail currents measured at 100 mV are shown at the right on an expanded time scale.

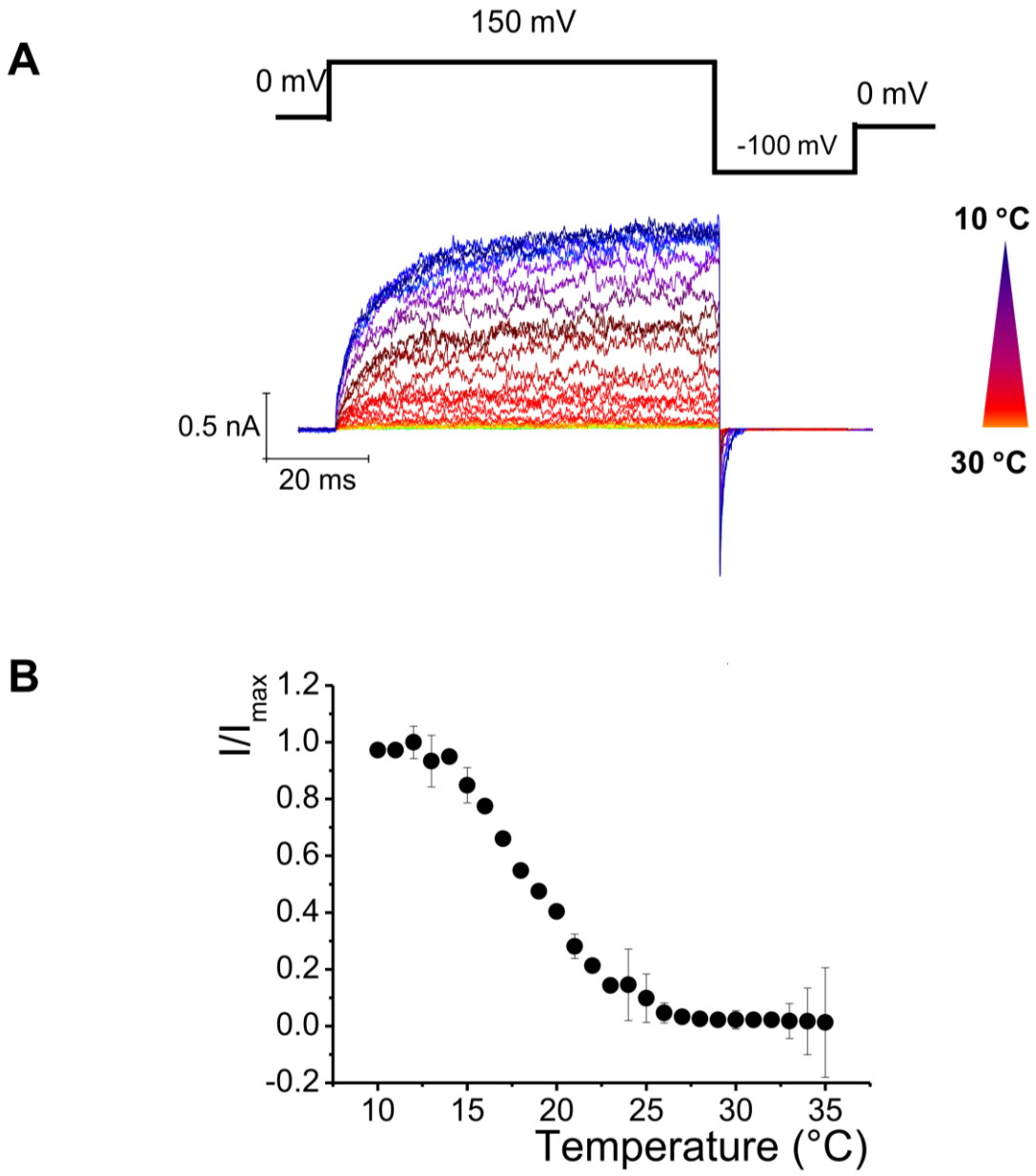

Figure 5: ***Analysis of temperature dependence of TRPM8 in oocytes of Xenopus laevis***. **(A)** Current records taken at 150 mV and at different temperature (35 °C to 10 °C). Each trace of ionic current is shown in a different color, where red colors represent high temperatures (e.g., 35 °C) and blue colors represent low temperatures (e.g., 10 °C). **(B)** Temperature versus relative current plot. The current was normalized by the maximum current obtained in each experiment (n=5).

Here, I can note that when the temperature increases, the deactivation kinetics of tail current become very fast, but activation kinetics does not change that much. I conclude that the channel close at high temperature because the deactivation rate increases more than the activation rate upon increasing temperature. Tail current amplitude was determined by fitting tail currents to exponential functions and extrapolating at time zero after the voltage step. Instantaneous tail currents were plotted against voltage and normalized to the maximal tail current ($Itail_{max}$) obtained at 15 °C (figure 6B). This plot shows that the *Itail* versus voltage curve of TRPM8 is shifted leftward along the voltage axis when the temperature changes from 30 to 15 °C. All these results are in agreement with previously published results (Brauchi, 2004; Nilius et al., 2005a; Latorre et al., 2007).

4.3. $V_{0.5}$ tends to the two asymptotes at high and low temperatures.

One of the allosteric model predictions indicates that the voltage for Po = 0.5, $V_{0.5\ \text{tends}}$, shows two asymptotic values: one at high temperatures (with all temperature sensors in resting conformation) and another at low temperatures (with all temperature sensors in activated conformation). To determine the effect of temperature on the $V_{0.5}$, I measured tail currents over a wider range of temperatures, 8 °C to 30 °C, using small temperature intervals of 2 °C. Instantaneous tail currents were normalized to the maximum values obtained for each temperature (Figure 7A) and plotted versus voltage. Tail current-voltage data were fitted using a Boltzmann function (Eq. 2). The parameters obtained are shown in Table 3. Figure 7B shows that at temperatures below 15 °C, $V_{0.5}$ remains constant, increases linearly in the 15 to 25 °C range and remains constant at higher temperatures, confirming the prediction of the model. Meanwhile, the voltage dependence of the TRPM8 channel increases in the 10 °C – 20 °C range and then decreases when the temperature is increased in the 20 ºC - 30 ºC (Figure 7C).

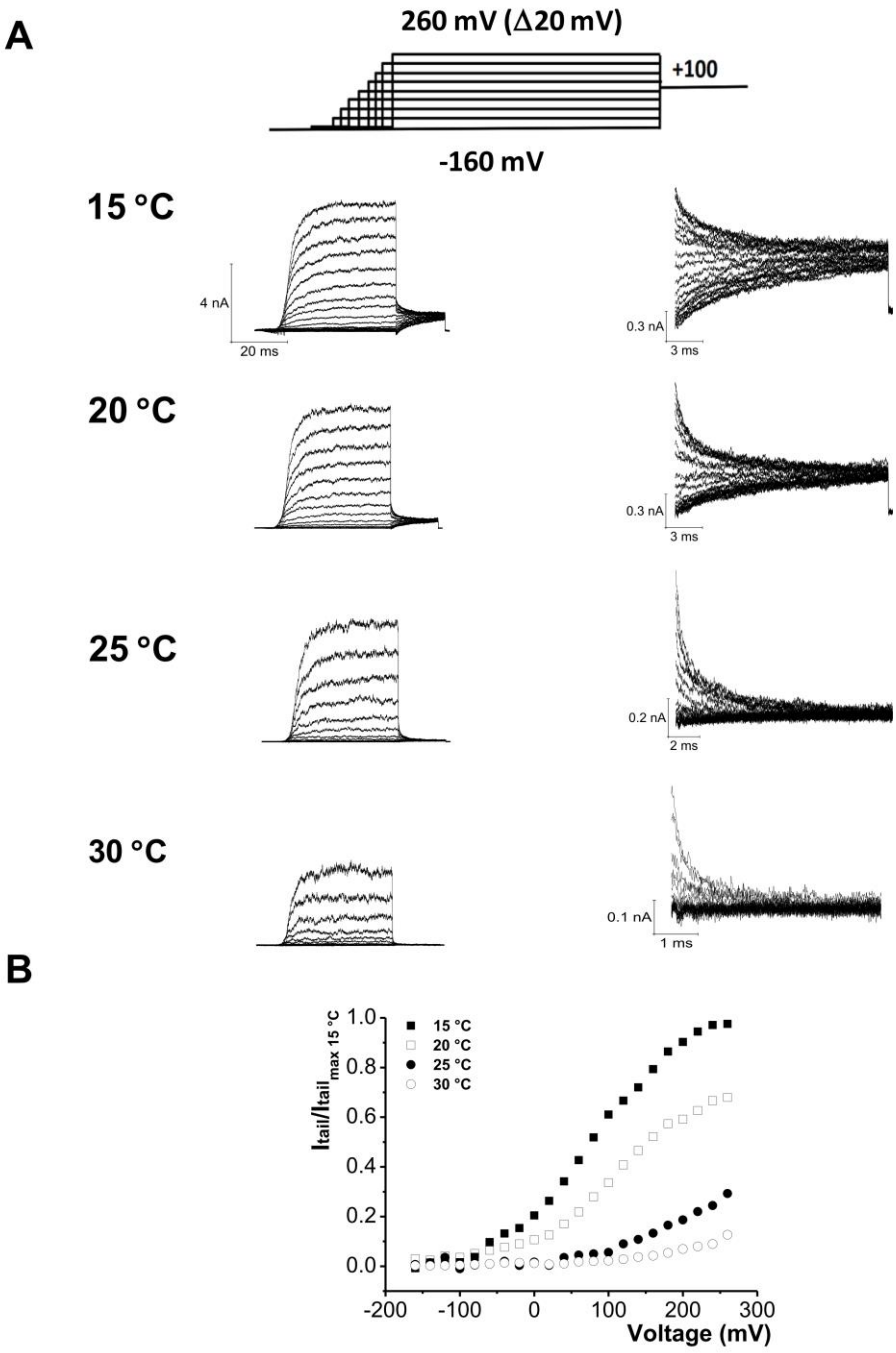

Figure 6: ***Voltage-dependency of TRPM8 channels***. **(A)** Macroscopic currents of TRPM8 at 15, 20, 25 and 30 °C. On the right, shows the tail current measured at 100 mV for each temperature, on an expanded time scale. **(B)** *Itail/Itail*$_{max\ 15\ ^{\circ}C}$ versus Voltage curves for channels at different temperatures. The *Itail* and Voltage relationships were normalized by maximal current obtained at 15 °C.

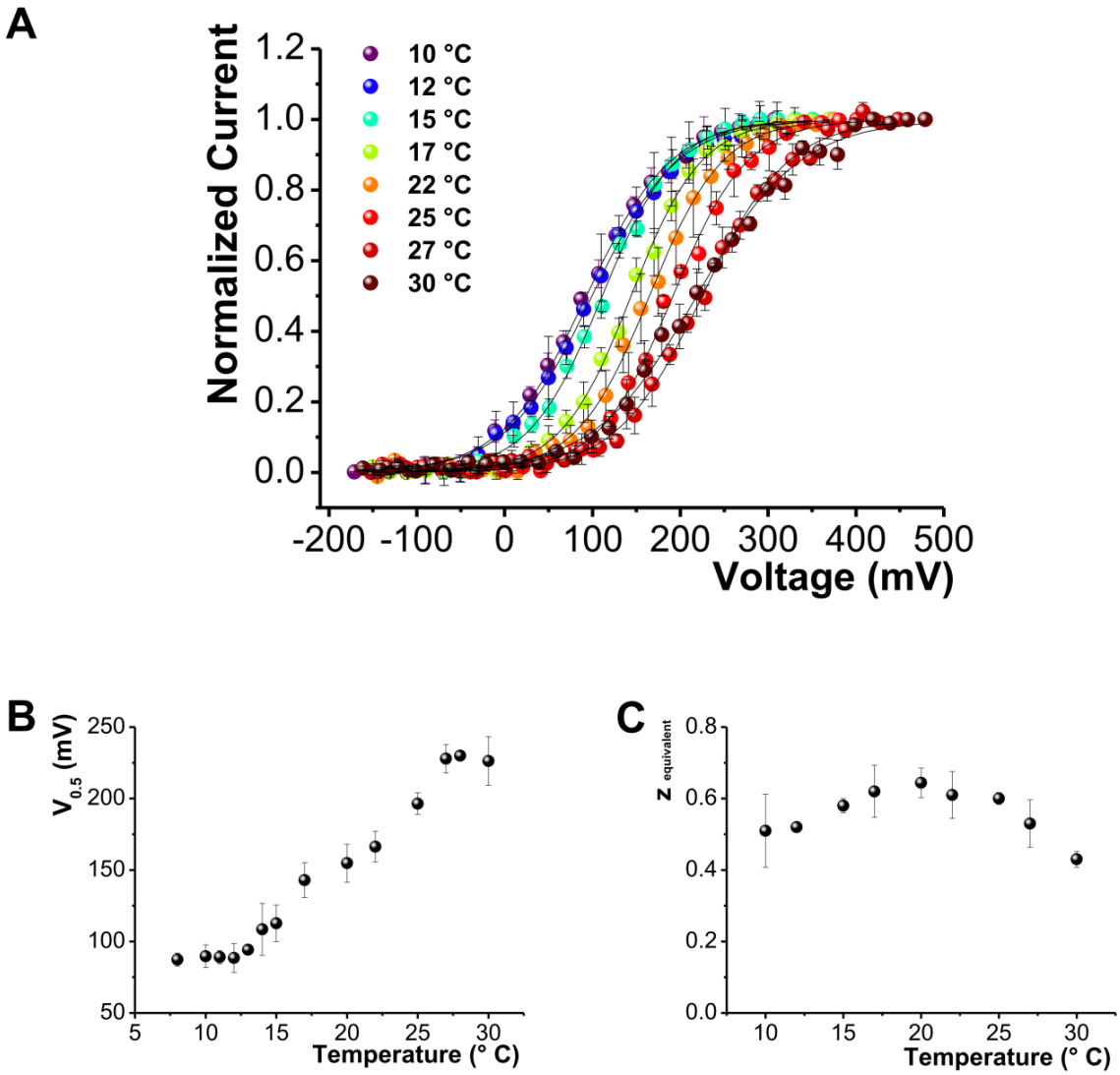

Figure 7. ***Effect of temperature on the behavior of $V_{0.5}$.*** **(A)** Tail current-voltage curves at different temperatures were normalized by maximal tail current at each different temperature. The solid lines indicate Boltzmann fits (Eq.2) to the experimental data. **(B)** $V_{0.5}$ as a function of temperature. Values of $V_{0.5}$ were obtained from the Boltzmann fits to the data shown in (A). Note that the relationship between $V_{0.5}$ and temperature is not linear and $V_{0.5}$ saturates at high and low temperatures. The current were obtained from *Itail* at 100 mV. **(C)** Average of the obtained z values plotted against Temperatures. Error bars are SD, n=4–7.

TABLE3

Parameters of the Boltzmann function estimated to Tail current-voltage curves at different temperatures normalized by maximal tail current at each different temperature.

Temperature (°C)	z	*Vm* (mV)
10	0.52	92
12	0.52	98
15	0.58	112
17	0.62	137
22	0.61	164
25	0.60	186
27	0.51	227
30	0.44	220

- The fit was done minimizing the relative distances squared to give a better fit of the lower open probabilities.

4.4. Voltage acts as a partial activator of TRPM8 channel.

Although all *Itail* versus Voltage curves reaches a plateau (Figure 7A), the absolute open probability at which they saturate at each temperature is unknown. In order to obtain the actual maximum open probability, we perform non-stationary noise analysis (Sigworth, 1980) at 260 mV. Figure 8, shows two representative recordings of noise analysis measured in the same patch at 10 °C and 30 °C. Figure 8A show the superimposed time course of the current on 200 repetitions. The variance is plotted as a function of the mean current for each isochrone (Figure 8 B) where the fitting with a parabola (Eq. 6, red line) gives a unitary current of 20 pA at 10 °C (average unitary channel current of 19 ± 0.04, n=8) and of 30 pA at 30 °C (average unitary channel current of 30 ± 0.2, n=7). Maximum open probability at 260 mV, $Po^{max,\ 260\ mV}$, (obtained according to the Eq. 7) at 10 °C was 0.91 (0.89 ± 0.06, n=8) and at 30 °C it was 0.41 (0.45 ± 0.03, n=7). $Po^{max,\ 260\ mV}$ obtained using noise analysis at 260 mV for each temperature were used to re-normalize the tail currents, which became expressed now as absolute open channel probability, *Po* (*V,T*) curves. *Po* versus Voltage curves are shown in Figure 8C, which notes that the voltage acts as a partial agonist because it is not able to activate fully the channel. Thus, as shown in Figure 8D, Po^{max} is less than 1.0, remains constant at temperatures lower than 15 °C and it is lower to the extent that the temperature increases.

4.5. Analysis of z_L in TRPM8 at very negative potential

Figure 9 A shows macroscopic currents at 20 °C, evoked in response to a voltage protocol between -160 mV at 300 mV. The conductance was determined from tail current amplitudes as described in the Materials and Methods section (3.3.1) and plotted against voltage (Figure 9 B) which gives a $V_{0.5}$ of 146 mV. Then, to obtain an absolute measure of the *Po*, the probabilities obtained using noise analysis at 260 mV for each temperature (Figures 9 C-D) were used to re-normalize the curves of tail currents. The time course of the current is represented in Figure 9 C, in which the currents measured during 200 repeat experiments are superimposed. The variance

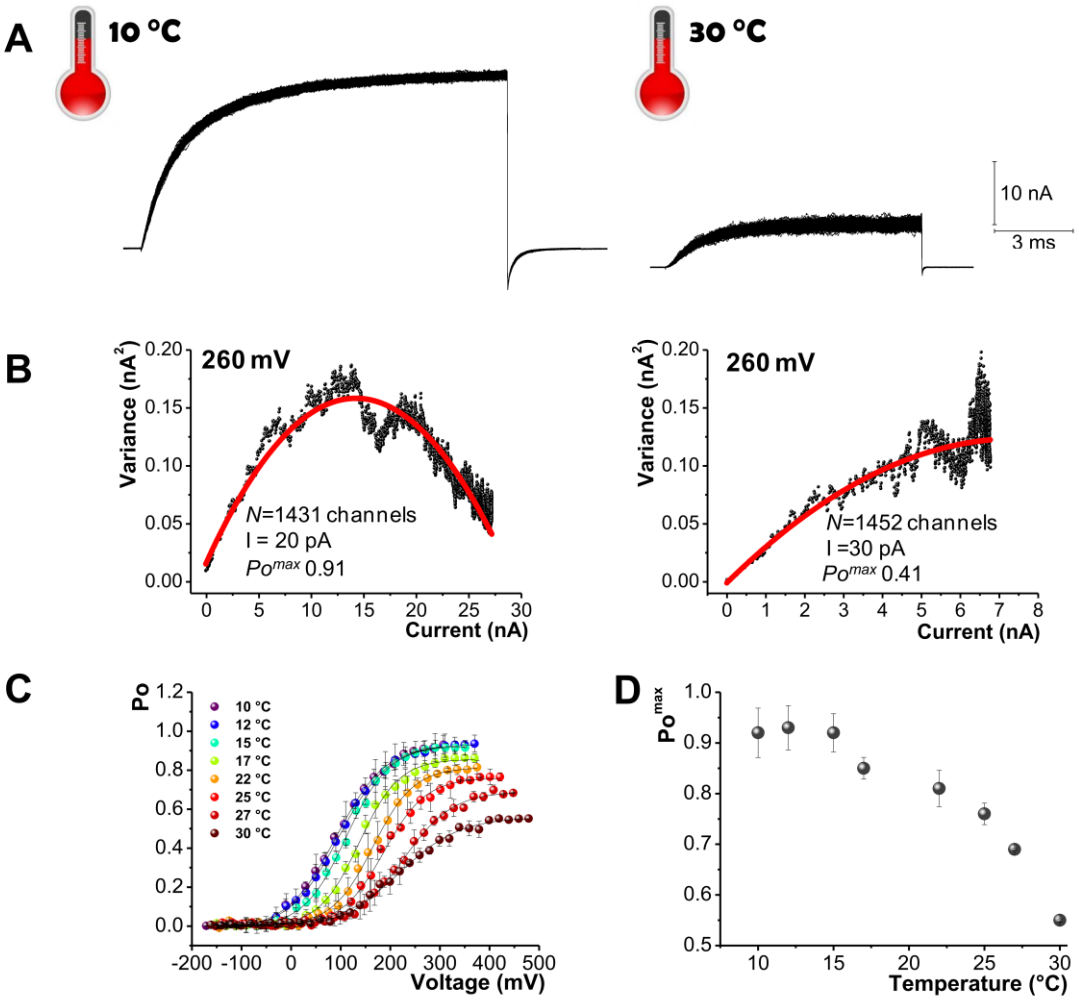

Figure 8. ***Effect of temperature on the open probability on TRPM8.*** **(A)** Superimposed current records of 200 sweeps recorded at 10 °C and 30 °C. **(B)** Variance versus mean current Plot. The red line represents a fit to the data using Equation 6. **(C)** *Po* versus voltage curve, performed at different temperatures. Each curve corresponds to the tail current-voltage curves shown in Figure 7A so that, the probabilities obtained using noise analysis at 260 mV for each temperature are used to re-normalize the curves of tail currents, obtaining the $Po(V,T)$. **(D)** Po^{max} versus temperature curve. Po^{max} were obtained from the values of the maximum probability of opening for each temperature, shown in Figure 8C. Error bars are SD, n=8.

is plotted as a function of the mean current for each isochrone in Figure 9 D, and fitted with de Eq. 6. This fit, gives the number of channels present in the patch and the unitary current that in this case are 1564 and 23 pA, respectively. In addition, I obtained a *Po* of 0.84, to the voltage and the temperature indicated used the Eq. 7 (Figure 9 E). Thus, the data (from 40 mV to 300 mV) of *Po* were plotted on a semi logarithmic scale and fitted with the Boltzmann function (eq. 2, solid line). The maximum voltage dependence of *Po* versus Voltage is indicated by the maximum slope (dashed line) which gives a value approximate for *z* of 0.65 (Figure 9 F). This slope is related to the voltage sensor–associated activation of the channels. However, while this slope does indicate the maximum voltage dependence of the TRPM8, it may not represent the limiting voltage dependence of channel.

In an allosteric model the closed to open transition of the channel may have an intrinsic voltage dependence unrelated to the movement of the voltage sensors. Thus, the open channel probability versus Voltage, reaches the limiting slope at very hyperpolarizing membrane voltage where voltage sensors are in the resting state whereby, the open probability is very low, reflecting the voltage dependence of just the closed-to-open conformational change (Horrigan and Aldrich, 1999, 2002). Our experimental approach was to measure *Po* under conditions that reduce the number of occupied states and thereby constrain a number of gating parameters. Thus, I measured *Po-V* relations at very negative voltages where voltage sensors are in the resting state (*J*=0) (Scheme 3A). This effectively reduces the number of occupied states to 10 (Scheme 3B). Scheme 3B predicts that when the voltage sensor is in resting conformation (smoothed zone in scheme 3A), the C-O transition (solid arrow) is governed by the equilibrium constant *L,* which is coupled to the equilibrium constant *K* by the allosteric factor *C*.

A

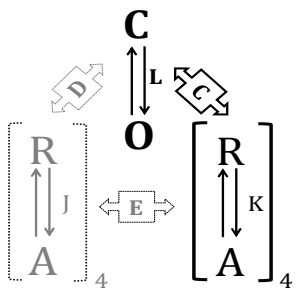

B

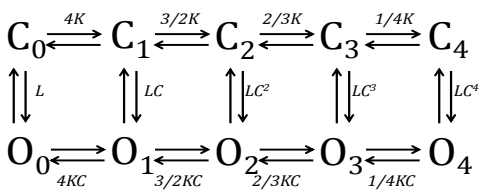

Scheme3

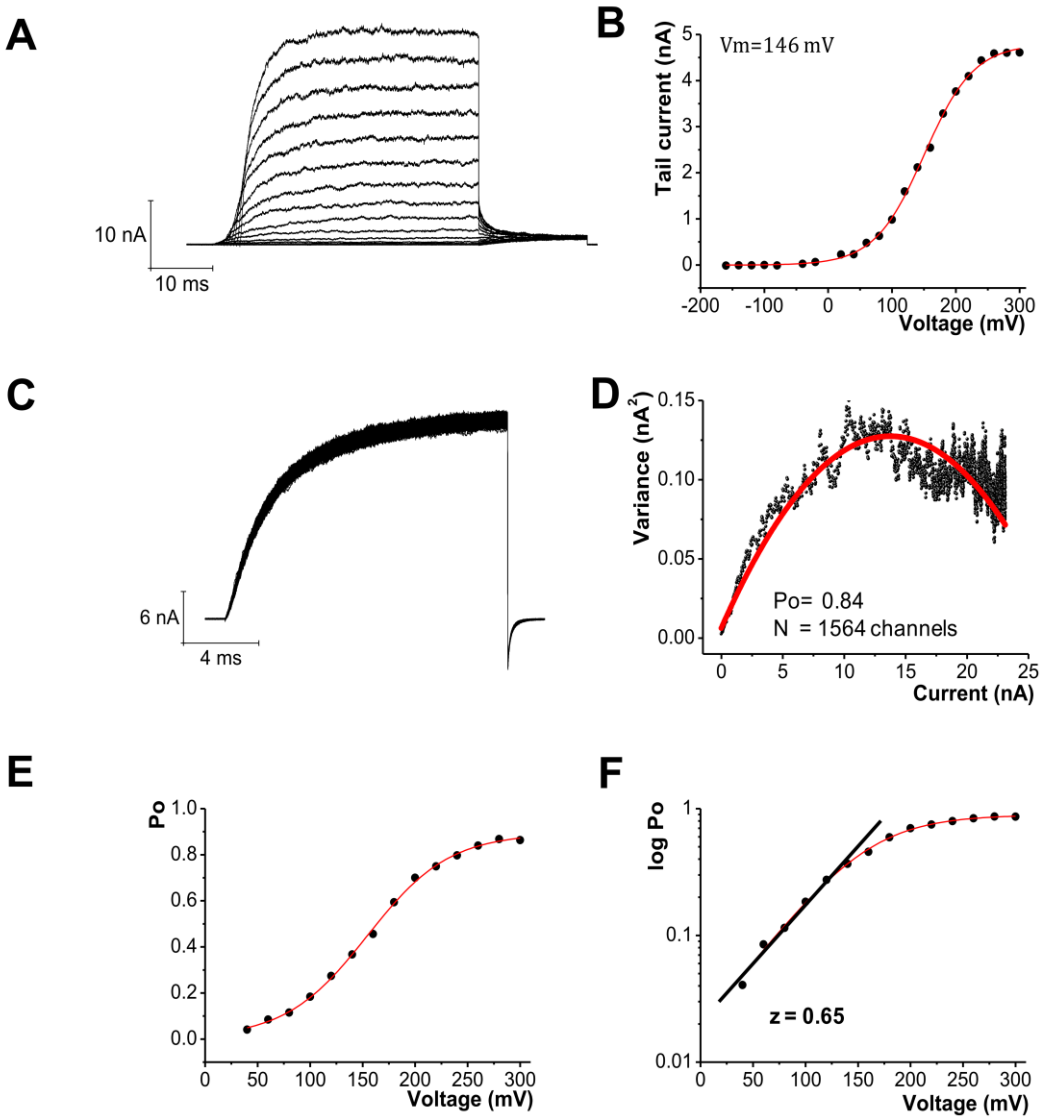

Figure 9. ***Steady state activation on TRPM8.*** **(A)** A family of current evoked by depolarizations from -160 to 300 in 20-mV steps, holding potential of -90 mV at 20°C. **(B)** Instantaneous tail current versus voltage was determined by measuring the tail current amplitude extrapolated to time = 0 after voltage jump (see methods). **(C)** The mean current was obtained from 200 current traces recorded from a holding voltage of -100 mV to a test potential of 260 mV at 20 °C. **(D)** Variance versus mean current plot. The red line represents the fit to the data using Equation 6. **(E)** *Po* versus Voltage data were obtained re-normalizing the curves of tail currents with the *Po* obtained to 260 mV at 20 °C. **(F)** Data shown in E were plotted on a semi logarithmic scale together with the Boltzmann fit (red line). The maximum slope of *Po* versus Voltage curve is indicated by the solid line (z=0.65).

In this condition, the model is confined to the C_n–O_n equilibrium (scheme 3B). Then, the open probability is given by the equation (Annex 2):

$$P_O = \frac{1}{1+\frac{(1+K)^4}{L(1+KC)^4}} \quad \textbf{Eq.17}$$

Where $L = L_O\, e^{(z_L FV/RT)}$ and $K = e^{-(\Delta H - T\Delta S)/RT}$. Thus, to determine the limiting slope in TRPM8 channels, I counted single unitary opening events per unit time in patches containing a known number of channels, at very negative potential (-40 to -250 mV) (i.e, in conditions of very low channel open probabilities). *Po* can be calculated from the mean open time of the events frequency divided by, *N*, the number of channels in the patch, as determined by noise analysis on the same patch. Single-channel measurements at more negative voltages (-100 mV to -250 mV) (Figure 10 A) reveal a marked decrease in the voltage dependence. As illustrated in the Scheme 3B, at very low voltages, where voltage sensors remain in resting states, the number of occupied state reduces to 10 and *Po* is described by Eq.17 (Annex 2), thus, when *Po* is small (*Po* << 0.01), $L\left(\frac{1+KC}{1+K}\right)^4 << 1$, Eq. 17 reduce to

$$P_o = L\left(\frac{1+KC}{1+K}\right)^4 = L_0\left(\frac{1+KC}{1+K}\right)^4 e^{\left(\frac{z_L V}{RT}\right)} \quad \textbf{Eq. 18}$$

Where z_L is the voltage dependence for the equilibrium constant *L* or the voltage dependence for opening channel. Single-channel measurements at 10 ºC or 30 ºC, is a very complicated task, for this reason, I defined L^* as the closed-to-open equilibrium with the allosteric contribution of temperature (in the absence of voltage sensor activation). Thus,

$$L_0^* = L_0 \left(\frac{1+KC}{1+K}\right)^4$$ **Eq.19**

Then, *Po* changes in the absence of voltage sensor activation becomes

$$P_O = L_0^* e^{\frac{(z_L V)}{RT}}$$ **Eq.20a**

$$lnP_O = lnL_0^* + \frac{z_L}{RT} V$$ **Eq. 20b**

Thus, in the absence of voltage sensor activation and at temperatures where the temperature sensor are not completely at rest or fully activated, the slope of ln*Po* versus very negative voltage, shows dependency of L_O*, therefore, linear intervals were fitted to Eq.20b, allowing the parameters to vary freely, obtained the values shown in the table 4. Finally, I performed a fit of the *Po* relationships to the allosteric model (Figure 10 C), for voltage dependence activation at different temperatures. The allosteric model predicts that the open probability as a function of voltage is given by the Eq. 1, which can also be expressed as:

$$P_O = \frac{1}{1 + \frac{(1 + J + JKE)^4}{L_0^* + (JD + JKCDE)^4}}$$ **Eq. 21**

Thus, based on the measured limiting slope previously performed, L_0^* was restricted to the values obtained using the Eq.20b for the fit (Table 4). The best-fit parameters obtained for each temperature, were: **15 °C**,*J*=0.3, z_J=0.45, V_J=110 mV, *D*=12.4, *C*=2.4, *E*=4.2, ΔH=-66 kcal/mol, ΔS=-222 cal/molK. **20 °C**:,*J*=0.32, z_J=0.41, V_J=150 mV, *D*=15.9, *C*=3.8, *E*=5.4,

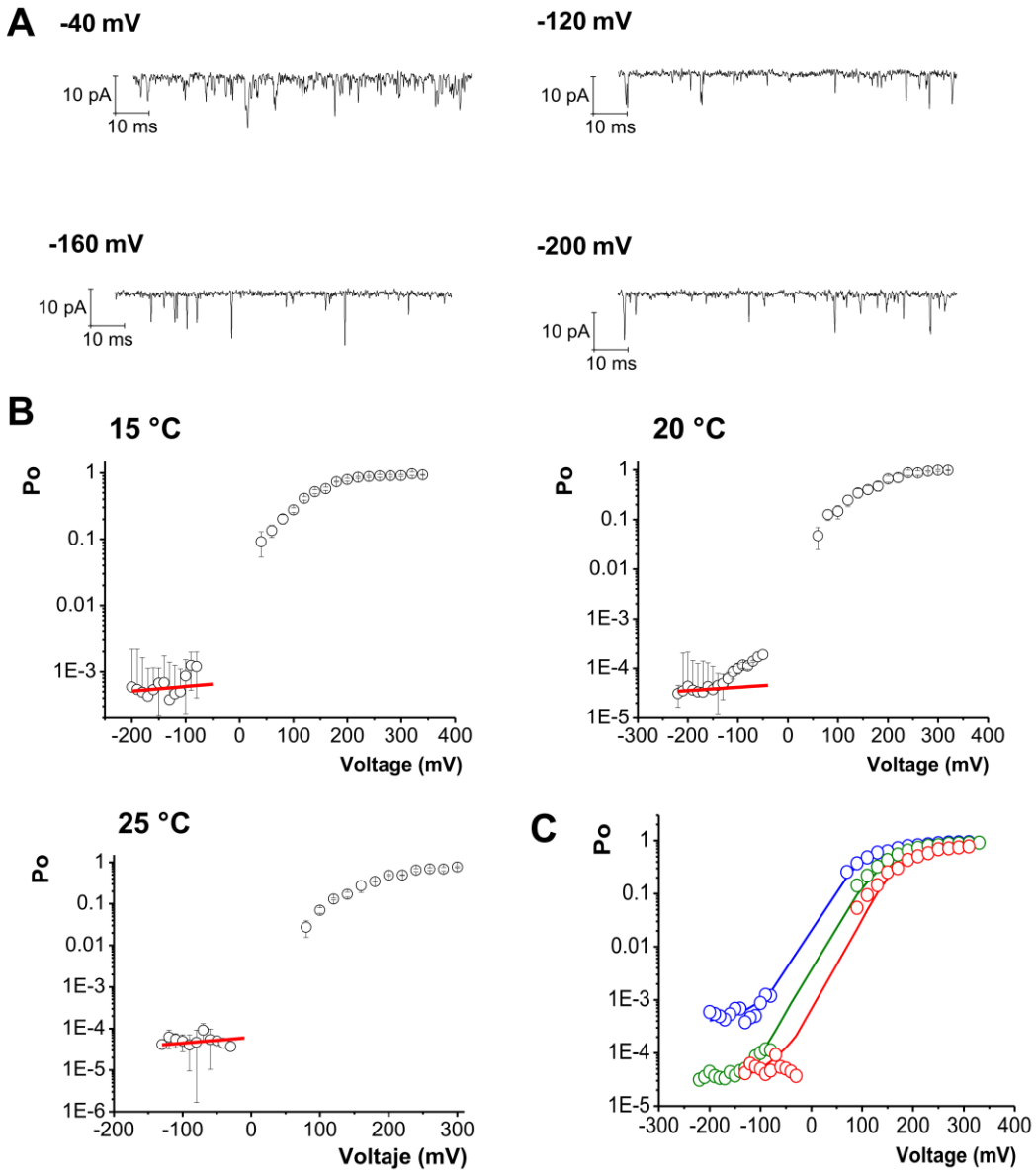

Figure 10*. Limiting slope in TRPM8*. **(A)** Single channel currents of TRMP8, were recorded at 20 °C and the indicated voltages and filtered at 20 kHz **(B)** Semilogarithmic *Po* versus V plots obtained from unitary events quantification (V < -40 mV) or macroscopic recordings (V > 50 mV) at 15 °C, 20 °C and 25 °C (open symbols). *Po* was calculated from the mean open time of the events times the event frequency divided by, *N*, the number of channels in the patch, as determined by noise analysis on the same patch. Linear intervals were fitted to Eq. 20b (red line). **(C)** Fit of the *Po* relationships to the allosteric model, for voltage dependence activation at different temperatures. The *Po* at different temperatures, were fitted to Eq. 21. The best-fit parameters obtained for each temperature, were: **15 °C**,J=0.3, z_J=0.45, V_J=110 mV, D=12.4, C=2.4, E=4.2, ΔH=-66 kcal/mol, ΔS=-222 cal/molK. **20 °C**:,J=0.32, z_J=0.41, V_J=150 mV, D=15.9, C=3.8, E=5.4, ΔH=-76 kcal/mol, ΔS=-260 cal/molK and **25 °C**: J=0.29, z_J=0.43, V_J=180 mV, D=15.5, C=2.63, E=9.39, ΔH=-96 kcal/mol, ΔS=-320 cal/molK. $L^*_{15\,°C}$, $L^*_{20\,°C}$ and $L^*_{25\,°C}$ were restricted to the values shown in Table 4.

TABLE 4

Parameters for limiting slope.

	L_0^*	s.d	z_L	s.d
15 °C	3.32E-4	2.6E-03	3.2E-03	9.6E-02
20 °C	3.28E-5	1.4E-04	5.8E-02	3.6E-02
25 °C	2.15E-5	5.7E-05	4.3E-02	3.1E-02

- L^*_0 and z_L are parameters obtained through measurement of single unitary opening events in patches containing hundreds of channels, at very negative potential (-40 to -250 mV). This open probability was fitted with equation 20b. SD is standard deviation about the mean. 15 °C (n=5), 20 °C (n=7) and 25 °C (n=5).

ΔH=-76 kcal/mol, ΔS=-260 cal/molK and **25 °C**: J=0.29, z_J=0.43, V_J=180 mV, D=15.5, C=2.63, E=9.39, ΔH=-96 kcal/mol, ΔS=-320 cal/molK. In conclusion, each curve de lnPo versus Voltage measured at different temperature, exhibits a break (with a very small slope at more negative potential) showing that the coupling between channel opening and voltage sensor activation is not strict. Thus, this behavior is well described by an allosteric model.

4.6. Temperature and voltage dependence of transitions between closed states of TRPM8 channels.

Figure 11 shows a family of current traces evoked in response to the voltage protocol shown in the upper part of the figure. The time course of activation has a sigmoid shape. On an expanded time scale can be noticed that current activation is preceded by a brief delay of ~200 μs before that the current takes an exponential growing time course (Figure 11, right). This delay suggests that TRPM8 channels undergo one or more transitions between closed states before opening. This proposition was examined using a classical strategy design by Cole and Moore (1960) known as the Cole-Moore shift (Cole and Moore, 1960). Figure 12 A shows superimposed ionic current records for TRPM8 at 20 °C, elicited by a 200 mV test voltage pulse for different conditioning prepulses ranging from -260 to -40 mV (see voltage protocol in Figure 12, right). In a voltage-dependent channel activated by depolarizing voltages, the delay should tend to disappear with more positive potentials, since those close states near the open state become populated. This is clearly reflected in the Figure 12 B, where the delay is essentially absent when the conditioning pulse is -40 mV. In the Figure 12 C, shown the delay duration (Δt) plotted versus conditioning voltage pulse at two different temperatures. The two Δt–V relationships in Figure 12 C are similar in shape and show a slight difference in magnitude, reflecting the independent of the temperature of the current delay.

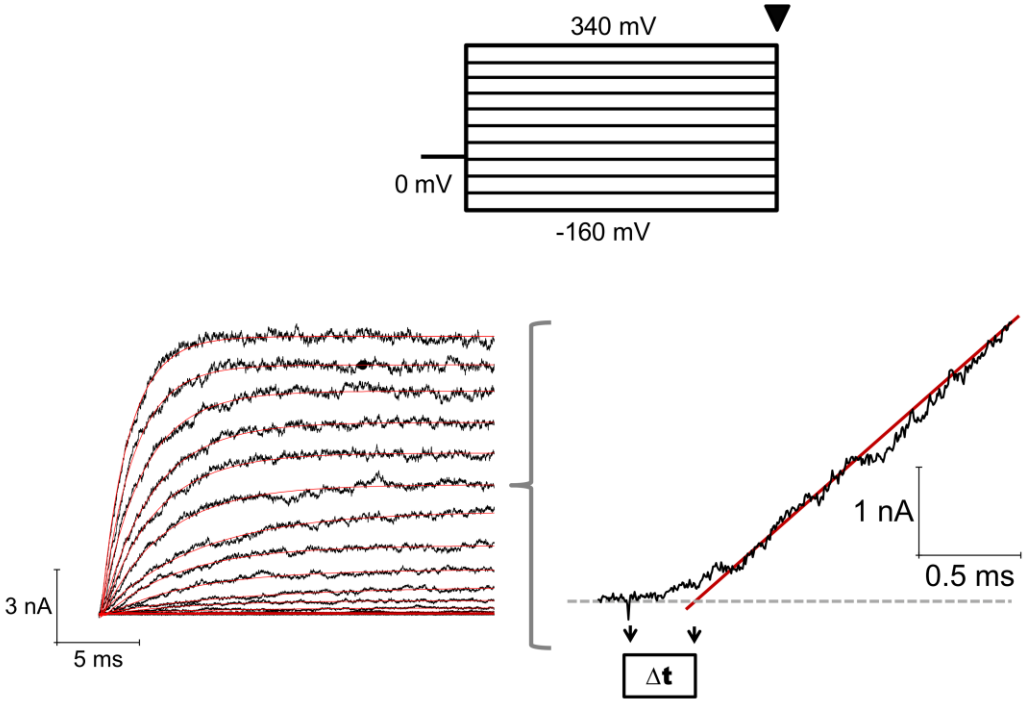

Figure 11. ***Delay in the current activation of TRPM8***. Current evoked by a voltage protocol shown at the top. The time course of activation is fit by a mono-exponential function (red lines). The current record obtained at 220 mV is plotted on an expanded time scale on the right of the figure. Current activation shows a delay. The delay duration (Δt) is defined as the time where the exponential fit intersects the time axis (red line).

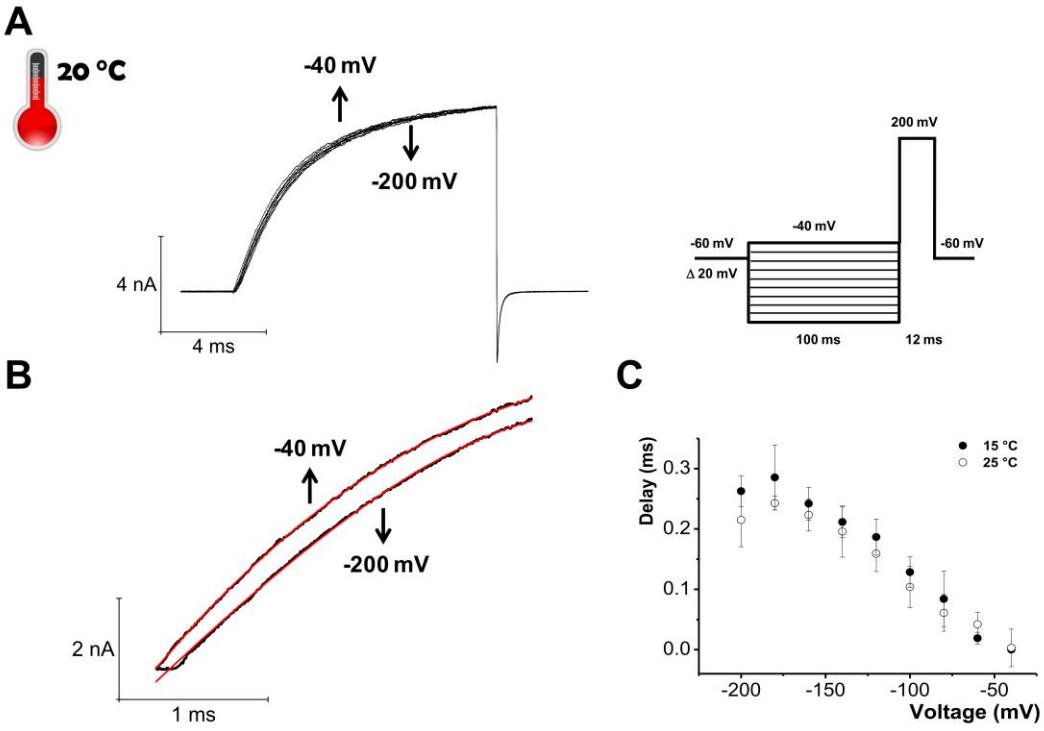

Figure 12: ***Kinetics of early transitions of the activation pathway using the Cole-Moore protocol.*** **(A)** Macroscopic ionic currents of TRPM8 elicited in response to conditioning prepulses shown in the pulse protocol (right). **(B)** Two current records obtained using prepulses of -40 mV and -200 mV are shown in an expanded time scale, showing a delay before current achieves an exponential time course (red line). **(C)** Delay duration is plotted versus prepulse voltage for two temperatures, 15 °C and 25 °C

In summary, TRPM8 channels undergo several closed state transitions prior to the closed to open channel, and the rates of these steps are independent of the temperature.

4.7. Voltage Dependence of the Activation and Deactivation Kinetics

After of short initial delay, the activation kinetic of TRPM8 channel follows an exponential time course. This observation suggests that its activation is dominated by a single rate limiting step. Thus, to study the properties of this transition, we examined the voltage dependency of the activation kinetic. Channels were activated by stepping from a holding potential of -90 mV to voltages between 20 mV and 300 mV at 10 °C, 140 mV and 340 mV at 20 °C, and 100 mV and 340 mV at 30 °C. Figure 13A shows representative current traces for TRPM8 channel activation to 260 mV and 200 mV at 10 °C, 20 °C and 30 °C where all traces are fitted by a single exponential function (Eq.3). Figure 13B shows the activation time constant obtained at several activation voltages for each temperature. $\tau_{activation}$ versus Voltage plot exhibits a bell-shaped voltage dependence with a maximum that shifts to higher voltage values with increasing temperature (Figure 13B). At cold temperature (10 °C) the activation time constant was about 4 times longer than at 30 °C. The observed behavior for the TRPM8 channel of τ versus voltage plot can be interpreted in terms of the allosteric model shown in the scheme 4a, where the allosteric factor is *D* and the equilibrium constant for voltage sensor activation is *J*, however, with the kinetic rate constants in place of the equilibrium constant (scheme 4b).

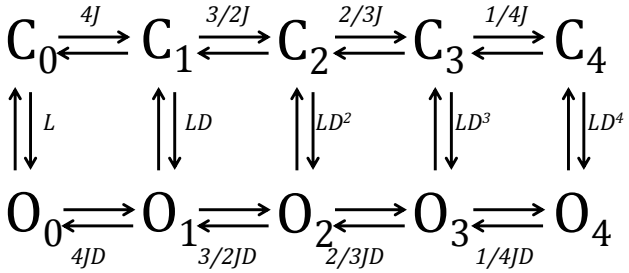

Scheme 4a

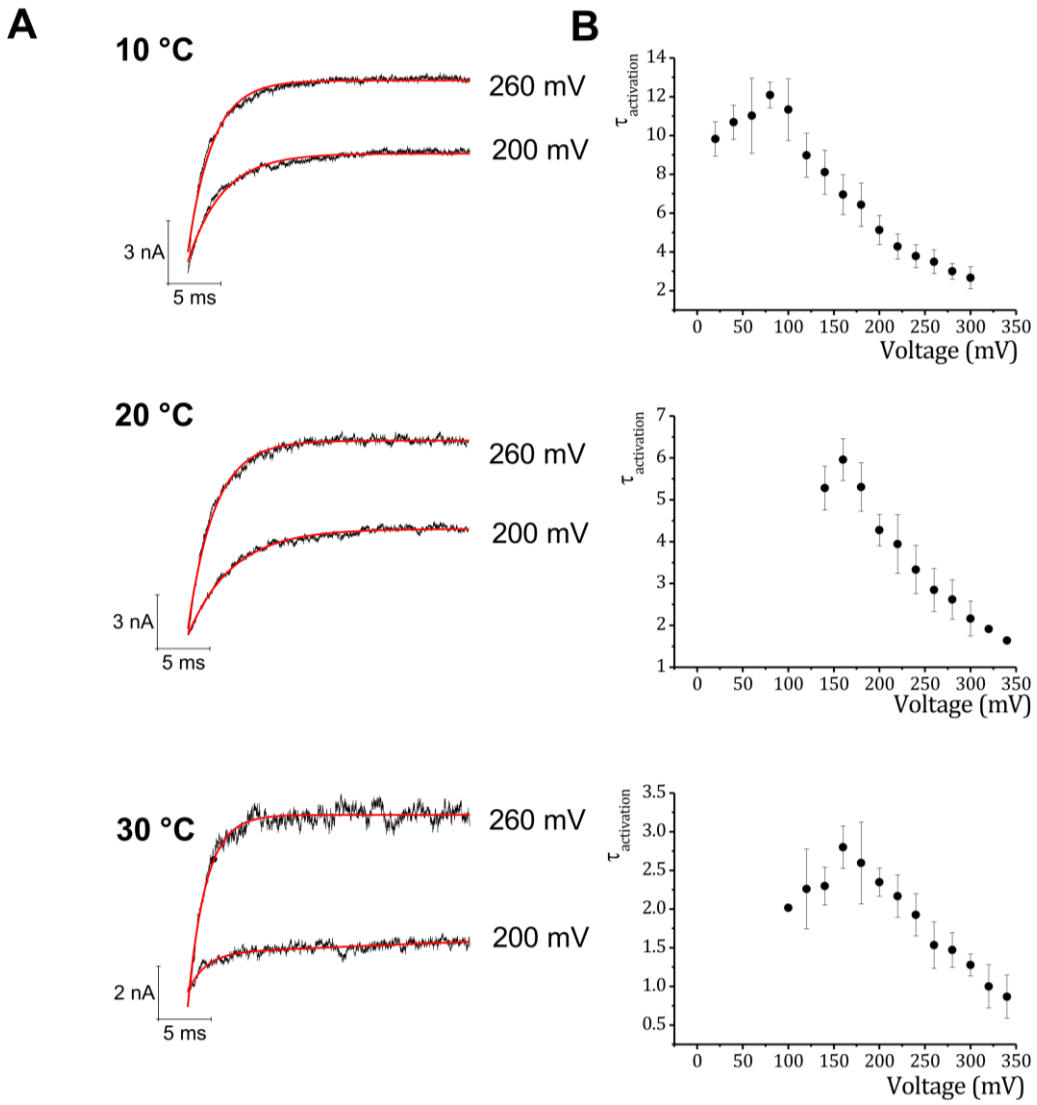

Figure 13. ***Voltage dependence of activation time constants.*** **(A)** Activation time constants ($\tau_{activation}$) were determined by fitting the current time course using equation 3. Representative traces are shown for 140, 200 and 300 mV at three different temperatures (10 °C, 20 °C and 30 °C). **(B)** $\tau_{activation}$ versus voltage relationships for each of the temperatures shown in the left side of the figure (n=4 for 10 °C, n=6 for 20 °C and n=5 for 30 °C).

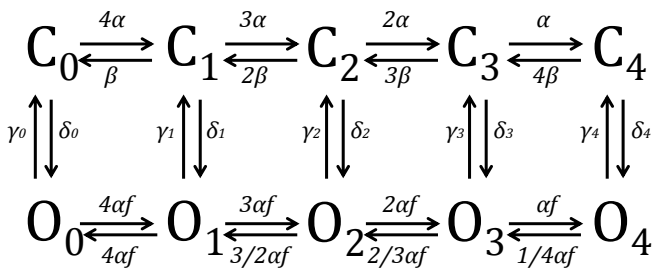

Scheme 4b

In this scheme, the time constant for current relaxation will be given by the γ_n and δ_n kinetic constants weighed by the relative probabilities of the O_n and C_n states. The rate constants that control the transitions between closed states are, α and β. These constants can be expressed as follows: $\alpha = \alpha_0 e^{(z_\alpha FV/RT)}$, $\beta = \beta_0 e^{(-z_\beta FV/RT)}$, $\delta_n = \delta_{n(0)} e^{(z_\delta FV/RT)}$, $\gamma_n = \gamma_{n(0)} e^{(-z_\gamma FV/RT)}$. The correspondence with the scheme 4a, is verified by the following equalities: $J = \alpha/\beta$, $L_0 = \delta_0/\gamma_0$, $z_J = z_\alpha + z_\beta$, $z_L = z_\delta + z_\gamma$, and $D = (\delta_{n+1}/\gamma_{n+1})/(\delta_n/\gamma_n) = f^2$. If voltage sensor activation is fast, and assumed to equilibrate on the timescale of channel opening, then τ is expressed by the equation:

$$\tau = [\sum(\gamma_i pO_i + \delta_i pC_i)]^{-1} \qquad \textbf{Eq. 22}$$

where *i* represent the number of activated voltage sensors, γ_i and δ_i are forward and backward rate constants for the *Ci-Oi* transitions and *pCi*, *pOi* are conditional occupancies of the open and closed states, i.e. $pC_i = p(C_i|C)$, $pO_i = p(O_i|O)$.

At extreme positive voltages, $\delta_n >> \gamma_n$ and all voltage sensors are activated *i*=4 (assuming four voltage sensor domains). Thus, the equation simplifies to

$$\tau = (\delta_4)^{-1} = \delta_4 e^{\left(\frac{z_\delta FV}{RT}\right)^{-1}} \qquad \textbf{Eq. 23}$$

where τ only depends on the opening rate constants.

At very negative potentials, all voltage sensors will be in their resting state (*i*=0), thus, τ depends only on the closing rate constants:

$$\tau = (\gamma_0)^{-1} = \gamma_0 e^{\left(-\frac{z_\gamma FV}{RT}\right)^{-1}} \quad \textbf{Eq. 24}$$

$$ln\tau = ln\gamma_0 - \frac{RT}{z_\gamma}V \quad \textbf{Eq. 25}$$

In other words, at very negative and very positive potentials, the voltage sensors are all in the resting state or all in the activated state, respectively. Thus, the limiting voltage dependencies of the macroscopic kinetics can reveal processes unrelated to voltage sensor movements. Because G-V saturates at ~250 mV at 10 °C, ~300 mV at 20 °C and ~400 mV at 30 °C (Figure 8 A), is more difficult that the $\tau_{activation}$ can be measured over a voltage range sufficiently large to measure accurately the value of the slope. For this reason, I analyzed the time course of deactivation fitting with a double exponential decay with a fast (τ_1) and a slow decay time constant (τ_2) (Figure 14A-B). Just as for $\tau_{activation}$ versus voltage plot, $\tau_{deactivation}$ show a bell-shaped which suggests that both time constants are voltage-dependent (Figure 15 and 16), showing, in both cases, a shift in the peak (to the right) when the increased temperature. The mean value in the peak at 15 °C for τ fast was 1.8 ± 0.15 msec (n=4), at 20 °C was 0.82 ± 0.22 msec (n=8) and 25 °C was 0.45 ± 0.05 msec (n = 4) (Figure 15) and to τ slow was 25 ± 1.4 msec at 15 ºC, 10 ± 2 msec at 20 ºC and 4.6 ± 1.7 msec at 25 ºC (Figure 16). To test the limiting behavior of $\tau_{deactivation}$, tail currents were measured at very negative voltages (Figure 15 A-B and Figure 16 A-B). Thus, at these voltages, the plot will reach a limiting slope that reflects now the portion of z_L asso ciated with the closing transition ($z\gamma$). Viewing Figure 15B, the curve has a limiting positive slope where the values to $z\gamma$ are 0.1 ± 0.06 (n=5); 0.02 ± 0.009 (n=7) and 0.02 ± 0.007 (n=7) at 15 °C, 20 °C and 25 °C, respectively (red line), whereas that figure 16 B, shows

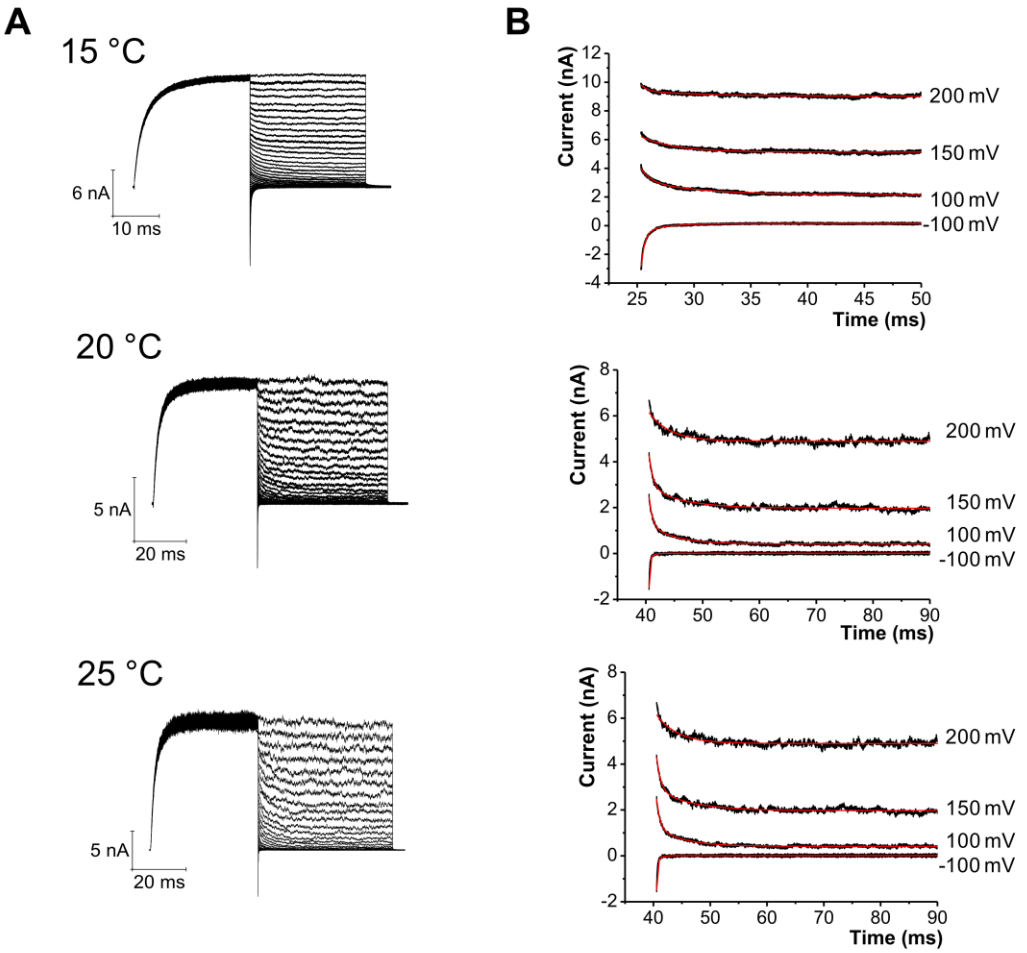

Figure 14. Deactivation current traces at different potential. **(A)** Representative recordings of macroscopic current decay at different temperatures. **(B)** The current were measured by fitting deactivation current traces by two exponentials (Eq.8). Representative traces are shown for -100, 100, 150 and 200 mV at three different temperatures

that values to z_γ are 0.04 ± 0.01 (n=5), 0.01 ± 0.007 (n =7) and 0.05 ± 0.01 (n=7) at 15 °C, 20 °C and 25 °C, respectively. It starts to veer, for both cases, upward at -100 mV to 15 °C and 20 °C and -50 mV to 25 °C, which, as expected, is the same position as the inflection point in the TRPM8 channel ln(*Po*) versus Voltage curve (Figure 10 B). The ln τ–V curves in the Figure 15 B and 16 B, were fitted with Eq. 25 (red lines). Thus, at more extreme potentials (negatives), voltage sensors are not activated and $\tau_{deactivation}$ reflects only γ_0 of the C-O rate constants, which is clearly independent of potential. The limiting voltage dependence of the macroscopic kinetics of TRPM8 channel, just like the measuring the limiting slope of the open probability at very negative potentials, reveals a potential independent process.

4.8. Temperature Dependence of the Activation and Deactivation Kinetic

To determine the temperature dependence of the activation and deactivation TRPM8 channel kinetics I obtained the activation energy (*Ea*) (see Materials and Methods, section 3.4.1) by plotting the inverse of the time constant (τ) versus 1/Temperature ($°K^{-1}$) (Arrhenius plot). The temperature dependence of the activation and deactivation rates is shown in Figure 17 A and B, respectively. The activation and deactivation (fast and slow) *Ea* are 5 kcal mol^{-1}, 26 kcal mol^{-1} and 38 kcal mol^{-1}, respectively, corresponding to approximate Q_{10} values of 1.4, 4.4 and 5.6. This means that the activation process of TRPM8 channel is less temperature dependent than the deactivation process. These data are consistent with those published previously for this channel, by Brauchi and col. (Brauchi, 2004), nevertheless, in this paper is indicates that the fast component of deactivation constant, is neither voltage- or temperature dependent, reason why only the slow component was used. In this thesis work, however, I determined that both component, fast and slow, are voltage and temperature sensitive and that both present a similar sensitivity to temperature. Is possible that the difference may be due to that in this thesis, the currents were filtered at 40 kHz, while in the paper published in 2004 (Brauchi, 2004), were filtered at 10 kHz, which could affect the accurate measurement of the fast component.

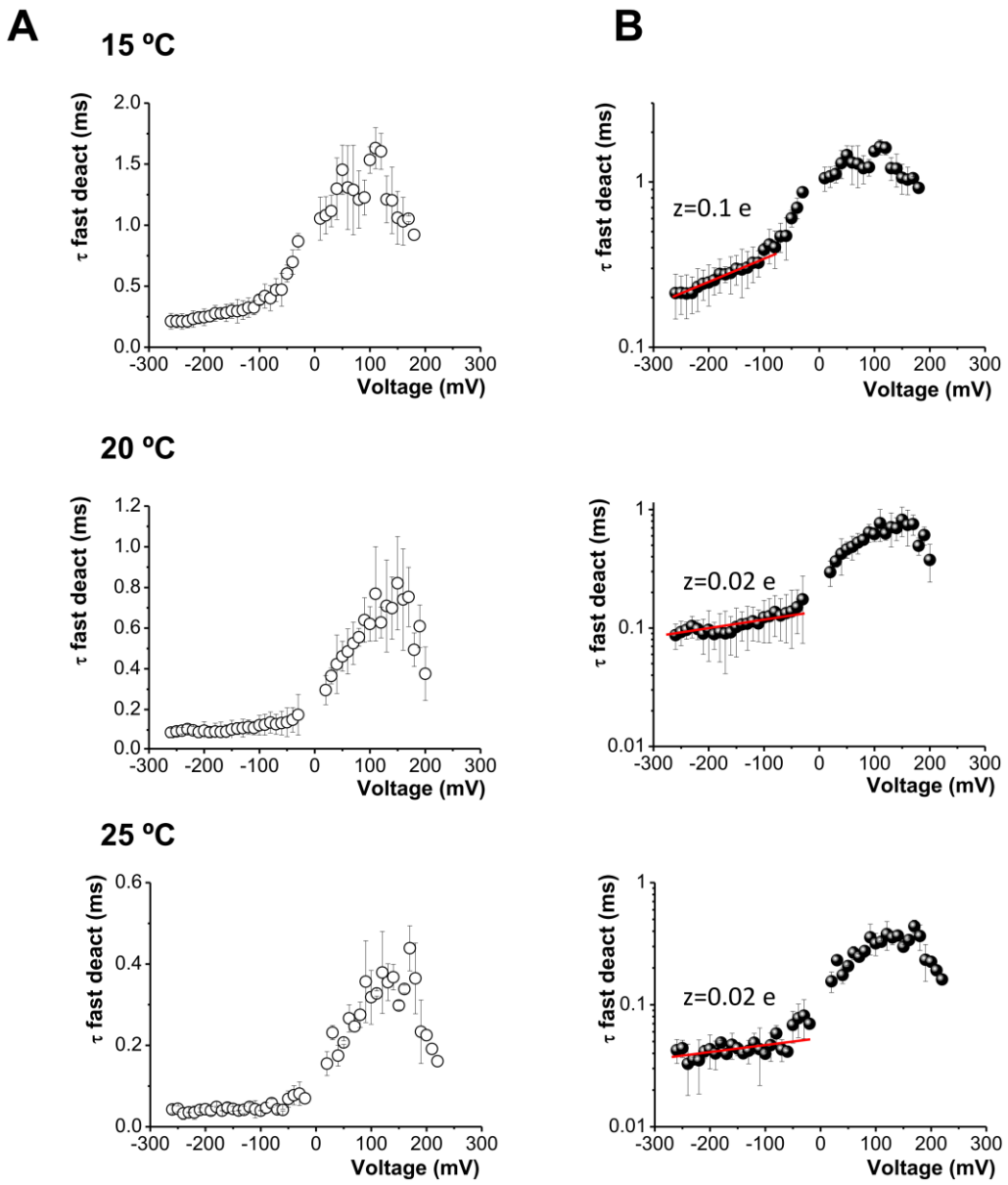

Figure 15. ***Voltage dependence of Tau fast on the deactivation process*** **(A)** τ fast $_{\text{deactivation}}$ versus Voltage relationships at different temperatures. The values of the time constants were obtained by fitting the data to equation 8. **(B)** Mean time constants of deactivation are plotted on a log scale versus voltage for the same experiments as in A (n= 5). This was done with the aim of obtain the $z\gamma$. Linear intervals were fitted to Eq. 25 (red line).

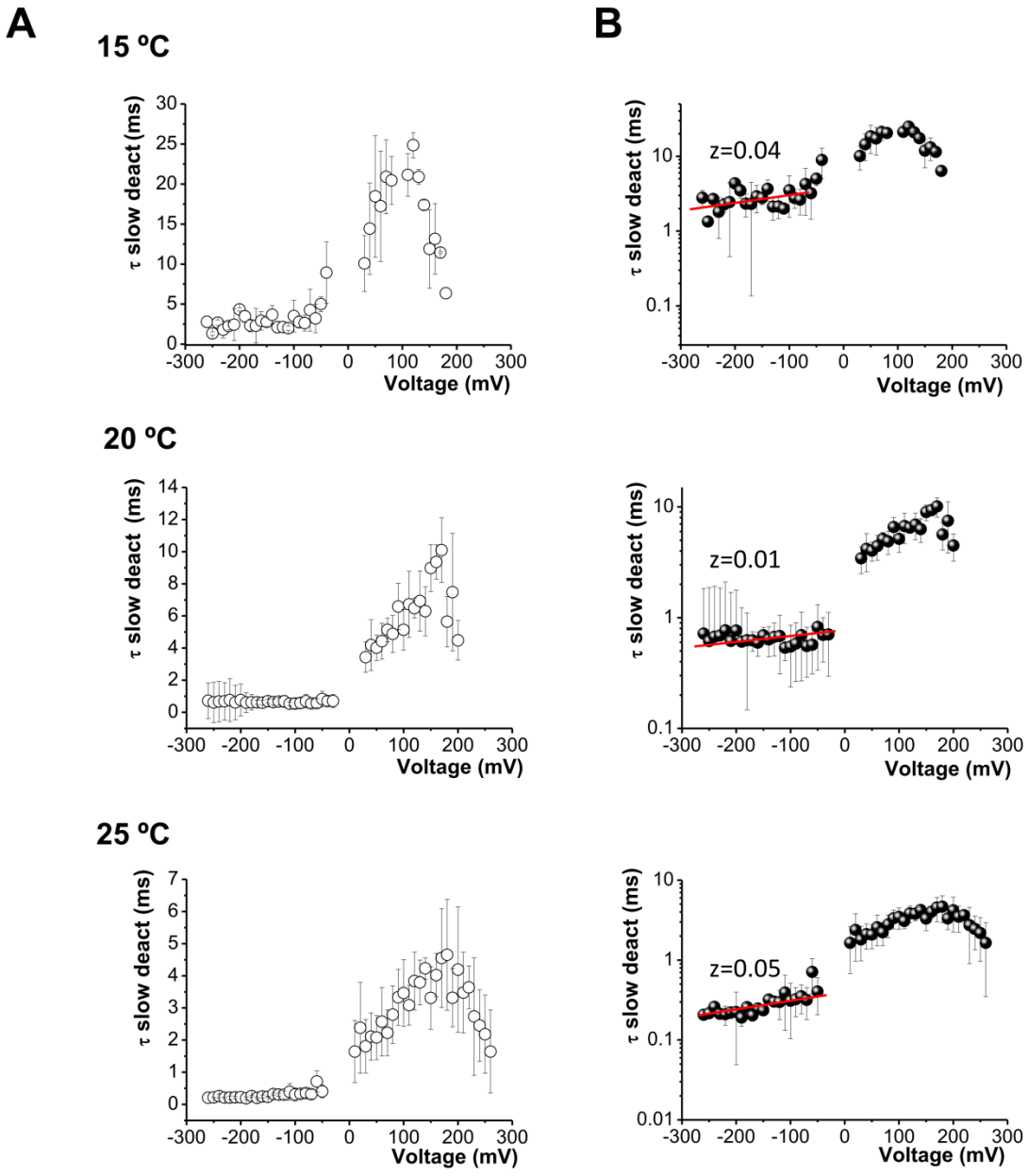

Figure 16. ***Voltage dependence of Tau slow on the deactivation process*** **(A)** τ slow $_{deactivation}$ versus Voltage relationships at different temperatures. The values of the time constants were obtained by fitting the data to equation 8. **(B)** Mean time constants of deactivation are plotted on a log scale versus voltage for the same experiments as in A (n= 5). This was done with the aim of obtain the $z\gamma$. Linear intervals were fitted to Eq. 25 (red line).

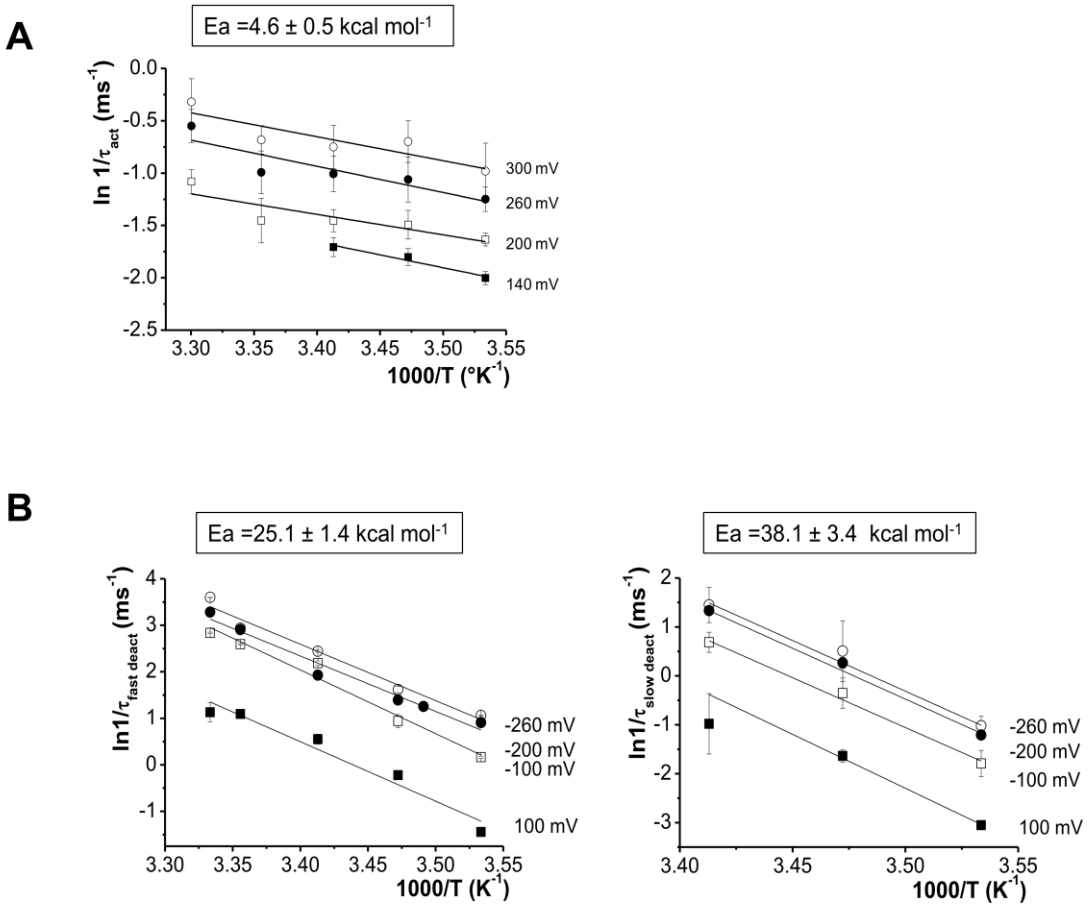

Figure 17. ***Arrhenius plot for activation and deactivation process on TRPM8.*** **(A)** Activation rates were calculated from the activation time constants of current traces elicited at 300, 260, 200 and 140 mV. **(B)** For deactivation process (fast and slow), the rates were calculated from the deactivation time constants of current traces elicited at -260, -200, -100 and 100 mV. Activation energies, *Ea*, were calculated directly from the slope of Arrhenius plots (Equation 10) at each voltage (solid lines).

4.9. Temperature Sensor

Coiled-coil domains of TRPM8, TRPM2 and TRPM4 channels have been recognized as central to the formation of tetramers (Launay et al., 2004; Erler et al., 2006). Their non-polar interactions promote the assembly of two, three or more heptads contributing to the stability of oligomeric proteins (Wagschal et al., 1999; Tripet et al., 2000) (Figure 3B). To determine the importance of the distal half of the TRPM8 carboxyl terminus in the channel modulation by temperature, we designed three truncated channel with different extensions: TRPM8CTΔ16 and TRPM8CTΔ25 with 16 and 25 last amino acids removed from the coiled-coil domain, respectively, and TRPM8CTΔ48 a deletion mutant, in which this domain was completely removed. Unlike the other mutants, TRPM8CTΔ48 showed no current activation when exposed to a voltage-pulse protocol. This was done at different temperatures and tested from three to six days after injection of RNA, without observing functional channel expression. This can be explained in two ways: (1) the channel was not expressed at the cell surface or (2) it reached the plasma membrane but it was not functional. This result demonstrates that at least a portion of coiled-coil is required for functional channel expression. Figure 18 shows that the temperature sensitivity of the channel as determined by the logQ_{10}, decreases proportionally to the shortening of the C-terminal. For this reason, I decided to study the energy contribution of each heptad of the coiled-coil to the temperature sensitivity of the channel. For this purpose, deletions TRPM8CTΔ8, TRPM8CTΔ15, TRPM8CTΔ22, TRPM8CTΔ29, TRPM8CTΔ36 and TRPM8CTΔ40 (Figure 18C) were made based on the alignment presented by Fujiwara and Minor (2008) (Figure 3 and 18C). Families of representative traces measured at 27 °C are shown in the Figure 19 A, for the wild type and their mutants TRPM8CTΔ8, TRPM8CTΔ15 and TRPM8CTΔ36, respectively. Subsequently, we measured the tail current-voltage curves at different temperatures, which were normalized by maximal tail current at each different temperature (Figure 19B), and by the open probabilities at 260 mV at each temperature (Figure 19C). The TRPM8CTΔ22, TRPM8CTΔ29 and TRPM8CTΔ40 mutants did not express detectable currents in oocytes. To analyze in more detail changes of the opening probability of TRPM8 due to deletion of the coiled-coil, I focus on

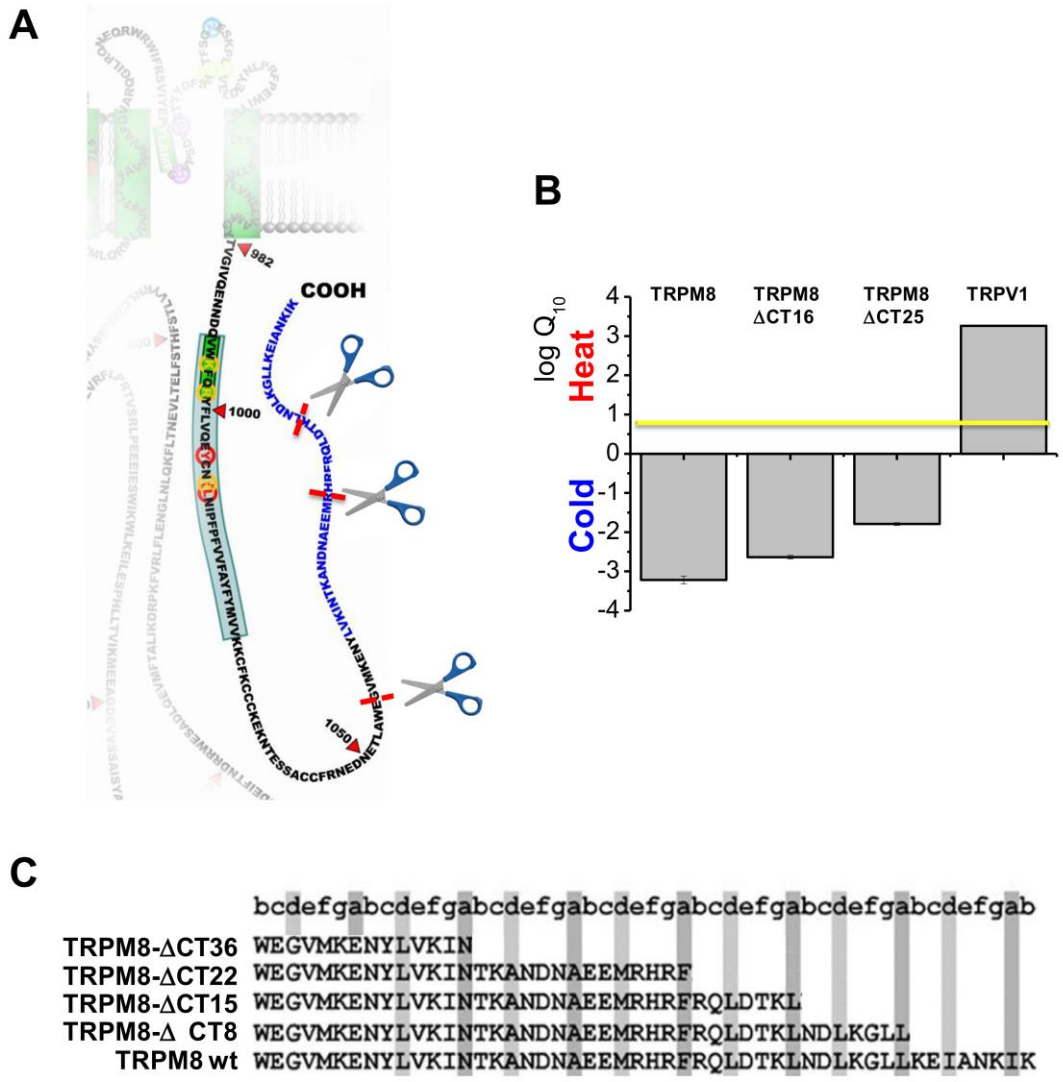

Figure 18*. The carboxyl terminus of TRPM8.* **(A)** In blue the domain corresponding to the Coiled-coil domain. Scissors define the different deletion mutants tested. **(B**) Relationship between Q_{10} and the long C-terminal end of TRPM8. The yellow line shows the value of logQ_{10} for proteins that are normally sensitive to temperature, whose value ranges between 1 and 3. **(C)** The coiled-coil primary structure of TRPM8 and the primary structure of the deletion mutants tested.

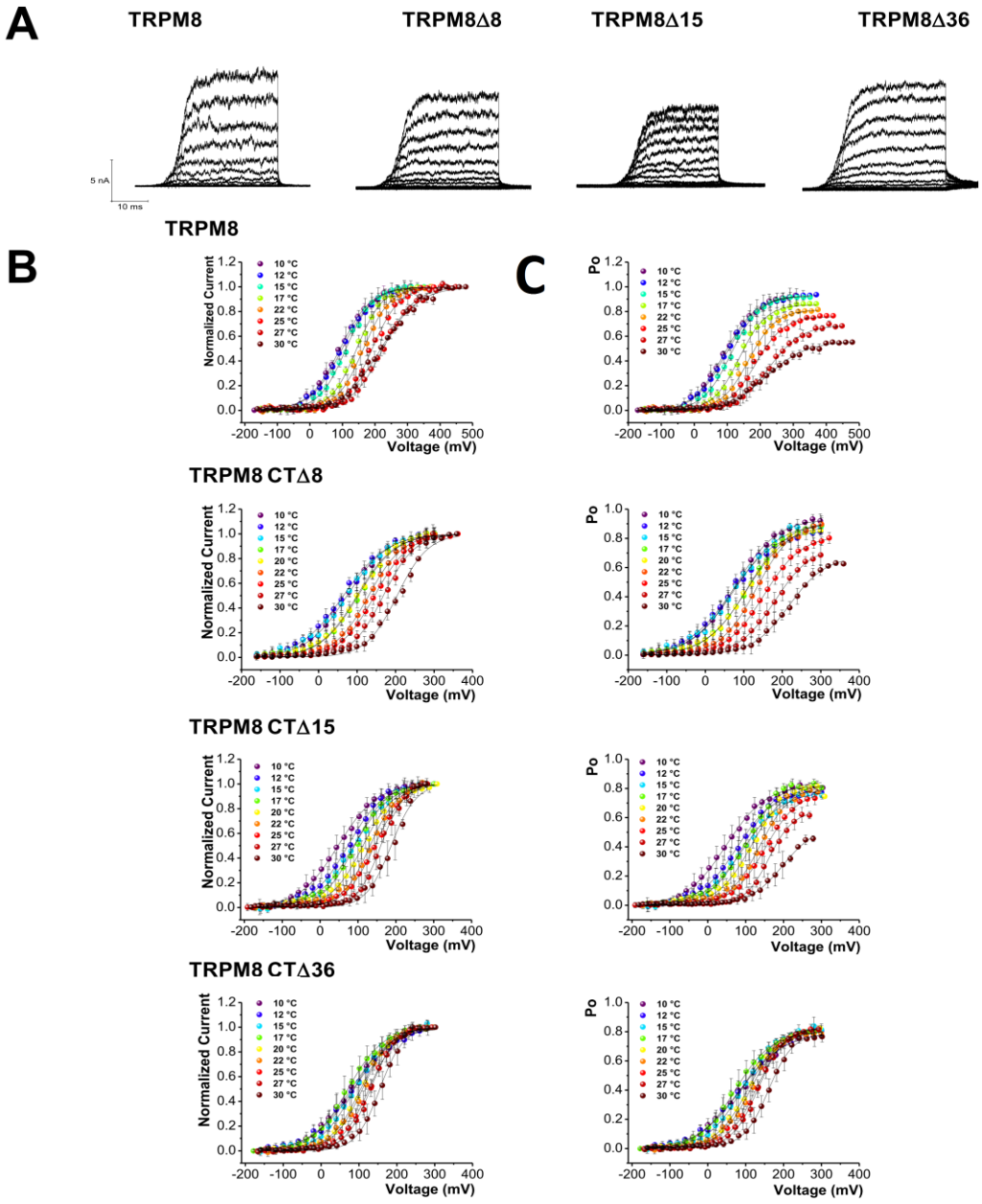

Figure 19: ***The effects of temperature on the channel open probability for deletions.*** **(A)** Shows representative current traces at 27 °C, for TRPM8 and for the suppression TRPM8ΔCT8, TRPM8ΔCT15 and TRPM8ΔCT36. **(B)** Tail current-voltage curves at different temperatures were normalized by maximal tail current at each different temperature. The solid lines indicate Boltzmann fits to the experimental data. **(C)** Each *Po* versus *voltage* curve, corresponds to the tail current-voltage curves performed at different temperatures shown in Figure 19 B so that, the probabilities obtained using noise analysis at 260 mV for each temperature are used to re-normalize the curves of tail currents. Error bars are SD, *n*=6–10

TRPM8CTΔ36, because it is the mutant that presents the biggest changes in this aspect (compare Figures 19 C for TRPM8 and TRPM8CTΔ36). Thus, Figure 20 shows a comparison of *Po* of TRPM8 and TRPM8CTΔ36 channels at 60 mV (Figure 20 A) and 300 mV (Figure 20 B), for different temperatures. At low temperatures (10 °C – 15 °C), the probability of opening for TRPM8CTΔ36, is smaller than the obtained by TRPM8 (Figure 20 A), however, at temperatures between 20-25 °C, the mutant have a higher open probability than TRPM8. Thus, although in general terms, the $Po^{max\ 60mv}$ of the mutant conserves a tendency to decrease with increasing temperature, its temperature sensitivity is less than the wild type channel. This behavior is evident to higher potentials, in this case, 300 mV (Figure 20 B), where open probability of TRPM8CTΔ36 was of 0.75, which practically does not change in the temperature interval considered (10 °C - 30 °C). Furthermore, we performed a thermodynamic analysis that yielded the equilibrium constants at 60 mV for the wild type, as well as for the mutants examined. Thus, the equilibrium constants obtained for each mutant, were used to construct Van't Hoff plots obtaining the enthalpy and entropy changes of the opening reaction (Figure 21). In the case of TRPM8, we can distinguish two phases, one between 10 °C- 17 °C (Phase 1) and other between 17 °C- 30 °C (Phase 2). The first phase is poorly sensitive to temperature with an enthalpy change of -25 kcal/mol and entropy change of –84 cal/mol K. The second phase is highly dependent on temperature with an enthalpy of -84 kcal/mol and entropy change of -291 cal/mol K. In the case of deletions TRPM8CTΔ8 and TRPM8CTΔ15, both have a similar phase 1 very similar energetically to TRPM8, however, the phase 2 shows a decrease in enthalpy and entropy changes every time that the coiled-coil is shortened. Thus, to the remove the last heptad (TRPM8CTΔ8) the enthalpy and entropy changes, diminishes in 29 kcal/mol and 100 cal/mol K with respect to the wild type protein, whereas for the case of TRPM8 CTΔ15 (deletion of the last two heptad) is reduced in 41 kcal/mol and 136 cal/mol K, respectively. For the mutant TRPM8CTΔ36, the temperature sensitivity of the channel practically is lost, showing in the phase 2, an enthalpy change of -27 kcal/mol and an entropy change of -87 cal/mol K (Figure 21).

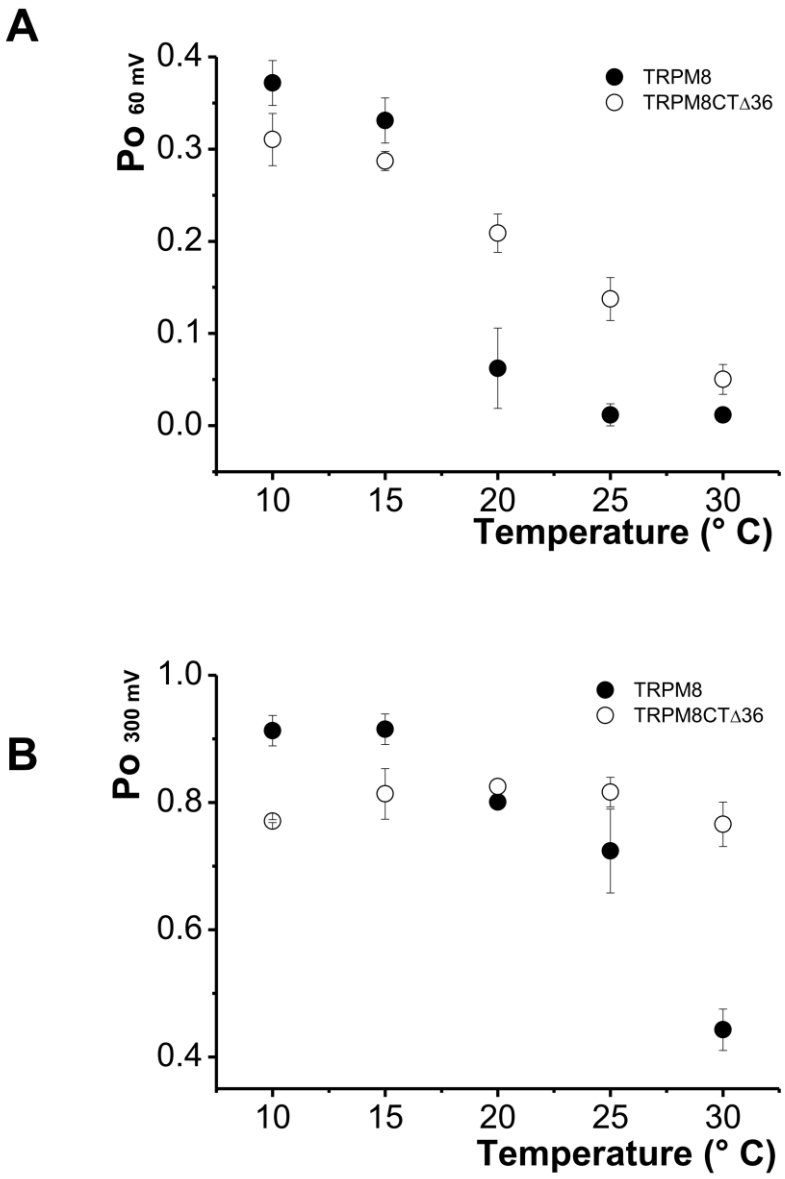

Figure 20: ***Comparison of Po of TRPM8 and TRPM8CTΔ36 channels at 60 mV and 300 mV at different temperatures.*** Open probabilities were obtained from the values shown in Figure 8C, for each voltage, 60 mV in A and 300 mV in B. Error bars are SD, *n*=6–10.

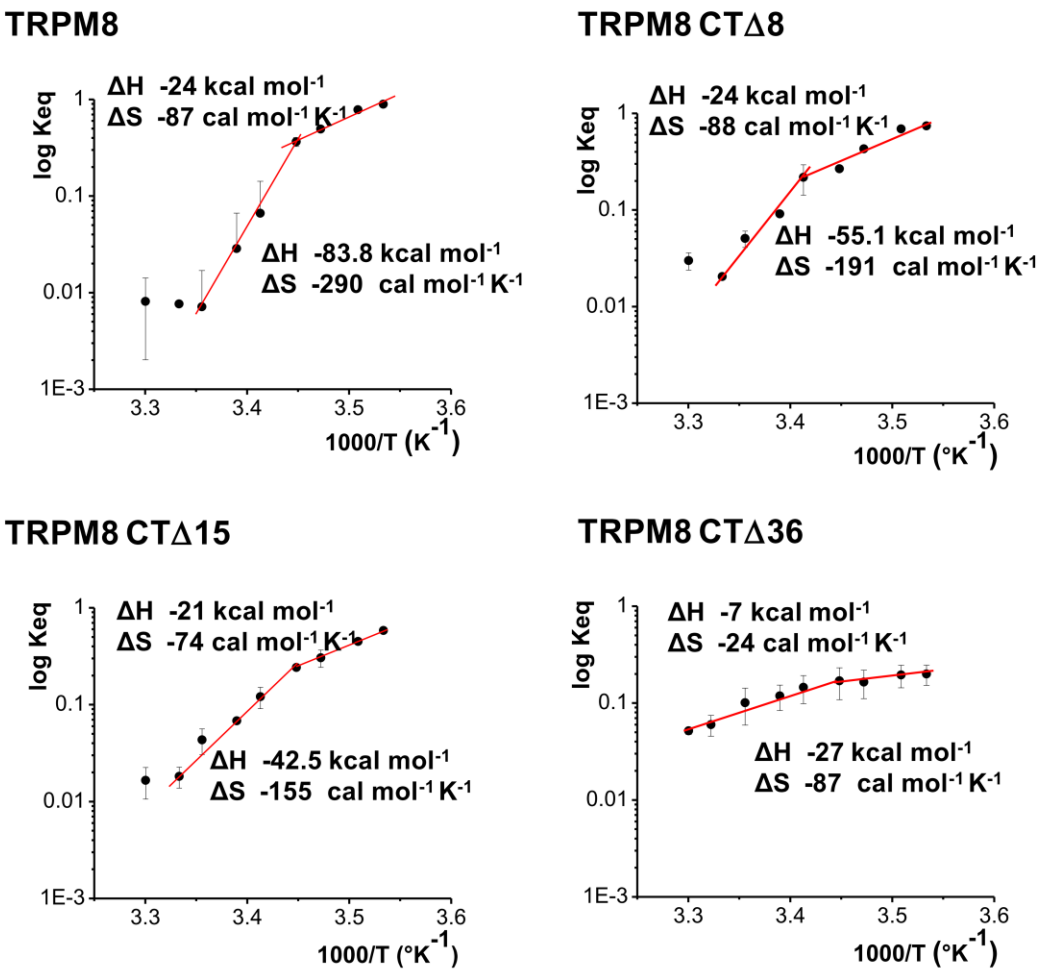

Figure 21: ***Thermodynamic analysis of TRPM8 and C-terminal deletion mutants.*** In each Van`t Hoff plot the enthalpy and entropy changes were calculate from the maximum slope and the intercept defined by the data obtained for each temperature range. Linear intervals were fitted to Eq. 16 (red line). Error bars are SD, *n*=6–10

Finally, Figure 22 shows the comparisons between the $V_{0.5}$ for mutants and wild type protein,

which, between 10 °C and 15 °C, practically not change. However, TRPM8 and TRPM8CTΔ36 present the greatest difference of ~ 80 mV at 30 °C. Furthermore, the mutants do not suffer significant changes in the *z* respect to the wild type channel between 10 °C and 20 °C, however, show a slight tendency to increase their value to the extent that the coiled-coil is shortened. Thus, at temperatures above 20 °C, the voltage dependence in the mutants does not decrease, as occurs for TRPM8. On the contrary, this dependence increases with decreasing number of heptad. Thus, at 30 °C, TRPM8CTΔ36 present a values of z of 0.8 while TRPM8 present a values of 0.4.

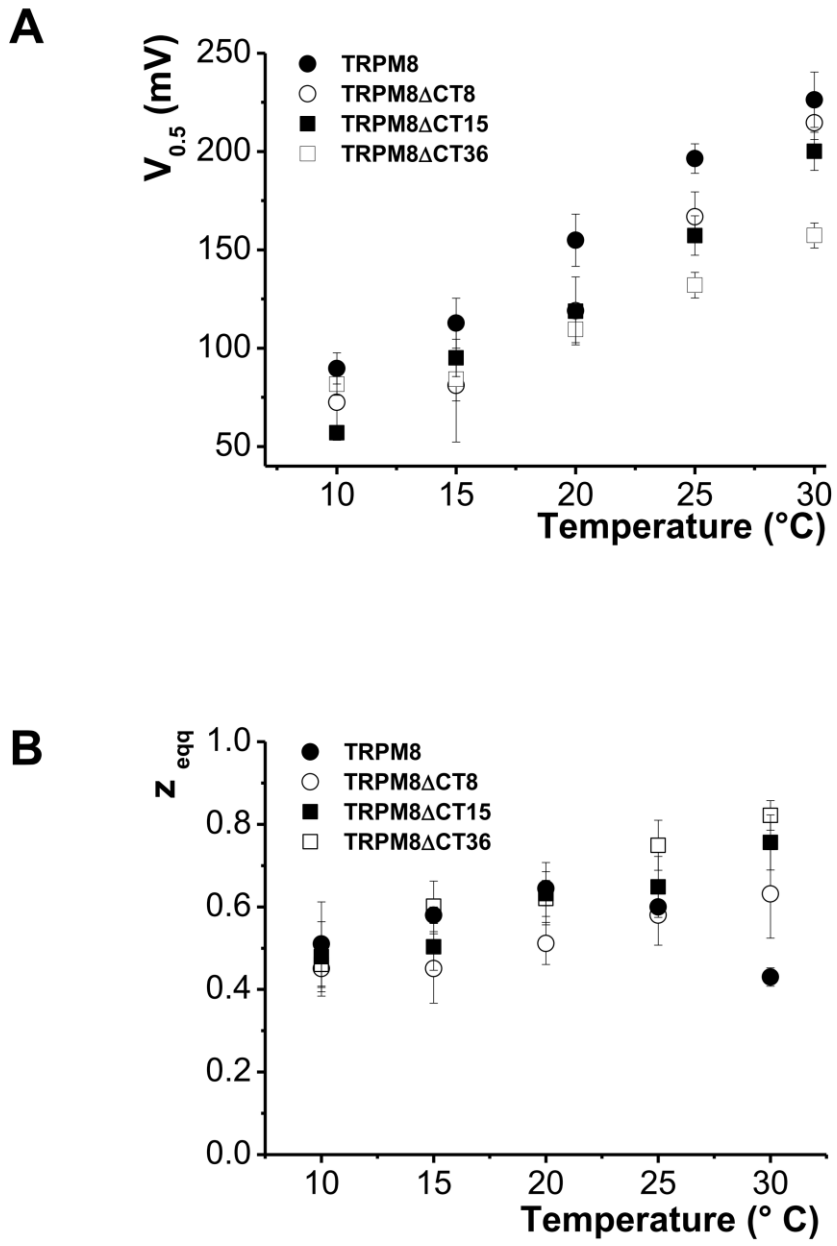

Figure 22. ***Changes in the $V_{0.5}$ and z, for the mutants.*** **(A)** Comparison $V_{0.5}$ of TRPM8 and the obtained for mutants. ***(B)*** Comparison between *z* of TRPM8 and mutants. These values were obtained using the equation 2. n=5-10.

5. DISCUSSION

In the first part of this thesis work, I set out new experiments to complement the information previously reported regarding the most appropriate gating kinetic model for TRPM8 (Brauchi, 2004; Latorre et al., 2007; Matta and Ahern, 2007; Latorre et al., 2009). The data presented in this thesis supports the validity and relevance of the allosteric model to explain the voltage dependence of steady state activation.

5.1. Voltage and temperature-dependent activation

To examine TRPM8 steady-state activation over a wide range of voltages, the conductance versus voltage (G-V) relationship was measured at different temperatures using macroscopic currents (Figure 6). As can be seen, the G–V curves fitted by a Boltzmann function (Figure 7A), shows an overlap between the curves at temperatures below 15 °C and over 27 °C, so that, $V_{0.5}$ saturates at high and low temperatures. This behavior cannot be explained on the basis of models in which voltage and temperature sensors are strictly coupled (two state model, linear model of the Hodgkin and Huxley type). These models predict a linear relationship between $V_{0.5}$ and temperature over the whole temperature range. As found experimentally (Figure7B), saturation of the $V_{0.5}$ at low and high temperatures is, however, predicted by allosteric models (Scheme 1). The Figure 8C shows that both, voltage and temperature can activate the channel independently to increase *Po*. Therefore, *Po* at the same voltage is larger with cold temperature (Figure 8D) and at the same temperature is larger with a more depolarized voltage, however, neither voltage or temperature are sufficient to fully activate the channel which causes that *Po* is always less than 1.

Furthermore, due to the allosteric coupling of the activation gate with the voltage and the

temperature, the opening of the channel due to one stimulus, voltage or temperature, will enhance the effect of the other via the allosteric coupling between the activation gate and the putative sensor voltage and/or temperature by an allosteric factor *E*. These indirect interactions mediated by channel opening also been seen for other channels as the high-conductance voltage- and Ca^{2+}-activated K^{+} (BK) channel (Cox et al., 1997; Horrigan and Aldrich, 2002).

5.2. Coupling between voltage sensors and the activation gate

The simplest obligatory model is the Hodgkin-Huxley type sequential model, C-C-C-C-O, in which four identical voltage sensors are activated independently by depolarization, and the channel remains closed until all four voltage-sensors are activated that opens the channel (Hille, 2001). This model assumes an obligatory coupling between voltage-sensor activation and channel opening: voltage-sensor must move to an active state in order for the channel to open, and channel opening is obligatory once all four voltage-sensors are activated. Thus, for any linear voltage-dependent model, the limiting voltage dependence of *Po* denotes the total gating charge moved during a transition from the resting closed state occupied at negative voltages to the open state. However, one prevalent model proposed for Shaker channels include a C-O transition after all four voltage-sensors are activated (Schoppa and Sigworth, 1998; Ledwell and Aldrich, 1999). This model shares similarity with the allosteric model proposed for TRPM8, being that the channels undergo two types of conformational change: voltage-sensor activation and channel opening, such that, although voltage sensor activation is obligatory for the channel to open, channel opening is not obligatory after voltage sensors are activated. For this reason, the voltage dependence of *Po* does not change even when *Po* is as low as 10^{-7} at very negative potentials (Schoppa and Sigworth, 1998), which differs from the results of TRPM8 channels. At extremely negative potentials (≤ −100), the voltage sensor of the TRPM8 channel is at the resting state and the probability of channel opening is small (Po ≤ 10^{-4} at 15 °C and ≤10^{-5} at 25 °C), so that, only voltage-independent opening can be detected (Figure 10). This differs from what happens at more positive voltages (> 80 mV), indicating that the activation gate can open

in an independent way while voltage sensors are in the resting state. Interestingly, L_0* values for TRPM8 at 25 °C, are about 15 times smaller than L_0* values at 15 °C (Table 4), suggesting that temperature affects channel opening through a pathway that does not involves sensor activation. Analysis of the kinetics of TRPM8 shows that the activation time course of the current at different temperatures is mono exponential after of a brief delay whereas that the deactivation of the macroscopic currents exhibit a double exponential. This delay is shortened when the prepulse reaches more depolarized values (Cole Moore shift), indicating that the channel transits between several voltage-dependent closed states. Similarly, large hyperpolarizing voltages will populate those closed states further removed from the open state. These changes in the delay not show temperature dependence, suggesting that the temperature-dependence of the voltage-dependent transition is weak, which strongly demonstrates, once more, that the voltage and temperature sensors are different entities. As shown in the Figures 13, 15 and 16, the time constants of TRPM8 current relaxation exhibits a bell-shaped voltage-dependence centered near the half activation voltage for TRPM8 at the corresponding temperatures. At limiting negative voltages, τ is determined by the time constant of the C_0–O_0 transition and at very positive voltages by the time constant of the C_4–O_4 transition. At intermediate voltages, τ, both activation and deactivation, represents a weighted sum of the rate constants for all C–O transitions (Eq. 20), where the relative weighting depends on the equilibrium distributions of different closed and open states. Thus, τ–V relationship measured at limiting negative voltages, determines the value of γ_0 and implies that channel closing is voltage independent (z_γ = 0.1 ± 0.06 at 15 °C,(n=5); z_γ = 0.02 ± 0.009 at 20 °C, (n=7); z_γ = 0.02 ± 0.007 at 25 °C, (n=7) and $z\gamma$= 0.04 ± 0.01 (n=5), 0.01 ± 0.007 (n =7) and 0.05 ± 0.01 (n=7) at 15 °C, 20 °C and 25 °C, for tau fast and tau slow of deactivation process, respectively).

5.3. Fitting allosteric model

To quantitatively evaluate the model, we selected eight *Po* versus Voltage curves, (n=5-8 for each temperature) to be simultaneously fitted using equation 1. Previously, I determined that *L* is

independent of potential and therefore z_L is not considered in this fitting. *C*, *D*, and *E* were only restricted to be higher than 0. Best fit was obtained with the following parameters: *C*=2.36, *D*= 11.93, *E*= 3.33, V_{0J}= 261 mV, z_J=0.33, ΔH=-57 kcal/mol, ΔS=-177 cal/mol (Figure 23). The solid lines in Figure 23 show the prediction of the *Po* in function of temperature. Thus, the allosteric model can reproduce the steady-state behavior on TRPM8 at different temperatures confirming that activation of voltage and temperature sensors additively affect the energy of the C-O transition. The procedure also gives values for enthalpy and entropy very similar to those obtained from the van't Hoff plot for TRPM8 wild type. On the other hand, with the results of Table 4, I can perform an approximation to obtain the value of *C, D* and *Po*. Thus, at 15 °C, $K \to \infty$ and $L^*_{0(15\,^\circ C)} = L_0 C^4$, while at 25 °C, $K \to 0$ and $L^*_{0(25\,^\circ C)} = L_0$. So, the ratio of L^* to both temperatures gives an approximate value for *C*, of 1.98 (see annex 3a). At very positive voltage, *J*→ ∞ and at very high temperature, *K*=0 and *Po* ≈ 0.5, $D^4 = L^{-1}$, thus, the value for *D* is 14.7 (see Annex 3b). Finally, at very positive voltage, *J*→ ∞ and at very cold temperature, *K*→ ∞, the *Po* is 0.93 (see Annex 3C). In this way, although these calculations only corresponds to an approximation, noteworthy that the result obtained by fitting to the value of *C* and *D*, coincides with the "theoretical value", 1.98 and 14.7 respectively, shown in the Annex III (pag.93), confirming the robustness of the adjustment. Also, the value calculated for *Po* at very positive voltage and at very cold temperature is 0.93, which coincides with the experimental value obtained to *Po* at 10 °C and 360 mV (Figure 8C) of 0.92. So, finally with all this background information, we can we can conclude that the allosteric model is able to reproduce successfully the TRPM8 channel gating behavior.

5.4. Temperature sensor

Coiled-coil domain, have a repeating pattern of seven amino acid residues called "heptad repeat", of the form (**a**-b-c-**d**-e-f-g)n, where **a** and **d** are generally apolar residues forming an amphipathic α-helix (Figure 3B). Coiled-coils may interact with each other and with other, which contributes to the stability of oligomeric proteins (Nooren et al., 1999;

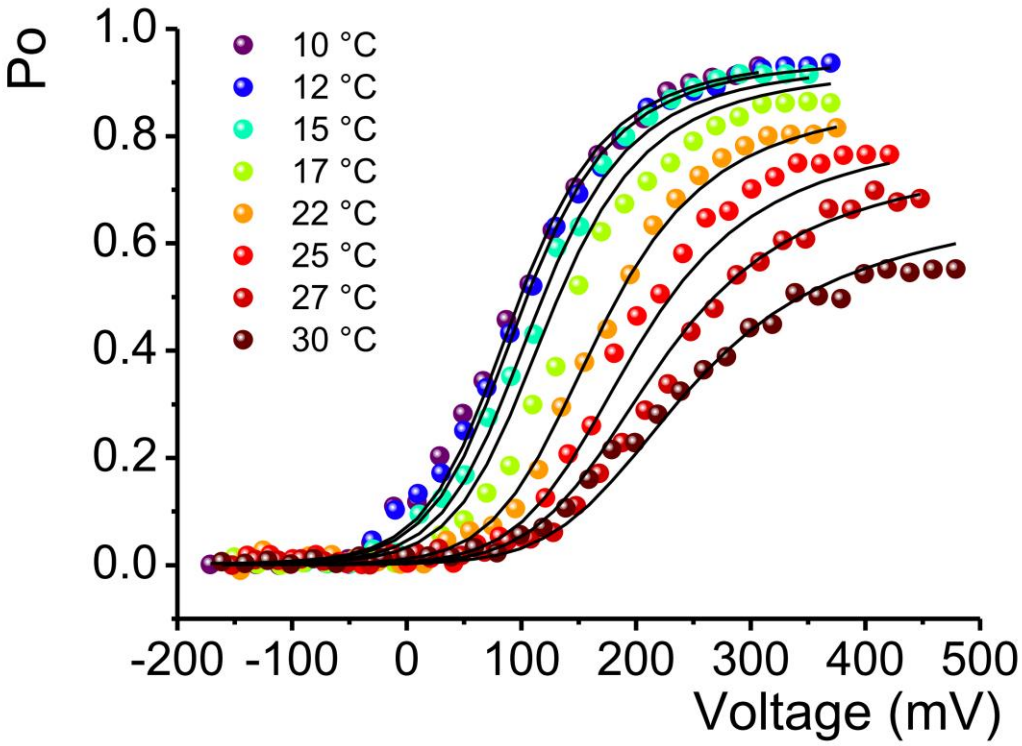

Figure 23. ***Predictions of the allosteric model.*** *Po* versus voltage data at different temperatures were fitted using equation 1 (solid curves) that defines the *Po* derived from the model given in Scheme 1**.** The best fit was obtained with the following parameters: C=2.36, D= 11.93, E= 3.33, V_{0J}= 261 mV, z_J=0.33, ΔH=-57 kcal/mol, ΔS=-177 cal/molK.

Wagschal et al., 1999; Tripet et al., 2000). For some time, the coiled-coil domains of TRPM8, TRPM2 and TRPM4, have been recognized as central to the formation of tetrameric proteins (Launay et al., 2002; Erler et al., 2006; Mei et al., 2006). In TRPM2, mutations in the coiled-coil that decrease subunit association also decrease channel activity (Mei et al., 2006). Removal of the TRPM2ΔCT, resulted in a significant, but not complete, reduction in subunit assembly which has been assessed by coimmunoprecipitation of wild type and TRPM2ΔC (Mei et al., 2006). TRPM2ΔCT, as well as point mutants at hydrophobic residues in the coiled-coil region, generate currents much smaller that the obtained for the wild type channel (Mei et al., 2006). Deletions of the coiled-coil domain of TRPM4 almost completely eliminated Ca^{2+}-activated whole-cell currents at +100 mV (Nilius et al., 2005b). Thus, from the results obtained for TRPM2 and TRPM4 channels, it can be inferred the truncations in the coiled-coil, do not induce loss of channel function, but resulted in a shift of the activation potential to extremely high positive voltages compared with the wild-type protein. In the case of TRPM8, it has been suggested that for a correct tetramerization and function of the channel, it would require the presence intact of coiled-coil domain. The fusion of the coiled-coil region to a transmembrane helix, either S6 of TRPM8 (Erler et al., 2006) or the transmembrane domain of CD8 (Tsuruda et al., 2006), produces a dominant-negative effect when coexpressed with wild-type TRPM8. Also, the L1089P mutation within the coiled-coil produces an inactive TRPM8 (Erler et al., 2006). Furthermore, Tsuruda and col. (Tsuruda et al., 2006), found that deletion of the TRPM8 coiled-coil prevented TRPM8 expression in HEK293T cells or *Xenopus laevis* oocytes. Thus, these results establish a clear role for coiled-coils in the TRPM8 channel assembly and in expression of functional channel at the plasma membrane. Furthermore, they have also demonstrated that the coiled-coil domains can form tetramers, proposing that C-terminal coiled-coil is an authentic tetramerization domain in these channels.

Previous studies of our laboratory suggest that the C-terminal end of the TRPM8 and TRPV1 determines thermosensation (Brauchi et al., 2006). They demonstrated that the exchange of the C-terminus between TRPM8 and TRPV1 channel, this last activated by heat, results in a TRPM8

channel heat-sensitive and in cold-sensitive TRPV1 channel. Thus, to determine the importance of the coiled-coil domain located on the distal region of C-terminal domain of TRPM8, we decided to delete each heptad repeat. For this, we designed the following deletions: TRPM8CTΔ8, TRPM8CTΔ15, TRPM8CTΔ22, TRPM8CTΔ29, TRPM8CTΔ36 and TRPM8CTΔ40. The mutants, with the exception of TRPM8CTΔ22, TRPM8CTΔ29 and TRPM8CTΔ40 were functional, highlighting the importance of the central heptads of the coiled-coil and of the last four amino acids which correspond to the amino-acid sequences located in the more proximal region of the coiled-coil, on the expression of the protein. These results show that for the channel tetramerization not required an intact coiled-coil structure, and therefore, the coiled-coil structure, is not the molecular determinant responsible for the tetramerization of the channel (Erler et al., 2006; Tsuruda et al., 2006). The gradual decrease in the ΔH of activation promoted by gradual deletions of the distal C-terminus, suggests that the coiled-coil region is a structural determinant, which determines the temperature sensitivity in TRPM8. Our results demonstrate that with the removal of each consecutive heptad, the enthalpy associated with gating of channel is reduced in a non-uniform manner, i.e. the heptads do not provide the same amount of energy to the process of gating in TRPM8 channels. Thus, the mutant TRPM8CTΔ8 present a reduction of 29 kcal/mol with respect to the wild protein, whereas the remaining deletions TRPM8CTΔ15 and TRPM8CTΔ36, show a decrease in enthalpy change of 41 and 58 kcal/mol respectively. With each deletion that I examined, are perturbed some parameters such as open probability and $V_{0.5}$ (Figure 20 and 22). Thus, the most dramatic effect of loss of sensitivity to temperature appears in the TRPM8CTΔ36 (Figure 20). As shown in the Figure 20A, at 60 mV and low temperatures (10 °C – 15 °C), the probability of opening for TRPM8CTΔ36, is smaller than the obtained by TRPM8, however, at temperatures between 20-25 °C, the mutant have a higher open probability than TRPM8, demonstrating that the mutant channel is less sensitive at temperature than the wild type protein. This behavior is evident to higher potentials, in this case, 300 mV (Figure 20 B), where the *Po* practically unchanged in the temperature range studied, being of 0.6 at 0.7 between 10 °C and 30 °C, in contrast to what happens with TRPM8 channel,

where in the same temperature range the *Po* at 300 mV, decreases from 0.9 to 0.4 with increasing temperature. This might be due, for example, that in this mutant, the rate of closure is less affected by the temperature increase in comparison to the wild type favoring the open state, however, this is only an idea and has not been analyzed in detail in this thesis work.

Finally, we have developed a homology model based on crystal structure of the coiled-coil domain of the channel enzyme TRPM7 (Fujiwara and Minor, 2008). In this model, TRPM8 coiled-coil is a four-stranded antiparallel coiled-coil that is held together by extensive core packing of polar interactions. This was done in order to estimate the energy contribution of each deletion *"in vitro"* by molecular dynamics (Figure 24 A). These values, just like the values obtained experimentally, were normalized (arbitrary unit). Thus, as shown the Figure 24 B, exists high correlation between the two data set, confirming that the energy changes due to the deletions show a non-linear relationship between the enthalpy and the coiled-coil heptad length, which means that each heptad is energetically different. Furthermore, when the heptad repeats are shortened; the channel is less sensitive to the temperature. In addition, we measured the energy contribution of each heptad coiled-coil of TRPM7 using the respective molecular model for this channel. Each heptad of TRPM7 produces a change enthalpy lower than those obtained by each heptad of TRPM8 (Figure 24 C), which confirms that TRPM8 is a protein highly temperature-dependent, due to large enthalpic and entropic changes produced by the coiled-coil domain of the carboxyl terminal.

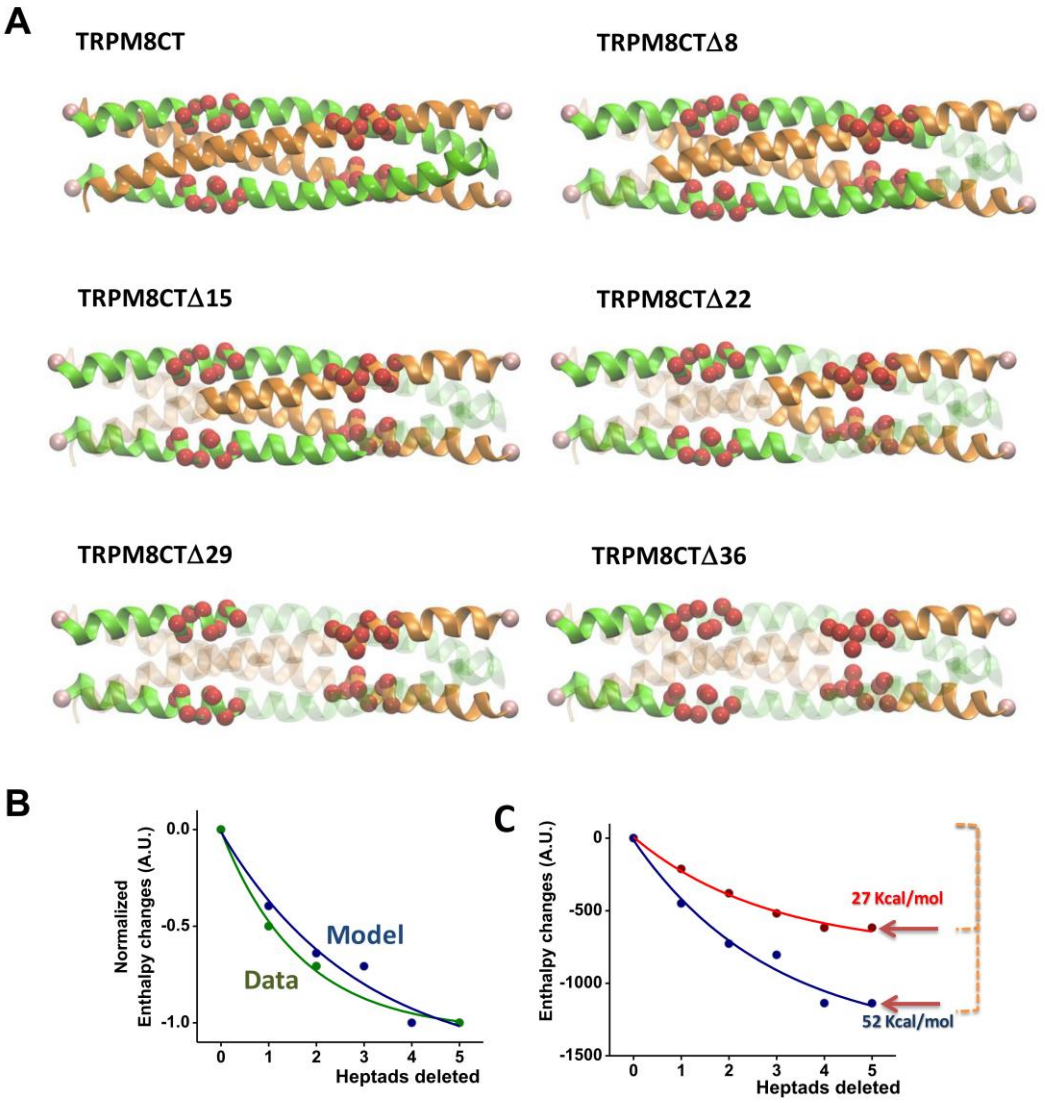

Figure 24: ***Heptad deletions reduce the temperature dependence in TRPM8***. **A**. Molecular model of the coiled-coil domain of the C- terminal that shows the deletion of each individual heptad. The coiled-coil of TRPM8 is shown in its antiparallel orientation, where each unit has a region of high flexibility (red balls) located on the fourth heptad characterized by not presenting a stable structure. **B.** Comparison between the experimentally obtained data (green circles) and the data obtained by molecular dynamics (blue circles) for TRPM8 and deletions. **C.** Energy comparison between the data obtained by molecular dynamics for heptads deleted for TRPM8 (blue circles) and for TRPM7 (red circles).

6. CONCLUSIONS

- Gating of TRPM8 can be explained by an allosteric kinetic model. Our results confirm that TRPM8 channel have different structures to sense the voltage and temperature, which can work together or separately. It is has been shown that other channels that response to many stimuli are allosteric proteins (BK channel).

- The gradual decrease in the ΔH of activation promoted by gradual deletions of the distal C-terminus, suggests that the coiled-coil region could be an important structural determinant for thermosensitivity in TRPM8.

- The energy changes due to the deletions show a non-linear relationship between the activation enthalpy and the coiled-coil heptad length. This means that entire structure is less stable when the heptad repeat is shortened; therefore the sensor (and the channel) is less sensitive to the temperature.

7. REFERENCE

Alessandri-Haber N, Joseph E, Dina OA, Liedtke W, Levine JD (2005) TRPV4 mediates pain-related behavior induced by mild hypertonic stimuli in the presence of inflammatory mediator. Pain 118:70-79.

Almers W (1978) Gating currents and charge movements in excitable membranes. Rev Physiol Biochem Pharmacol 82:96-190.

Alvarez O, Gonzalez C, Latorre R (2002) Counting channels: a tutorial guide on ion channel fluctuation analysis. Adv Physiol Educ 26:327-341.

Babes A (2009) Ion channels involved in cold detection in mammals: TRP and non-TRP mechanisms. Biophys Rev 1:193-200.

Bandell M, Story GM, Hwang SW, Viswanath V, Eid SR, Petrus MJ, Earley TJ, Patapoutian A (2004) Noxious cold ion channel TRPA1 is activated by pungent compounds and bradykinin. Neuron 41:849-857.

Bargal R, Avidan N, Ben-Asher E, Olender Z, Zeigler M, Frumkin A, Raas-Rothschild A, Glusman G, Lancet D, Bach G (2000) Identification of the gene causing mucolipidosis type IV. Nat Genet 26:118-123.

Bassi MT, Manzoni M, Monti E, Pizzo MT, Ballabio A, Borsani G (2000) Cloning of the gene encoding a novel integral membrane protein, mucolipidin-and identification of the two major founder mutations causing mucolipidosis type IV. Am J Hum Genet 67:1110-1120.

Bautista DM, Siemens J, Glazer JM, Tsuruda PR, Basbaum AI, Stucky CL, Jordt SE, Julius D (2007) The menthol receptor TRPM8 is the principal detector of environmental cold. Nature 448:204-208.

Bautista DM, Jordt SE, Nikai T, Tsuruda PR, Read AJ, Poblete J, Yamoah EN, Basbaum AI, Julius D (2006) TRPA1 mediates the inflammatory actions of environmental irritants and proalgesic agents. Cell 124:1269-1282.

Bodding M, Wissenbach U, Flockerzi V (2007) Characterisation of TRPM8 as a pharmacophore receptor. Cell Calcium 42:618-628.

Brauchi S, Orio P, Latorre R (2004) Clues to understanding cold sensation: thermodynamics and electrophysiological analysis of the cold receptor TRPM8. Proc Natl Acad Sci U S A 101:15494-15499.

Brauchi S, Orta G, Salazar M, Rosenmann E, Latorre R (2006) A hot-sensing cold receptor: C-terminal domain determines thermosensation in transient receptor potential channels. J Neurosci 26:4835-4840.

Brauchi S, Orta G, Mascayano C, Salazar M, Raddatz N, Urbina H, Rosenmann E, Gonzalez-Nilo F, Latorre R (2007) Dissection of the components for PIP2 activation and thermosensation in TRP channels. Proc Natl Acad Sci U S A

104:10246-10251.
Brauchi S, Orio,P., Latorre R. (2004) Clues to understanding cold sensation: thermodynamics and electrophysiological analysis of the cold receptor TRPM8. Proc Natl Acad Sci USA 101:15494-15499
Brauchi S. OG, Salazar M., Rosenmann E., Latorre R. (2006) A hot-sensing cold receptor: C-terminal domain determines thermosensation in transient receptor potential channels. J Neurosci 26:4835-4840.
Cain DM, Khasabov SG, Simone DA (2001) Response properties of mechanoreceptors and nociceptors in mouse glabrous skin: an in vivo study. J Neurophysiol 85:1561-1574.
Campero M, Serra J, Ochoa JL (1996) C-polymodal nociceptors activated by noxious low temperature in human skin. J Physiol 497 (Pt 2):565-572.
Caterina MJ, Rosen TA, Tominaga M, Brake AJ, Julius D (1999) A capsaicin-receptor homologue with a high threshold for noxious heat. Nature 398:436-441.
Caterina MJ, Schumacher MA, Tominaga M, Rosen TA, Levine JD, Julius D (1997) The capsaicin receptor: a heat-activated ion channel in the pain pathway. Nature 389:816-824.
Caterina MJ, Leffler A, Malmberg AB, Martin WJ, Trafton J, Petersen-Zeitz KR, Koltzenburg M, Basbaum AI, Julius D (2000) Impaired nociception and pain sensation in mice lacking the capsaicin receptor. Science 288:306-313.
Cesare P, McNaughton P (1996) A novel heat-activated current in nociceptive neurons and its sensitization by bradykinin. Proc Natl Acad Sci U S A 93:15435-15439.
Clapham DE (2003) TRP channels as cellular sensors. Nature 426:517-524.
Colburn RW, Lubin ML, Stone DJ, Jr., Wang Y, Lawrence D, D'Andrea MR, Brandt MR, Liu Y, Flores CM, Qin N (2007) Attenuated cold sensitivity in TRPM8 null mice. Neuron 54:379-386.
Cole KS, Moore JW (1960) Potassium ion current in the squid giant axon: dynamic characteristic. Biophys J 1:1-14.
Colquhoun SFJ (1995) Fitting and statistical analysis of single-channel records. Single-Channel Recording Sakmann B, Neher E, editors Plenum Press, New York: 483–587.
Cosens DJ, Manning A (1969) Abnormal electroretinogram from a Drosophila mutant. Nature 224:285-287.
Cox DH, Cui J, Aldrich RW (1997) Allosteric gating of a large conductance Ca-activated K+ channel. J Gen Physiol 110:257-281.
Crick FHC (1953) The packing of α-helices: Simple coiled-coils. Acta Crystallogr 6:689-697.
Chuang HH, Neuhausser, W. M., and Julius, D. (2004) The Super-Cooling Agent Icilin Reveals a Mechanism of Coincidence Detection by a Temperature-Sensitive TRP Channel. Neuron 43:859-869.
Chung MK, Lee H, Mizuno A, Suzuki M, Caterina MJ (2004) 2-aminoethoxydiphenyl borate activates and sensitizes the heat-gated ion channel TRPV3. J Neurosci 24:5177-5182.
Dascal N (1987) The use of Xenopus oocytes for the study of ion channels. CRC Crit Rev Biochem 22:317-387.

Davis JB, Gray J, Gunthorpe MJ, Hatcher JP, Davey PT, Overend P, Harries MH, Latcham J, Clapham C, Atkinson K, Hughes SA, Rance K, Grau E, Harper AJ, Pugh PL, Rogers DC, Bingham S, Randall A, Sheardown SA (2000) Vanilloid receptor-1 is essential for inflammatory thermal hyperalgesia. Nature 405:183-187.

De Petrocellis L, Chu CJ, Moriello AS, Kellner JC, Walker JM, Di Marzo V (2004) Actions of two naturally occurring saturated N-acyldopamines on transient receptor potential vanilloid 1 (TRPV1) channels. Br J Pharmacol 143:251-256.

Delany NS, Hurle M, Facer P, Alnadaf T, Plumpton C, Kinghorn I, See CG, Costigan M, Anand P, Woolf CJ, Crowther D, Sanseau P, Tate SN (2001) Identification and characterization of a novel human vanilloid receptor-like protein, VRL-2. Physiol Genomics 4:165-174.

Denis V, Cyert MS (2002) Internal Ca(2+) release in yeast is triggered by hypertonic shock and mediated by a TRP channel homologue. J Cell Biol 156:29-34.

Dhaka A, Viswanath V, Patapoutian A (2006) Trp ion channels and temperature sensation. Annu Rev Neurosci 29:135-161.

Dhaka A, Murray AN, Mathur J, Earley TJ, Petrus MJ, Patapoutian A (2007) TRPM8 is required for cold sensation in mice. Neuron 54:371-378.

Doerner JF, Gisselmann G, Hatt H, Wetzel CH (2007) Transient receptor potential channel A1 is directly gated by calcium ions. J Biol Chem 282:13180-13189.

Erler I, Al-Ansary DM, Wissenbach U, Wagner TF, Flockerzi V, Niemeyer BA (2006) Trafficking and assembly of the cold-sensitive TRPM8 channel. J Biol Chem 281:38396-38404.

Eswar N, Webb B, Marti-Renom MA, Madhusudhan MS, Eramian D, Shen MY, Pieper U, Sali A (2006) Comparative protein structure modeling using Modeller. Curr Protoc Bioinformatics Chapter 5:Unit 5 6.

Fujiwara Y, Minor DL, Jr. (2008) X-ray crystal structure of a TRPM assembly domain reveals an antiparallel four-stranded coiled-coil. J Mol Biol 383:854-870.

Gaudet CBPaR (2007) The Role of the N Terminus and Transmembrane Domain of TRPM8 in Channel Localization and Tetramerization. The Journal of Biological Chemistry 282:36474-36480.

Gaudet R (2008) A primer on ankyrin repeat function in TRP channels and beyond. Mol Biosyst 4:372-379.

Gong Z, Son W, Chung YD, Kim J, Shin DW, McClung CA, Lee Y, Lee HW, Chang DJ, Kaang BK, Cho H, Oh U, Hirsh J, Kernan MJ, Kim C (2004) Two interdependent TRPV channel subunits, inactive and Nanchung, mediate hearing in Drosophila. J Neurosci 24:9059-9066.

Grandl J, Hu H, Bandell M, Bursulaya B, Schmidt M, Petrus M, Patapoutian A (2008) Pore region of TRPV3 ion channel is specifically required for heat activation. Nat Neurosci 11:1007-1013.

Grimm C, Kraft R, Sauerbruch S, Schultz G, Harteneck C (2003) Molecular and functional characterization of the melastatin-related cation channel TRPM3. J Biol Chem 278:21493-21501.

Hamill OP, Marty A, Neher E, Sakmann B, Sigworth FJ (1981) Improved patch-clamp techniques for high-resolution current recording from cells and cell-free

membrane patches. Pflugers Arch 391:85-100.
Hardie RC, Minke B (1992) The trp gene is essential for a light-activated Ca2+ channel in Drosophila photoreceptors. Neuron 8:643-651.
Hofmann T, Chubanov V, Gudermann T, Montell C (2003) TRPM5 is a voltage-modulated and Ca(2+)-activated monovalent selective cation channel. Curr Biol 13:1153-1158.
Horrigan FT, Aldrich RW (1999) Allosteric voltage gating of potassium channels II. Mslo channel gating charge movement in the absence of Ca(2+). J Gen Physiol 114:305-336.
Horrigan FT, Aldrich RW (2002) Coupling between voltage sensor activation, Ca2+ binding and channel opening in large conductance (BK) potassium channels. J Gen Physiol 120:267-305.
Hu HZ, Gu Q, Wang C, Colton CK, Tang J, Kinoshita-Kawada M, Lee LY, Wood JD, Zhu MX (2004) 2-aminoethoxydiphenyl borate is a common activator of TRPV1, TRPV2, and TRPV3. J Biol Chem 279:35741-35748.
Huang J, Zhang X, McNaughton PA (2006) Modulation of temperature-sensitive TRP channels. Semin Cell Dev Biol 17:638-645.
Hui K, Guo Y, Feng ZP (2005) Biophysical properties of menthol-activated cold receptor TRPM8 channels. Biochem Biophys Res Commun 333:374-382.
Humphrey W, Dalke A, Schulten K (1996) VMD: visual molecular dynamics. J Mol Graph 14:33-38, 27-38.
Hwang SW, Cho H, Kwak J, Lee SY, Kang CJ, Jung J, Cho S, Min KH, Suh YG, Kim D, Oh U (2000) Direct activation of capsaicin receptors by products of lipoxygenases: endogenous capsaicin-like substances. Proc Natl Acad Sci U S A 97:6155-6160.
Jordt SE, Bautista DM, Chuang HH, McKemy DD, Zygmunt PM, Hogestatt ED, Meng ID, Julius D (2004) Mustard oils and cannabinoids excite sensory nerve fibres through the TRP channel ANKTM1. Nature 427:260-265.
Karashima Y, Talavera K, Everaerts W, Janssens A, Kwan KY, Vennekens R, Nilius B, Voets T (2009) TRPA1 acts as a cold sensor in vitro and in vivo. Proc Natl Acad Sci U S A 106:1273-1278.
Kim J, Chung YD, Park DY, Choi S, Shin DW, Soh H, Lee HW, Son W, Yim J, Park CS, Kernan MJ, Kim C (2003) A TRPV family ion channel required for hearing in Drosophila. Nature 424:81-84.
Kiselyov K, Chen J, Rbaibi Y, Oberdick D, Tjon-Kon-Sang S, Shcheynikov N, Muallem S, Soyombo A (2005) TRP-ML1 is a lysosomal monovalent cation channel that undergoes proteolytic cleavage. J Biol Chem 280:43218-43223.
Kohn WD, Kay CM, Hodges RS (1995) Protein destabilization by electrostatic repulsions in the two-stranded alpha-helical coiled-coil/leucine zipper. Protein Sci 4:237-250.
Krylov D, Barchi J, Vinson C (1998) Inter-helical interactions in the leucine zipper coiled coil dimer: pH and salt dependence of coupling energy between charged amino acids. J Mol Biol 279:959-972.
Kwan KY, Allchorne AJ, Vollrath MA, Christensen AP, Zhang DS, Woolf CJ, Corey DP (2006) TRPA1 contributes to cold, mechanical, and chemical nociception but is

not essential for hair-cell transduction. Neuron 50:277-289.
LaPlante JM, Falardeau J, Sun M, Kanazirska M, Brown EM, Slaugenhaupt SA, Vassilev PM (2002) Identification and characterization of the single channel function of human mucolipin-1 implicated in mucolipidosis type IV, a disorder affecting the lysosomal pathway. FEBS Lett 532:183-187.
Latorre R, Brauchi S, Orta G, Zaelzer C, Vargas G (2007) ThermoTRP channels as modular proteins with allosteric gating. Cell Calcium 42:427-438.
Launay P, Fleig A, Perraud AL, Scharenberg AM, Penner R, Kinet JP (2002) TRPM4 is a Ca2+-activated nonselective cation channel mediating cell membrane depolarization. Cell 109:397-407.
Launay P, Cheng H, Srivatsan S, Penner R, Fleig A, Kinet JP (2004) TRPM4 regulates calcium oscillations after T cell activation. Science 306:1374-1377.
Ledwell JL, Aldrich RW (1999) Mutations in the S4 region isolate the final voltage-dependent cooperative step in potassium channel activation. J Gen Physiol 113:389-414.
Liedtke W, Choe Y, Marti-Renom MA, Bell AM, Denis CS, Sali A, Hudspeth AJ, Friedman JM, Heller S (2000) Vanilloid receptor-related osmotically activated channel (VR-OAC), a candidate vertebrate osmoreceptor. Cell 103:525-535.
Littleton JT, Ganetzky B (2000) Ion channels and synaptic organization: analysis of the Drosophila genome. Neuron 26:35-43.
Liu B, Qin F (2005) Functional control of cold- and menthol-sensitive TRPM8 ion channels by phosphatidylinositol 4,5-bisphosphate. J Neurosci 25:1674-1681.
Lupas AN, Gruber M (2005) The structure of alpha-helical coiled coils. Adv Protein Chem 70:37-78.
Macpherson LJ, Geierstanger BH, Viswanath V, Bandell M, Eid SR, Hwang S, Patapoutian A (2005) The pungency of garlic: activation of TRPA1 and TRPV1 in response to allicin. Curr Biol 15:929-934.
Manzoni M, Monti E, Bresciani R, Bozzato A, Barlati S, Bassi MT, Borsani G (2004) Overexpression of wild-type and mutant mucolipin proteins in mammalian cells: effects on the late endocytic compartment organization. FEBS Lett 567:219-224.
Marti-Renom MA, Stuart AC, Fiser A, Sanchez R, Melo F, Sali A (2000) Comparative protein structure modeling of genes and genomes. Annu Rev Biophys Biomol Struct 29:291-325.
Matta JA, Ahern GP (2007) Voltage is a partial activator of rat thermosensitive TRP channels. J Physiol 585:469-482.
McKemy DD, Neuhausser, W. M., and Julius, D. (2002) Identification of a cold receptor reveals a general role for TRP channels in thermosensation. Nature 416:52-58.
McNamara FN, Randall A, Gunthorpe MJ (2005) Effects of piperine, the pungent component of black pepper, at the human vanilloid receptor (TRPV1). Br J Pharmacol 144:781-790.
Mei ZZ, Xia R, Beech DJ, Jiang LH (2006) Intracellular coiled-coil domain engaged in subunit interaction and assembly of melastatin-related transient receptor potential channel 2. J Biol Chem 281:38748-38756.
Montell C (2005) The TRP superfamily of cation channels. Sci STKE 2005:re3.
Montell C, Rubin GM (1989) Molecular characterization of the Drosophila trp locus: a

putative integral membrane protein required for phototransduction. Neuron 2:1313-1323.
Montell C, Birnbaumer L, Flockerzi V (2002a) The TRP channels, a remarkably functional family. Cell 108:595-598.
Montell C, Birnbaumer L, Flockerzi V, Bindels RJ, Bruford EA, Caterina MJ, Clapham DE, Harteneck C, Heller S, Julius D, Kojima I, Mori Y, Penner R, Prawitt D, Scharenberg AM, Schultz G, Shimizu N, Zhu MX (2002b) A unified nomenclature for the superfamily of TRP cation channels. Mol Cell 9:229-231.
Moqrich A, Hwang SW, Earley TJ, Petrus MJ, Murray AN, Spencer KS, Andahazy M, Story GM, Patapoutian A (2005) Impaired thermosensation in mice lacking TRPV3, a heat and camphor sensor in the skin. Science 307:1468-1472.
Muraki K, Iwata Y, Katanosaka Y, Ito T, Ohya S, Shigekawa M, Imaizumi Y (2003) TRPV2 is a component of osmotically sensitive cation channels in murine aortic myocytes. Circ Res 93:829-838.
Nadler MJ, Hermosura MC, Inabe K, Perraud AL, Zhu Q, Stokes AJ, Kurosaki T, Kinet JP, Penner R, Scharenberg AM, Fleig A (2001) LTRPC7 is a Mg.ATP-regulated divalent cation channel required for cell viability. Nature 411:590-595.
Nauli SM, Alenghat FJ, Luo Y, Williams E, Vassilev P, Li X, Elia AE, Lu W, Brown EM, Quinn SJ, Ingber DE, Zhou J (2003) Polycystins 1 and 2 mediate mechanosensation in the primary cilium of kidney cells. Nat Genet 33:129-137.
Nilius B, Owsianik G (2011) The transient receptor potential family of ion channels. Genome Biol 12:218.
Nilius B, Talavera K, Owsianik G, Prenen J, Droogmans G, Voets T (2005a) Gating of TRP channels: a voltage connection? J Physiol 567:35-44.
Nilius B, Prenen J, Janssens A, Owsianik G, Wang C, Zhu MX, Voets T (2005b) The selectivity filter of the cation channel TRPM4. J Biol Chem 280:22899-22906.
Nilius B, Prenen J, Droogmans G, Voets T, Vennekens R, Freichel M, Wissenbach U, Flockerzi V (2003) Voltage dependence of the Ca2+-activated cation channel TRPM4. J Biol Chem 278:30813-30820.
Nooren IM, Kaptein R, Sauer RT, Boelens R (1999) The tetramerization domain of the Mnt repressor consists of two right-handed coiled coils. Nat Struct Biol 6:755-759.
Palmer CP, Zhou XL, Lin J, Loukin SH, Kung C, Saimi Y (2001) A TRP homolog in Saccharomyces cerevisiae forms an intracellular Ca(2+)-permeable channel in the yeast vacuolar membrane. Proc Natl Acad Sci U S A 98:7801-7805.
Park U, Vastani N, Guan Y, Raja SN, Koltzenburg M, Caterina MJ (2011) TRP vanilloid 2 knock-out mice are susceptible to perinatal lethality but display normal thermal and mechanical nociception. J Neurosci 31:11425-11436.
Peier AM, Reeve AJ, Andersson DA, Moqrich A, Earley TJ, Hergarden AC, Story GM, Colley S, Hogenesch JB, McIntyre P, Bevan S, Patapoutian A (2002) A heat-sensitive TRP channel expressed in keratinocytes. Science 296:2046-2049.
Peier AM, Moqrich, A., Hergarden, A. C., Reeve, A. J., Andersson, D. A., Story, G. M., Earley, T. J., Dragoni, I., McIntyre, P., Bevan, S., and Patapoutian, A. (2002) A TRP channel that senses cold stimuli and menthol. Cell 108:705-715.
Perraud AL, Fleig A, Dunn CA, Bagley LA, Launay P, Schmitz C, Stokes AJ, Zhu Q,

Bessman MJ, Penner R, Kinet JP, Scharenberg AM (2001) ADP-ribose gating of the calcium-permeable LTRPC2 channel revealed by Nudix motif homology. Nature 411:595-599.
Petersen CC, Berridge MJ, Borgese MF, Bennett DL (1995) Putative capacitative calcium entry channels: expression of Drosophila trp and evidence for the existence of vertebrate homologues. Biochem J 311 (Pt 1):41-44.
Phillips AM, Bull A, Kelly LE (1992) Identification of a Drosophila gene encoding a calmodulin-binding protein with homology to the trp phototransduction gene. Neuron 8:631-642.
Qin N, Neeper MP, Liu Y, Hutchinson TL, Lubin ML, Flores CM (2008) TRPV2 is activated by cannabidiol and mediates CGRP release in cultured rat dorsal root ganglion neurons. J Neurosci 28:6231-6238.
Reid G FM (2002) Ion channels activated by cold and menthol in cultured rat dorsal root ganglion neurones. Neurosci Lett 324:164-168.
Rohacs T, Lopes CM, Michailidis I, Logothetis DE (2005) PI(4,5)P2 regulates the activation and desensitization of TRPM8 channels through the TRP domain. Nat Neurosci 8:626-634.
Ross RA (2003) Anandamide and vanilloid TRPV1 receptors. Br J Pharmacol 140:790-801.
Runnels LW, Yue L, Clapham DE (2001) TRP-PLIK, a bifunctional protein with kinase and ion channel activities. Science 291:1043-1047.
Sano Y, Inamura K, Miyake A, Mochizuki S, Yokoi H, Matsushime H, Furuichi K (2001) Immunocyte Ca2+ influx system mediated by LTRPC2. Science 293:1327-1330.
Schlingmann KP, Weber S, Peters M, Niemann Nejsum L, Vitzthum H, Klingel K, Kratz M, Haddad E, Ristoff E, Dinour D, Syrrou M, Nielsen S, Sassen M, Waldegger S, Seyberth HW, Konrad M (2002) Hypomagnesemia with secondary hypocalcemia is caused by mutations in TRPM6, a new member of the TRPM gene family. Nat Genet 31:166-170.
Schoppa NE, Sigworth FJ (1998) Activation of shaker potassium channels. I. Characterization of voltage-dependent transitions. J Gen Physiol 111:271-294.
Sidi S, Friedrich RW, Nicolson T (2003) NompC TRP channel required for vertebrate sensory hair cell mechanotransduction. Science 301:96-99.
Sigg D, Bezanilla F (1997) Total charge movement per channel. The relation between gating charge displacement and the voltage sensitivity of activation. J Gen Physiol 109:27-39.
Sigworth FJ (1980) The variance of sodium current fluctuations at the node of Ranvier. J Physiol 307:97-129.
Smith GD, Gunthorpe MJ, Kelsell RE, Hayes PD, Reilly P, Facer P, Wright JE, Jerman JC, Walhin JP, Ooi L, Egerton J, Charles KJ, Smart D, Randall AD, Anand P, Davis JB (2002) TRPV3 is a temperature-sensitive vanilloid receptor-like protein. Nature 418:186-190.
Starace DM, Bezanilla F (2004) A proton pore in a potassium channel voltage sensor reveals a focused electric field. Nature 427:548-553.
Stayner C, Zhou J (2001) Polycystin channels and kidney disease. Trends Pharmacol Sci

22:543-546.
Story GM, Peier AM, Reeve AJ, Eid SR, Mosbacher J, Hricik TR, Earley TJ, Hergarden AC, Andersson DA, Hwang SW, McIntyre P, Jegla T, Bevan S, Patapoutian A (2003) ANKTM1, a TRP-like channel expressed in nociceptive neurons, is activated by cold temperatures. Cell 112:819-829.
Strotmann R, Harteneck C, Nunnenmacher K, Schultz G, Plant TD (2000) OTRPC4, a nonselective cation channel that confers sensitivity to extracellular osmolarity. Nat Cell Biol 2:695-702.
Stuhmer W, Methfessel C, Sakmann B, Noda M, Numa S (1987) Patch clamp characterization of sodium channels expressed from rat brain cDNA. Eur Biophys J 14:131-138.
Sun M, Goldin E, Stahl S, Falardeau JL, Kennedy JC, Acierno JS, Jr., Bove C, Kaneski CR, Nagle J, Bromley MC, Colman M, Schiffmann R, Slaugenhaupt SA (2000) Mucolipidosis type IV is caused by mutations in a gene encoding a novel transient receptor potential channel. Hum Mol Genet 9:2471-2478.
Talavera K, Yasumatsu K, Voets T, Droogmans G, Shigemura N, Ninomiya Y, Margolskee RF, Nilius B (2005) Heat activation of TRPM5 underlies thermal sensitivity of sweet taste. Nature 438:1022-1025.
Todaka H, Taniguchi J, Satoh J, Mizuno A, Suzuki M (2004) Warm temperature-sensitive transient receptor potential vanilloid 4 (TRPV4) plays an essential role in thermal hyperalgesia. J Biol Chem 279:35133-35138.
Togashi K, Hara Y, Tominaga T, Higashi T, Konishi Y, Mori Y, Tominaga M (2006) TRPM2 activation by cyclic ADP-ribose at body temperature is involved in insulin secretion. EMBO J 25:1804-1815.
Tominaga M, Caterina MJ, Malmberg AB, Rosen TA, Gilbert H, Skinner K, Raumann BE, Basbaum AI, Julius D (1998) The cloned capsaicin receptor integrates multiple pain-producing stimuli. Neuron 21:531-543.
Trevisani M, Smart D, Gunthorpe MJ, Tognetto M, Barbieri M, Campi B, Amadesi S, Gray J, Jerman JC, Brough SJ, Owen D, Smith GD, Randall AD, Harrison S, Bianchi A, Davis JB, Geppetti P (2002) Ethanol elicits and potentiates nociceptor responses via the vanilloid receptor-1. Nat Neurosci 5:546-551.
Tripet B, Wagschal K, Lavigne P, Mant CT, Hodges RS (2000) Effects of side-chain characteristics on stability and oligomerization state of a de novo-designed model coiled-coil: 20 amino acid substitutions in position "d". J Mol Biol 300:377-402.
Tsuruda PR, Julius D, Minor DL, Jr. (2006) Coiled coils direct assembly of a cold-activated TRP channel. Neuron 51:201-212.
Venkatachalam K, Montell C (2007) TRP channels. Annu Rev Biochem 76:387-417.
Venkatachalam K, Hofmann T, Montell C (2006) Lysosomal localization of TRPML3 depends on TRPML2 and the mucolipidosis-associated protein TRPML1. J Biol Chem 281:17517-17527.
Vlachova V TJ, Susankova K, Lyfenko A, Ettrich R, Vyklicky L (2003) Functional role of C-terminal cytoplasmic tail of rat vanilloid receptor 1. J Neurosci 23:1340-1350.
Voets T (2012) Quantifying and Modeling the Temperature-Dependent Gating of TRP

Channels. Rev Physiol Biochem Pharmacol.
Voets T, Droogmans G, Wissenbach U, Janssens A, Flockerzi V, Nilius B (2004) The principle of temperature-dependent gating in cold- and heat-sensitive TRP channels. Nature 430:748-754.
Voets T, Owsianik, G., Janssens, A., Talavera, K., and Nilius, B. (2007) TRPM8 voltage sensor mutants reveal a mechanism for integrating thermal and chemical stimuli. Nat Chem Biol 3:174-182.
Wagschal K, Tripet B, Hodges RS (1999) De novo design of a model peptide sequence to examine the effects of single amino acid substitutions in the hydrophobic core on both stability and oligomerization state of coiled-coils. J Mol Biol 285:785-803.
Walder RY, Landau D, Meyer P, Shalev H, Tsolia M, Borochowitz Z, Boettger MB, Beck GE, Englehardt RK, Carmi R, Sheffield VC (2002) Mutation of TRPM6 causes familial hypomagnesemia with secondary hypocalcemia. Nat Genet 31:171-174.
Walker RG, Willingham AT, Zuker CS (2000) A Drosophila mechanosensory transduction channel. Science 287:2229-2234.
Watanabe H, Vriens J, Suh SH, Benham CD, Droogmans G, Nilius B (2002a) Heat-evoked activation of TRPV4 channels in a HEK293 cell expression system and in native mouse aorta endothelial cells. J Biol Chem 277:47044-47051.
Watanabe H, Davis JB, Smart D, Jerman JC, Smith GD, Hayes P, Vriens J, Cairns W, Wissenbach U, Prenen J, Flockerzi V, Droogmans G, Benham CD, Nilius B (2002b) Activation of TRPV4 channels (hVRL-2/mTRP12) by phorbol derivatives. J Biol Chem 277:13569-13577.
Wes PD, Chevesich J, Jeromin A, Rosenberg C, Stetten G, Montell C (1995) TRPC1, a human homolog of a Drosophila store-operated channel. Proc Natl Acad Sci U S A 92:9652-9656.
Wissenbach U, Bodding M, Freichel M, Flockerzi V (2000) Trp12, a novel Trp related protein from kidney. FEBS Lett 485:127-134.
Woolfson DN (2005) The design of coiled-coil structures and assemblies. Adv Protein Chem 70:79-112.
Xu H, Blair NT, Clapham DE (2005) Camphor activates and strongly desensitizes the transient receptor potential vanilloid subtype 1 channel in a vanilloid-independent mechanism. J Neurosci 25:8924-8937.
Xu H, Delling M, Jun JC, Clapham DE (2006) Oregano, thyme and clove-derived flavors and skin sensitizers activate specific TRP channels. Nat Neurosci 9:628-635.
Xu H, Ramsey IS, Kotecha SA, Moran MM, Chong JA, Lawson D, Ge P, Lilly J, Silos-Santiago I, Xie Y, DiStefano PS, Curtis R, Clapham DE (2002) TRPV3 is a calcium-permeable temperature-sensitive cation channel. Nature 418:181-186.
Zhu X, Chu PB, Peyton M, Birnbaumer L (1995) Molecular cloning of a widely expressed human homologue for the Drosophila trp gene. FEBS Lett 373:193-198.
Zurborg S, Yurgionas B, Jira JA, Caspani O, Heppenstall PA (2007) Direct activation of the ion channel TRPA1 by Ca2+. Nat Neurosci 10:277-279.

ANNEX I

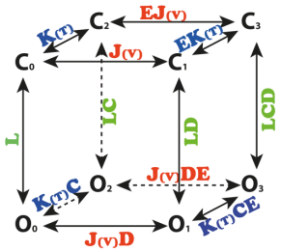

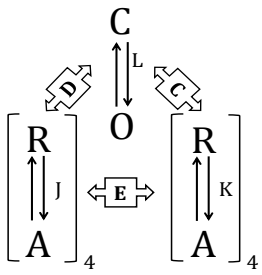

$$\frac{O_1}{O_0} = JD \quad , \quad \frac{O_2}{O_0} = KC \quad , \quad \frac{O_3}{O_0} = KCEJD \quad , \quad \frac{O_0}{C_0} = L,$$
$$\frac{O_0}{C_1} = \frac{L}{J} \quad , \quad \frac{O_0}{C_2} = \frac{L}{K} \quad , \quad \frac{O_0}{O_3} = \frac{L}{KEJ}$$

$$P_O = \frac{O_0+O_1+O_2+O_3}{O_0+O_1+O_2+O_3+C_0+C_1+C_2+C_3}$$

$$P_O = \frac{1+\frac{O_1}{O_0}+\frac{O_2}{O_0}+\frac{O_3}{O_0}}{1+\frac{O_1}{O_0}+\frac{O_2}{O_0}+\frac{O_3}{O_0}+\frac{C_0}{O_0}+\frac{C_1}{O_0}+\frac{C_2}{O_0}+\frac{C_3}{O_0}}$$

$$P_O = \frac{1+JD+KC+KCEJD}{1+JD+KC+KCEJD+\frac{1}{L}+\frac{J}{L}+\frac{K}{L}+\frac{KEJ}{L}}$$

$$P_o = \frac{1}{1+\frac{(1+J+K+KEJ)}{L(1+JD+KC+KCEJD)}}$$

Assuming that the channel contains four voltage-sensing domains and four sensors of temperature

$$P_o = \frac{1}{1+\frac{(1+J+K+KEJ)^4}{L(1+JD+KC+KCEJD)^4}}$$

ANNEX II

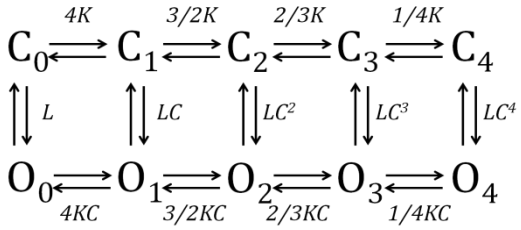

$$4KC = \frac{O_1}{O_0} \quad , \quad 6K^2C^2 = \frac{O_2}{O_0} \quad , \quad 4K^3C^3 = \frac{O_3}{O_0} \quad , \quad K^4C^4 = \frac{O_4}{O_0}$$

$$\frac{1}{L} = \frac{C_0}{O_0} \quad , \quad \frac{4K}{L} = \frac{C_1}{C_0} \quad , \quad \frac{6K^2}{L} = \frac{C_2}{C_0} \quad , \quad \frac{4K^3}{L} = \frac{C_3}{C_0} \quad , \quad \frac{K^4}{L} = \frac{C_4}{C_0}$$

$$P_O = \frac{O_0 + O_1 + O_2 + O_3 + O_4}{O_0 + O_1 + O_2 + O_3 + O_4 + C_0 + C_1 + C_2 + C_3 + C_4}$$

$$P_O = \frac{1 + \frac{O_1}{O_0} + \frac{O_2}{O_0} + \frac{O_2}{O_0} + \frac{O_3}{O_0} + \frac{O_4}{O_0}}{1 + \frac{O_1}{O_0} + \frac{O_2}{O_0} + \frac{O_2}{O_0} + \frac{O_3}{O_0} + \frac{O_4}{O_0} + \frac{C_0}{O_0} + \frac{C_1}{O_0} + \frac{C_2}{O_0} + \frac{C_3}{O_0} + \frac{C_4}{O_0}}$$

$$P_O = \frac{1 + 4DK + 6D^2K^2 + 4D^3K^3 + D^4K^4}{1 + 4DK + 6D^2K^2 + 4D^3K^3 + D^4K^4 + \frac{1}{L} + \frac{4K}{L} + \frac{6K^2}{L} + \frac{4K^3}{L} + \frac{K^4}{L}}$$

$$P_O = \frac{(1 + KC)^4}{(1 + KC)^4 + \frac{1}{L}(1 + K)^4}$$

$$P_O = \frac{1}{1 + \frac{(1 + K)^4}{L(1 + KC)^4}}$$

ANNEX III

$$Po = \frac{1}{1+\frac{(1+J+K+JKE)^4}{L(1+JD+KC+JKDEC)^4}}$$

a. At very negative voltages, *J*=0

$$P_O = \frac{1}{1+\frac{(1+K)^4}{L(1+KC)^4}}$$

- At very high temperatures (25 °C), $K \rightarrow 0$

$$P_O = \frac{1}{1+\frac{1}{L^*}}$$

Then, if $L^* << 0$,

$$P_O = \frac{1}{\frac{1}{L^*}}$$

$$P_O = L^* = 2.1E-5$$

(This value was obtained of table 4)

Furthermore, considering that

$$L_0^* = L_0\left(\frac{1+KC}{1+K}\right)^4 \text{ (See equation 19)}$$

If $K \rightarrow 0$, $L_0^* \rightarrow L_0$

Thus, at very low temperatures (15 °C), $K \rightarrow \infty$

$$P_O = \frac{1}{1+\frac{1}{L^*}} = L^* = 3.32E-4$$

(This value was obtained of table 4)

Where

$$L_0^* = L_0 C^4$$

Thus, the ration between Po at 15 °C and 25 °C shows that

$$\frac{P_{0\,(15\,°C)}}{P_{O\,(25\,°C)}} = \frac{LC^4}{L} = \frac{3.32\ E{-}4}{2.15\ E{-}5}$$

Thus, when the temperature decreases, *Po* increases 10 times, $C^4 = 15.4$, $C = 1.98$

b. At very positive voltage, *J* → ∞ and at high temperature, *K* →0.

$$P_o = \frac{1}{1+\frac{(1+J)^4}{L(1+JD)^4}} = \frac{1}{1+\frac{1}{LD^4}}$$

Furthermore, experimentally, at this temperatures, *Po* ≈ 0.5

$$LD^4 = 1 \qquad D^4 = L^{-1}$$

$$D^4 = (2.15\ E - 5)^{-1}$$
$$D = 14.69$$

c. At very positive voltage, *J*→∞ and at very cold temperature, *K*→∞

$$P_o = \frac{1}{\frac{(JKE)^4}{L(JKDEC)^4}} \qquad P_o = \frac{1}{1+\frac{1}{L(DC)^4}} \qquad LD^4 = 1 \quad , C^4 = 15.4$$

$$P_O = \frac{1}{1+\frac{1}{15}} = 0.93$$ Experimental value for ***Po*=0.92**